Analysis of the relevance of exosomes for the spread of hepatitis B virus

Thesis

For the award of the degree of

Doctor of Natural Sciences, Doctor philosophiae naturalis (Dr. phil. nat.)

Submitted to the

Department of Biochemistry, Chemistry and Pharmacy

Johann Wolfgang Goethe University

Frankfurt am Main – Germany

Presented by

Qingyan Wu

Born in Xinjiang Uygur Autonomous Region, China

Frankfurt am Main (2022)

(D 30)

vom Fachbereich Biochemie, Chemie, Pharmazie (14) der
Johann Wolfgang Goethe-Universität als Dissertation angenommen.

Dekan: Prof. Dr. Clemens Glaubitz

Gutachter: Prof. Dr. Rolf Marschalek
Prof. Dr. Eberhard Hildt

Datum der Disputation: December 20th, 2022

Table of contents

List of Figures

List of Abbreviations

Abbreviation	Meaning
%	percent
ε	epsilon
(-) strand	negative sense strand
(+) stranded	positive sense strand
aa	amino acid residue
AGL	antigenic loop
Alix	apoptosis-linked gene-2 (ALG-2)-interacting protein X
APS	ammonium peroxydisulphate
ATP	adenosine triphosphate
bps	base pairs
BSA	bovine Serum Albumin
ccc-DNA	covalently closed circular DNA
CCR5	C-C chemokine receptor type 5
CHMP	charged multivesicular body protein
CTD	C-terminal arginine-rich domain
CXCR-4	C-X-C chemokine receptor type 4
DEPC	diethyl pyrocarbonate
DMEM	Dulbecco's Modified Eagle's Medium
DMSO	dimethyl sulfoxide
DNA	deoxyribonucleic acid
dNTP	deoxynucleotide triphosphates
DR1/2	direct repeat 1/2
dsDNA	double-stranded DNA
dslDNA	double-stranded linear DNA
DTT	dithiothreitol
EBV	Epstein-Barr virus
ECL	enhanced Chemiluminescence
EDTA	ethylenediamine tetraacetic acid
EIAV	Equine infectious anemia virus
ELISA	enzyme-linked immunosorbent assay
ER	endoplasmic reticulum
ESCRT	endosomal sorting complex required for transport
FA	formaldehyde
FBS	fetal bovine serum
FEN-1	flap endonuclease 1

HAV	Hepatitis A virus
HBV	Hepatitis B virus
HBcAg/HBc/C	Hepatitis B core antigen
HBeAg	Hepatitis B e antigen
HBsAg	HBV surface antigen
HBx/X	Hepatitis B x antigen
HCC	hepatocellular carcinoma
HCV	Hepatitis C virus
HDV	Hepatitis D virus
HEV	Hepatitis E virus
HIV	Human immunodeficiency virus
HRP	horseradish peroxidase
HRS	hepatocyte growth factor-regulated tyrosine kinase substrate
HSPGs	heparan sulfate proteoglycans
HSV-1	Herpes simplex virus 1
IgG	immunoglobulin G
ILVs	intraluminal vesicles
kb	kilobases
KO	knockout
LB	lysogeny broth
LHBs/L	large hepatitis B surface antigen
LIG1/3	DNA ligase 1/3
LMP1	latent membrane protein 1
MHBs/M	middle hepatitis B surface antigen
MHC	major histocompatibility complex
MOI	multiplicity of infection
mRNA	messenger ribonucleic acid
MVBs	multivesicular bodies
NP-40	nonyl phenoxypolyethoxylethanol
NPCs	nuclear pore complexes
NT	non-target
NTA	nanoparticle tracking analysis
NTCP	sodium taurocholate cotransporting polypeptide
NTD	N-terminal assembly domain
ORF	open reading frame
P	polymerase
PA	phosphatidic acid

PBS	phosphate Buffered Saline
PBMCs	peripheral blood mononuclear cells
PCR	polymerase chain reaction
PD-L1	programmed-death ligand-1
PI3P	phosphatidylinositol 3-phosphate
PLD2	phospholipase D2
PM	plasma membrane
PRD	proline-rich domain
PTA	phosphotungstic acid hydrate
PVDF	polyvinylidene difluoride membrane
qPCR	quantitative polymerase chain reaction
RBD	receptor binding domain
rcDNA	relaxed circular DNA
RIPA	radio-immunoprecipitation assay
RH	RNase H domain
rpm	revolutions per minute
RPMI-1640	Roswell Park Memorial Institute Medium 1640
RT	room temperature
RT domain	reverse transcriptase domain
S/CO	sample to cut-off value
SDS	sodium dodecyl sulfate
SEM	standard error of the mean
STAM1/2	signal transducing adaptor molecule 1/2
TAR	transactivation response element
TDP2	tyrosyl-DNA phosphodiesterase 2
TEM	transmission electron microscopy
TEMED	N,N,N’,N’-Tetramethylethylenediamine
TM	transmembrane domain
TP	terminal protein domain
Tsg101	tumor susceptibility gene 101
UEV	ubiquitin E2 variant
VPS	vacuolar protein-sorting-associated protein
Vta1	vesicle trafficking 1

1 Introduction

1.1 The Hepatitis B virus

1.1.1 Global Impact and Epidemiology of Hepatitis B virus (HBV) infection

The saga of the discovery of the 'Australia antigen' [1], HBV surface antigen (HBsAg), in 1965 is considered an important milestone in understanding the pathogenesis of infectious hepatitis [2, 3]. A hepatitis B infection can lead to an acute infection or a chronic infection. An acute infection can persist up to 6 months, a positive HBV test for over 6 months after the first blood test result is diagnosed as chronic infection. Serological evidence for HBV infection shows that over 2 billion people are either past or presently infected [4]. The World Health Organization reported in 2019 that there are approximately 1.5 million new infections annually [5] and an estimated 296 million people living with chronic infection around the world [6]. Clinical studies have shown that chronic HBV infection is highly associated with an increased risk to develop cirrhosis, liver failure or hepatocellular carcinoma. Worldwide, the consequences of HBV infection cause more than 620,000 deaths each year [7]. Although safe and effective HBV vaccines have reduced the incidence of new HBV infections in most countries, HBV remains a major health problem as no large-scale effective vaccination strategies are in place in many countries with a high prevalence burden. Moreover, many chronic HBV infected patients do not receive effective and timely treatment and a complete cure for the established chronic infection is still far from being achieved [8, 9]. Therefore, understanding the life cycle of HBV and interactions with its host cells offer new insights for the development of better therapeutic approaches and vaccine opportunities.

As one of the most widespread infectious diseases in the world, the prevalence of chronic HBV infection shows a different geographical distribution. The global seroprevalence of HBsAg was reported to be 3.61% with high prevalence (> 8.00%) in countries of the African region (about 8.83%) and high-intermediate endemicity (5.00% – 7.99%) in countries of the Western Pacific region (about 5.25%) (**Figure 1**) [10, 11]. In contrast, low HBsAg prevalence (< 2.00%) was observed in most countries of the Americas (except Haiti) and Western Europe as well as in Australia and Japan of the Western Pacific region [11]. HBsAg prevalence was low-intermediate (2.00% – 4.99%) in the Eastern Mediterranean and European region, but the prevalence increased eastward in Europe, the prevalence in Djibouti, Sudan and Somalia also has higher HBsAg prevalence than other countries in the Eastern Mediterranean [11]. HBsAg prevalence in Southeast Asian overall varied widely, with low prevalence in India, Indonesia, and Nepal, while other countries had low-intermediate to high-intermediate prevalence levels [11]. Thus, a combination of active and effective monitoring, screening, enhanced vaccination, and effective treatment strategies will contribute to the elimination of HBV as a public health threat.

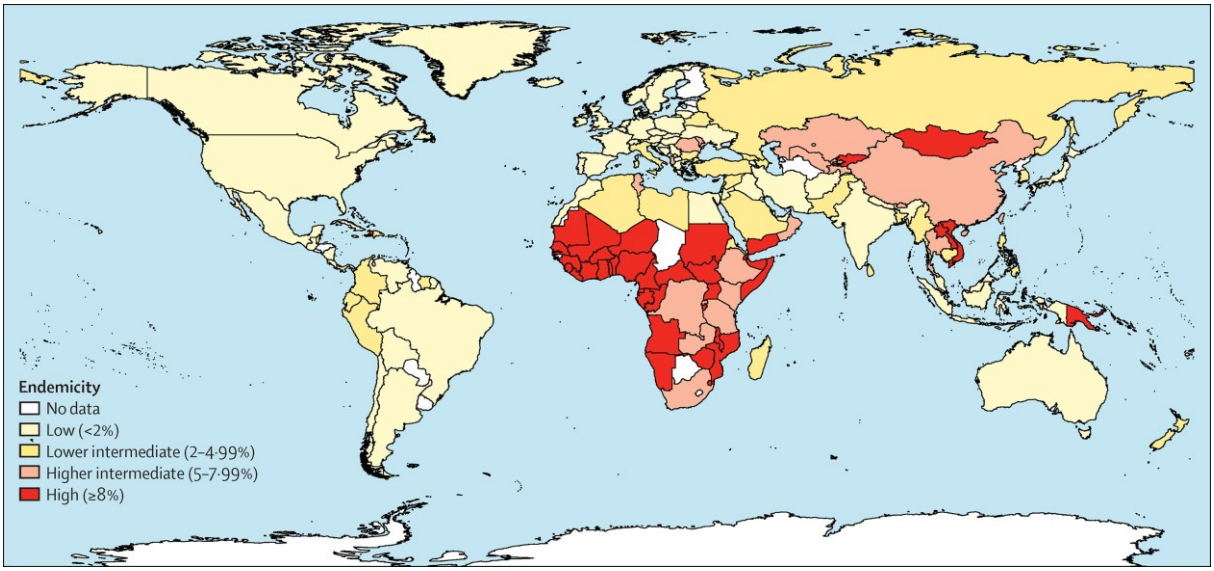

Figure 1. Global prevalence of chronic hepatitis B virus infection (HBsAg) estimation. Based on data published between 1965 and 2013. Image retrieved from [11].

1.1.2 HBV classification and genome organization

HBV is classified into the family of *hepadnaviridae*, sometimes also referred to as para-retroviruses or retroid viruses due to the replication of the double-stranded DNA (dsDNA) genome by reverse transcription of a pre-genomic RNA (pgRNA) template [12]. The hepadnaviridae are subdivided into orthohepadnavirus (including human hepatitis B virus, woodchuck hepatitis B virus and ground squirrel hepatitis B virus) and avihepadnavirus (like duck hepatitis B virus and heron hepatitis B virus) [13]. Besides the unique life cycle, replication through a pre-genomic RNA template, hepadnaviridae also share the features of a narrow host range and tissue tropism, a RNA-dependent DNA polymerase and a partially double-stranded genomic DNA [12].

The genome of all Hepadnaviridae is a partially dsDNA, 3.1 to 3.3 kilobases (kb) in length, comprising a complete coding strand (minus-strand) and an incomplete non-coding strand (plus-strand) [14, 15]. The circular configuration is maintained by the cohesive overlap between the 5’ ends of positive and negative DNA strands, with an overlap complementary length of approximately 50 base pair (bps) for the avihepadnaviruses and 240 bps for the orthohepadnaviruses [14, 15]. The DNA genome of HBV is about 3.2 kb in size and has a reverse transcriptase, also known as polymerase protein, covalently linked to the 5’ end of the minus-strand, and a capped RNA oligomer attached to the 5’ end of the plus-strand (**Figure 2**). Two direct repeat elements, DR1 and DR2, are essential for HBV DNA replication and genome circularization (**Figure 2**) [16, 17].

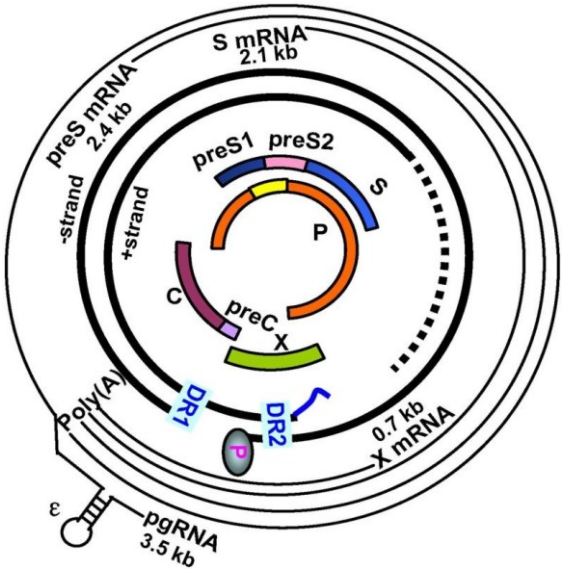

Figure 2. Schematic diagram of HBV genome organization. The innermost filled boxes represent the P (polymerase)-open reading frame (ORF) fully overlapping with the preS/S-ORF, and partially overlapping with the preC/C-ORF and the X-ORF. The next black partially double coil surrounding the ORF represents the viral double-stranded, relaxed circular DNA with the P protein (small, filled circle) attached to the 5' end of the (-) stranded DNA and the 3' end of the (+) stranded DNA (dotted line) is incomplete. A capped RNA oligomer is linked to the 5' end of the (+) strand (short wavy line). The vertical blue bars on relaxed circular DNA indicate direct repeat elements 1 and 2 (DR1 and DR2). The outmost circled lines denote the four classes of viral RNAs transcribed from the covalently closed circular (ccc) DNA template: 0.7-kb X mRNA, 2.1-kb preS2/S mRNA, 2.4-kb preS1 mRNA, and 3.5-kb pgRNA. The 3.5-kb precore mRNA encoding HBeAg was not shown. The RNA encapsidation signal, epsilon (ε), situated near the 5' end of the pgRNA. Image retrieved from [18].

There are four different unidirectional promoters (core, SPI, SPII, and X) and four open reading frames in the HBV genome that transcribe four different classes of HBV RNAs. 0.7-kb X mRNA for translating HBx protein, 2.1-kb preS2/S mRNA for middle (MHBs) and small (SHBs) hepatitis B surface proteins, 2.4-kb preS1 mRNA encoding the large hepatitis B surface protein (LHBs), and 3.5-kb pgRNA is used to encode the core and P proteins (in addition, 3.5 kb precore mRNA for the non-structurally secreted protein: HBeAg) [18]. All viral RNAs share the same 3' sequences since there is only one polyadenylation signal in the viral genome (**Figure 2**). The promoters of core, preS1, preS2/S and X are further augmented by two enhancer elements (I and II) and also by the weak transcriptional transactivator, HBx [19]. Each nucleotide in the HBV genome has coding capacity, the P gene overlaps with the 3' end of core gene, the entire envelope gene, and the 5' end of X gene (**Figure 2**). Consequently, the HBV genome is the smallest DNA virus, but it is also characterized as one of the most compact and extremely economical viruses.

1.1.3 HBV genotypes and serotypes

Based on an intergroup divergence of at least 7.5% across the complete genome, HBV has been classified into 10 genotypes (A-J) [20–23]. Genotypes A-D, F and I were further divided

into at least 35 sub-genotypes based on intergroup nucleotide differences of between approximately 4% and 8% across the genome (**Table 1**) [21–23]. Based on HBsAg antigenic heterogeneity, 9 serological subtypes have been identified (ayw1, ayw2, ayw3, ayw4, ayr, adw2, adw4, adrq+, and adrq-) [21, 22]. 'a' as the common determinant present in HBV strains, the expression specificities of y/d and w/r are defined by substitutions at amino acids 122 and 160 of the HBsAg, respectively [24–26].

Different genotypes and sub-genotypes display distinct geographic distributions (**Table 1**) and are influential in both the clinical manifestation and heterogeneous clinical outcomes in chronic HBV infection. For example, patients infected with genotype C have an increased and earlier risk of liver inflammation, cirrhosis and hepatocellular carcinoma (HCC) compared to those infected with other genotypes [27]. An acute infection of HBV genotype A is correlated to a relatively high risk for developing a chronic infection [28]. With respect to interferon treatment, patients infected with genotypes A or B had better efficacy than genotypes C, D and G [29]. But no significant distinction has been found in the treatment to nucleos(t)ide analogue therapy across genotypes/subgenotypes [30].

Table 1 Comparison of virological characteristics of HBV genotypes

Genotype	Genome length (nt)	Differentiating features	Sub-genotype	Geographic distribution
A	3221	6-nucleotide (nt) insertion near the 3' terminal of core gene	A1-A4	A1: Africa, Southern Asia A2: Europe, North America and Japan A3: Western Africa
B	3215	B1 and B5 without recombination with genotype C in the precore/core region	B1-B5	B1: Japan; B2: East Asia B3, B7, B9: Southeast Asia B6: Canada
C	3215	the oldest HBV genotype	C1-C16	C1-C3: Southeast Asia, East Asia C4: Australian; C5: Philippines C6-C16: Indonesia
D	3182	33-nt deletion at the N terminus of the preS1 region	D1-D7	D1: Middle East; D2: Europe and Africa D3: worldwide; D5: India; D7: Tunisia and Cuba
E	3212	3-nt deletion at the N terminus of the preS1 region	-	West and central Africa
F	3215	The Intra-genotypic divergence was 14%	F1-F4	Central and South Americas, and Alaska
G	3248	36-nt insert at the core region; 3-nt deletion at the N terminus of the preS1 region; two stop codons at positions 2 and 28 of the precore region,	-	France, Germany, and the Americas

		HBeAg negative		
H	3215	Closely related to genotype F	-	Central America, Mexico, and Nicaragua
I	3215	Genotype A, C, G recombination	I1 and I2	Southern China, Vietnam, Laos, India
J	3182	33-nt deletion at the N terminus of the preS1 region	-	Japan

Table retrieved and modified from [18].

1.1.4 Structure of HBV Virions and Subviral Particles

One well-known feature of HBV is the secretion of large amounts of virions and subviral particles. A complete HBV virion (Dane particle) is a spherical particle with a diameter of about 42 nm containing an outer envelope (assembled by HBV surface antigen (HBsAg)) and an inner nucleocapsid (assembled by HBV core antigen (HBcAg)) in which the partially double-stranded relaxed circular DNA genome is encapsulated [31] (**Figure 3**).

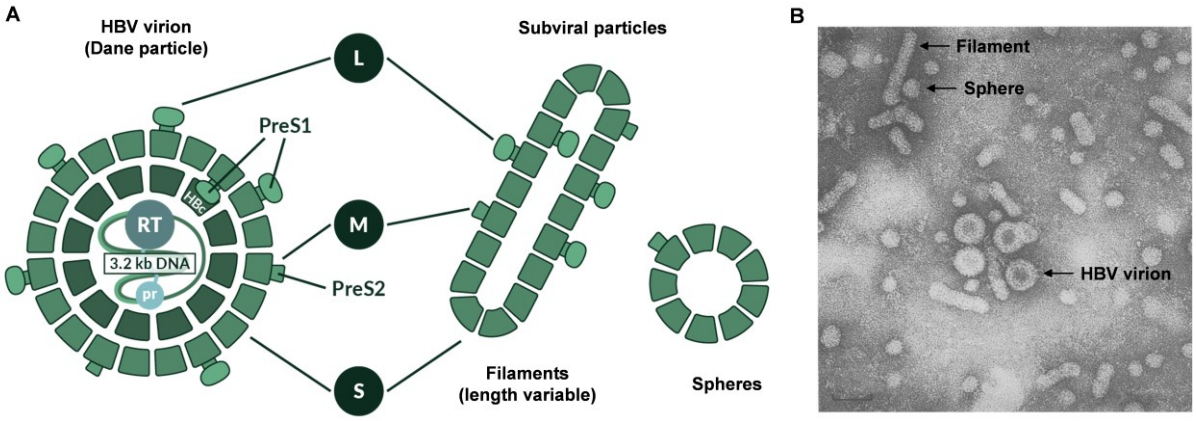

Figure 3. Schematic diagram of HBV virion, sphere, and filament. (A) The envelope of infectious HBV virion consists of three viral surface proteins: LHBs, MHBs, and SHBs. The icosahedral capsid encapsulates a double-stranded relaxed circular DNA (rcDNA), a viral polymerase and cellular protein kinase(s). The viral surface proteins in addition form filaments with variable length or spheres with a diameter of about 22-nm. **(B)** Electron microscopy image of negative stained HBV virions, filament, and sphere. Image retrieved and modified from [32, 33].

The nucleocapsid of HBV virions is composed of 180 or 240 subunits of HBcAg, arranged in an icosahedral symmetry with triangulation (T) numbers of 3 or 4 [34, 35]. The N-terminal assembly region (first 149 amino acid residues (aa)) of core protein is responsible to form the capsid shell [36–38]. The arginine-rich C-terminal domain is required for nucleocytoplasmic shuttling of the core/capsid [39, 40], viral replication, and pgRNA/reverse transcriptase

encapsidation [41]. Besides one copy of rcDNA and viral polymerase, nucleocapsid probably contains cellular protein kinase(s) [42, 43].

The envelope of HBV virions consists of a lipid bilayer derived from host hepatocyte and three different viral surface proteins (LHBs, MHBs, and SHBs) (**Figure 3**). The LHBs, MHBs and SHBs are estimated to be present in the envelope of Dane particles with a ratio of approximately 1:1:4. These surface proteins are translated from a single continuous ORF by using three separate in-phase start codons and a shared stop codon (**Figure 4A**).

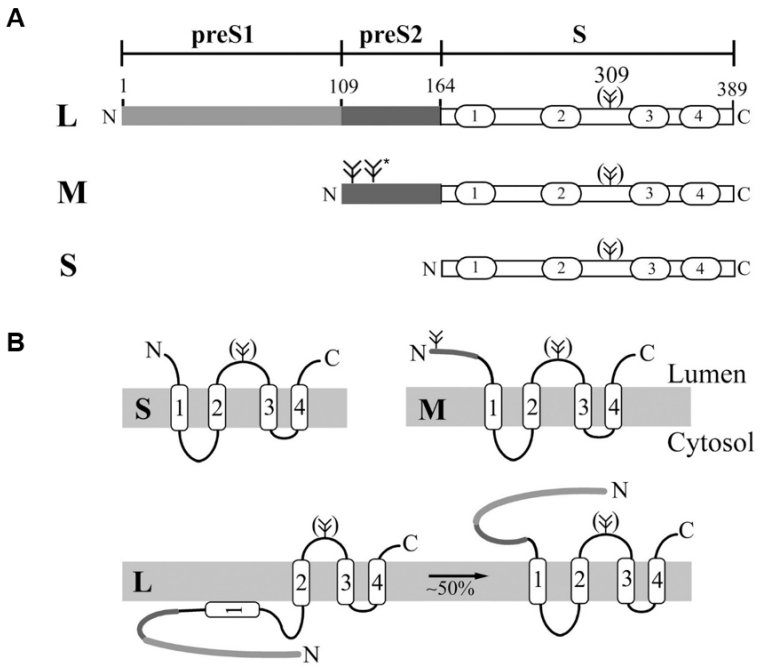

Figure 4. Schematic representation of the structure of the HBV envelope proteins and their proposed transmembrane topologies. (A) HBV envelope proteins comes in three forms: LHBs protein with preS1, preS2 and S domain, MHBs protein with preS2 and S domain, and SHBs only with S domain. The short wavy line at the N-terminus of LHBs represents the myristoylation. Four transmembrane domains (TMI-IV) are present in the S domain. "(Ⲩ)" denotes only the part of the proteins being glycosylated [44]. In the preS2 domain of MHBs there also exists an N-glycosylation site denoted with "Ⲩ", and an O-glycosylation site present in genotypes C and D denoted as "Ⲩ*" [45–48]. **(B)** Proposed transmembrane topologies of SHBs, MHBs and LHBs. Image retrieved and modified from [49].

The proposed transmembrane topologies of the surface proteins are shown in **Figure 4B**. The SHBs, MHBs and LHBs are initiated to be synthesized as multi-spanning transmembrane proteins at the endoplasmic reticulum (ER), where a fraction of them acquires the N-linked glycosylation (N146 in the S domain, within the antigenic loop (AGL) region [48]). The MHBs exhibit a topology like that of SHBs, with their N and C termini protruding into the ER lumen. However, LHBs are characterized by a dual topology of the preS region. Upon maturation, LHBs form a dual transmembrane topology by disposing their hydrophilic N-terminal preS1+preS2 domain either at the cytosol (corresponding to the virion inside, i-preS) or the ER lumen (corresponding to the virion outside, e-preS) (**Figure 4B**) [50,

51]. Both topologies of LHBs play a crucial role in the viral life cycle, with the i-preS recruiting the capsid during the assembly and the e-preS binding to the receptors during virus entry [52, 53]. The N-terminus myristoylation at glycine 2 of LHBs is essential for viral infectivity [52, 54, 55]. Since myristoylation occurs at the cytosol, the initial topology of the LHBs is i-preS. During maturation, ~50% of i-preS post-translationally translocate to e-preS [49]. Moreover, the cytoplasmic preS2 region serves as a transcriptional activator by activating protein kinase C (PKC) [56, 57].

In addition to infectious virions, large amounts of non-infectious HBsAg subviral particles (SVPs) (10^3- to 10^6-fold excess over HBV virion) are found in the blood of HBV positive patients and in HBV-producing cells. These HBsAg SVP structures are spheres (approximately 22 nm in diameter) or 22-nm diameter filaments of variable length, they are formed exclusively from envelope proteins and lack the viral genome and any other HBV proteins (**Figure 3**). The spheres are assembled mainly by the SHBs, containing smaller amounts of the MHBs, and very small traces of the LHBs [58]. However, the filaments are characterized by a higher content of the LHBs, with about equal amounts of MHBs and LHBs proteins [59, 60] (**Figure 3**).

Recent evidence indicates DNA-free empty virions (enveloped capsids without viral genome or pgRNA inside) [61–63] and RNA-containing particles (enveloped capsids with HBV RNA or pgRNA inside) [64, 65] also existed in the blood of infected patients. Besides enveloped particles, nonenveloped capsids (naked capsids) have been found in HBV-replicating cells. Interestingly, they are rarely found in the blood of HBV infected patients, but some infected individuals produce large amounts of anti-core antibodies [66–68]. Undoubtedly, the major functional significance of the SVP is to block the neutralizing effect of the host antibodies [31].

1.2 Viral life cycle

1.2.1 Attachment

In more than 50 years since HBV was discovered, the fundamentals of its life cycle and morphogenesis have been roughly illuminated. The attachment of HBV to the host cell surface is considered to be multi-step, involving multiple receptors with different affinities.

The initial low-affinity interaction of HBV with heparan sulfate proteoglycans (HSPGs) promotes viral enrichment at the plasma membrane, beginning the life cycle of HBV [69, 70] (**Figure 5, step 1**). HSPGs have been described to be associated with the primary attachment to cells of many viruses, including HIV-1 [71], herpes simplex virus [72], human papillomavirus [73] and flavivirus [74, 75]. HBV was found to interact exclusively with highly sulfated HSPGs [69, 70] that are predominantly present on the surface of hepatocytes [76], specifically with glypican 5 [77], which is strongly expressed in the liver. These discoveries

partially clarify the intense hepatotropism of HBV. However, these findings do not explain how those HBV that are sequestered in non-liver cells avoid binding to HSPGs. The current study indicates that the attachment of HBV to HSPGs is mediated by electrostatic interactions between only two positively charged residues (R122 and K141) positioned in the AGL of HBV S domain and the negatively charged HSPGs [78].

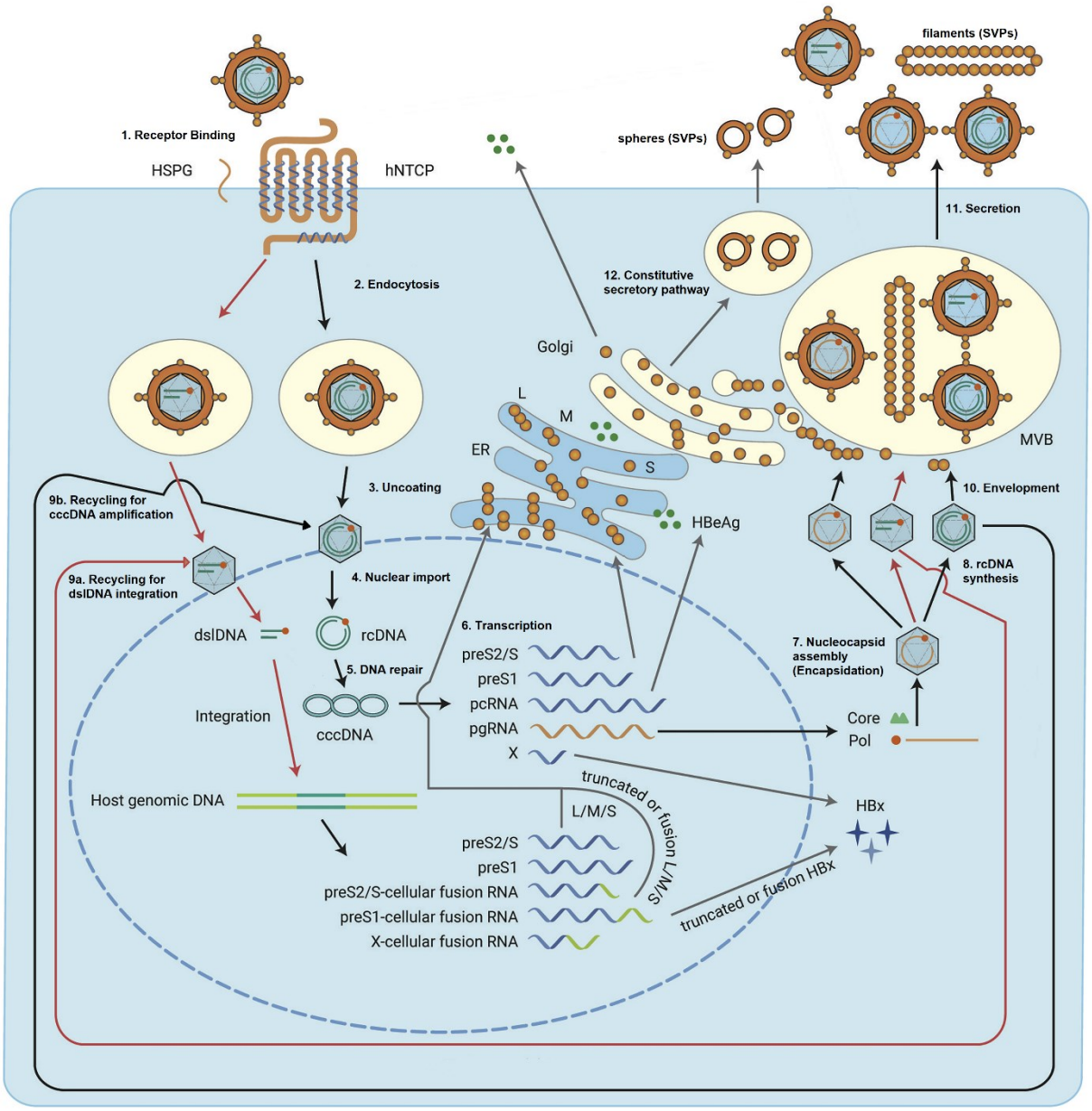

Figure 5. Model of the HBV life cycle. 1. By binding to the receptors HBV attachment to the hepatocyte membrane. **2.** Entry into host cells by endocytosis. **3.** Viral uncoating. **4.** Nuclear import of the nucleocapsid, rcDNA is delivered to the nucleus. **5.** rcDNA is repaired to form cccDNA. **6.** Transcription of pregenomic RNA (pgRNA) and other sub-genomic RNAs. **7.** Encapsidation of pgRNA-polymerase into the nucleocapsid. **8.** Reverse transcription of pgRNA into rcDNA. **9a** and **9b**. Nuclear Recycling of rcDNA or dslDNA. **10**. Nucleocapsid acquires viral envelope at the multivesicular body (MVB) to accomplish the assembly of the virus. **11**. Viruses and filaments are released by the exosome delivery pathway. **12**. Spheres are released via the constitutive secretory pathway. Image retrieved and modified from [79].

This reversible and low-affinity interaction allows HBV to stabilize at the cell surface and facilitates the movement of HBV along the cell surface until it binds with a specific receptor with high affinity. As a bile acid transporter expressed almost exclusively on the sinusoidal (basolateral) membranes of hepatocytes [80], sodium taurocholate cotransporting polypeptide (NTCP) was revealed as a critical entry receptor for HBV and HDV in 2012 [81] (**Figure 5, step 1**). Specifically, the myristoylated N-terminal 2-48 amino acids of the LHBs protein mediates the specific high-affinity attachment with NTCP receptor [82–85].

1.2.2 Viral entry, intracellular trafficking and nucleocapsid transportation

After binding to the specific receptor NTCP, the subsequent entry of HBV into hepatocytes is probably triggered by clathrin-mediated endocytosis [86, 87], in which different host factors are involved (**Figure 5, step 2**). In the early stage of infection, electron microscopy analysis also revealed the presence of HBV particles in clathrin-coated vesicles [87]. However, the entry of viruses is known to often involve multiple host factors, the co-receptor(s) and cell factors necessary for NTCP mediates HBV internalization remain to be elucidated. NTCP is obviously required for effective HBV infection, but not sufficient. Although overexpression of NTCP increases the efficiency of HBV infection in the hepatoma cell lines, it requires extremely high titers [81, 88, 89]. Hitherto non-identified liver-specific factors are probably required for robust HBV infection.

After endocytosis, the enveloped virus needs to be regulated by fusion with the cellular membrane or other mechanisms to escape from the endosomes and release the nucleocapsid (**Figure 5, step 3**). Several findings have demonstrated that HBV could be transported from early endosomes to late endosomes after endocytosis using host factors like activation of epidermal growth factor receptor [90, 91]. Viral uncoating probably takes place in late endosomes. Currently, the precise manner in which HBV flees the endosome is not fully understood. Several studies have reported different views. The fusogenic domains that have been identified in HBV include: the low pH-dependent N-terminal 9-24 amino acids of preS1 [92], the pH-independent fusogenic domain C-terminal 41-52 amino acid of preS2 [93], and the low pH-dependent fusogenic domain N-terminal 1-23 amino acids of S [94], suggest that this process is likely to be dependent on the fusion. However, it has also been reported that there is no fusion in this process, it is the function of the translocation motif (TLM) which was identified in the preS domain of HBV to enable the translocation across the endosomal membrane [95].

After being released, the nucleocapsid is assumed to be transported to the vicinity of the nuclear pore complex. A microtubule-dependent approach [96] and the dynein L11 motor protein that interacts directly with the nucleocapsid [97] are thought to potentially facilitate transport of the nucleocapsid to the nucleus (**Figure 5, step 4**). The HBV nucleocapsids can

pass through nuclear pore complexes (NPCs) as an intact particle [98, 99], and only the capsids with a mature genome are disassembled in NPCs by an unknown mechanism. This import process is probably regulated by the direct interaction of capsid with importin α/β [100] and nucleoporin 153 [101]. Several studies revealed that in NPCs, separation of capsid structures and the polymerase-genome complex is mediated by the phosphorylation at C-terminus of the HBc protein and by the importin α- and β-dependent manner [102–105]. In addition, a bipartite nuclear localization signal localized in the N terminal protein (TP) domain of the polymerase was assumed to mediate the final genome complex import into the nucleus [106].

1.2.3 Covalently closed circular DNA (cccDNA) formation

Once inside the nucleus, the partially double-stranded rcDNA is repaired and converted into the covalently closed circular DNA (cccDNA) (**Figure 5, step 5**). The DNA repair mechanisms involved in this conversion remain currently opaque. Theoretically, it is believed that repair begins with the HBV polymerase being removed from the 5’ end of minus-strand by tyrosyl-DNA phosphodiesterase 2 (TDP2) [107] and/or flap endonuclease 1 (FEN-1) [108, 109], a process that is perhaps also regulated by other nucleases and proteases (**Figure 6**). Subsequently, the minus-strand is repaired by removing a 10 nucleotide DNA flap (used to link the HBV polymerase to the minus-strand) by FEN-1 (or other nucleases) and then by joining the nick by DNA ligase 1 and/or 3 (LIG1/3) [109, 110] (**Figure 6**). The repair of plus-strand is currently thought to resemble the synthesis of DNA lagging strand with five protein factors required, involving the following steps: the use of host DNA polymerases (proliferating cell nuclear antigen [111], replication factor C complex [111] and DNA polymerase delta [112]) to synthesis of incomplete DNA strand; cleavage of the displaced 5’-capped RNA primer by FEN-1; and the nick ligation by LIG1/3(**Figure 6**) [109, 110].

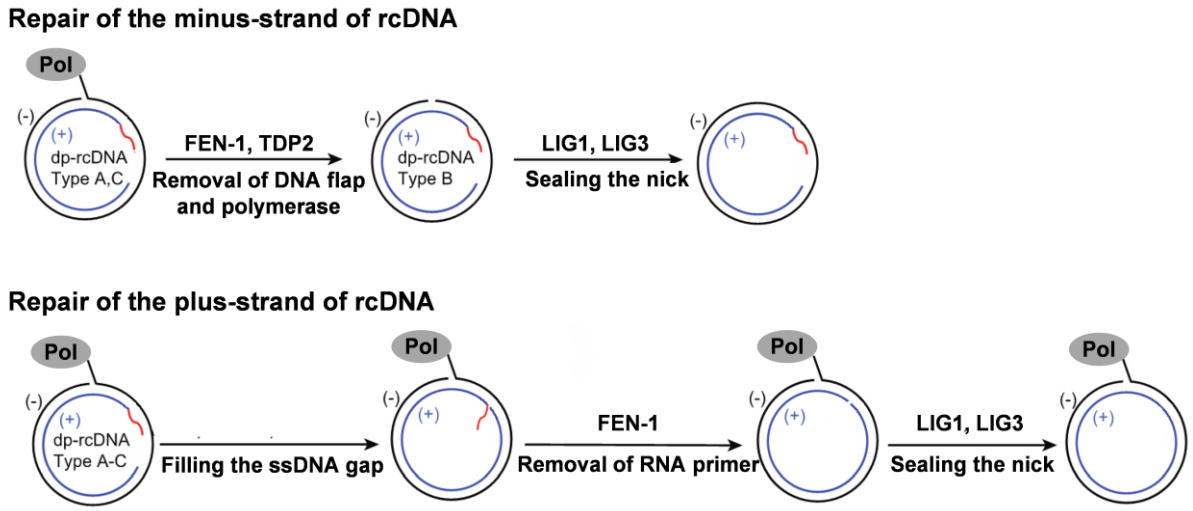

Figure 6. A putative model for the conversion of HBV rcDNA to cccDNA. For minus-strand repair, HBV polymerase (Pol) is removed by tyrosyl-DNA phosphodiesterase 2 (TDP2) and/or flap endonuclease 1 (FEN-1). The DNA flap is removed by FEN-1 and the nick is sealed by DNA ligase 1/3 (LIG1/3). The repair of the plus-strand is like the synthesis of the DNA lagging strand, with the ssDNA gap filled by various host DNA polymerases, RNA primer removed by FEN-1 and the nick sealed by DNA ligase 1/3 (LIG1/3). Image retrieved and modified from [113].

After formation, cccDNA is assembled with host factors (histones, transcription factors and other host factors) and viral proteins (HBx, HBc) in the form of a minichromosome. Maintenance of the cccDNA pool in the nucleus is critical for persistent viral infection. Cure of chronic infection requires elimination of cccDNA. Due to the high stability and long persistence this is a major obstacle on the way to a curative HBV therapy [114, 115]. Samples from HBV-infected patients showed that cccDNA copy numbers were maintained from 0.01 to 9 copies in each cell and have a half-life of over 9 months [114–117]. Currently, there is no clear mechanism for the regulation of maintenance/stability of cccDNA, with cytokine stimulation, antigen status and immune responses thought to be the main factors [118]. Elimination of cccDNA is essential to cure chronic HBV infection.

1.2.4 Viral RNA and protein synthesis

Taking cccDNA as a template, the pregenomic RNA (pgRNA) and other subgenomic RNAs are transcribed under the mediation of the host RNA polymerase II machinery [119] (**Figure 5, step 6**). The transcription is regulated by four promoters on the viral genome (core, SPI, SPII, and X). Hepatocyte enriched transcriptional factors, chromatin modifying enzymes, hepatocyte nuclear factors and potentially viral regulatory HBx protein [120] are also recruited to the cccDNA in this process [121]. Like host chromosomes, transcription is subject to epigenetic regulation, such as methylation of cccDNA [122], histone acetylation [121, 123, 124]. Afterwards, the transcribed viral RNA species are exported to the cytoplasm for protein synthesis. The core protein and polymerase are translated from 3.5-kb pgRNA,

HBeAg translated from 3.5-kb precore mRNA (**Figure 7**). 2.4-kb preS1 mRNA and 2.1-kb preS2/S mRNA RNA coding for the three envelope proteins, 0.7-kb mRNA encoding for HBx protein. In addition to serving as the transcript for HBc protein and polymerase synthesis, pgRNA is also the template for the rcDNA synthesized by reverse transcription.

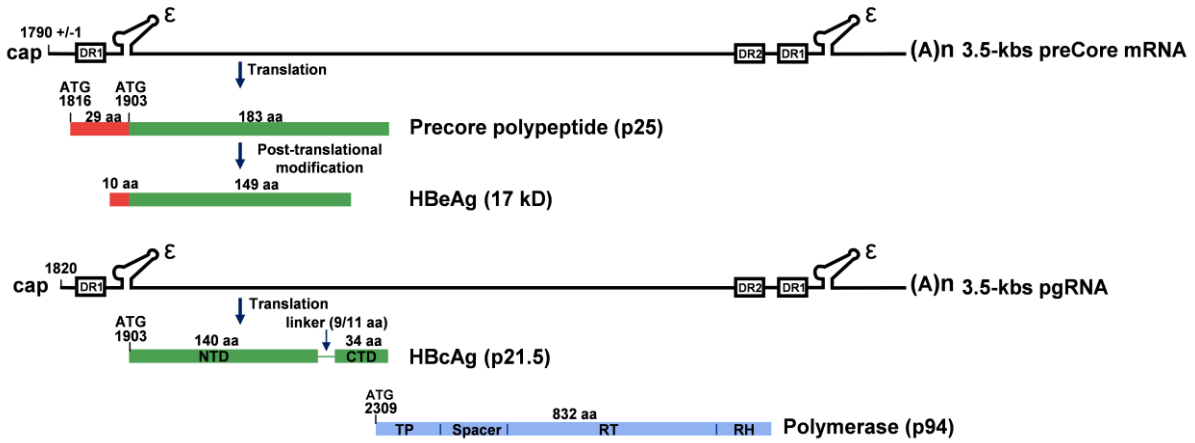

Figure 7. Schematic illustration of the HBV 3.5-kb precore mRNA and 3.5-kb pgRNA. The 3.5-kb precore mRNA transcribes a precore polypeptide, which is then post-transcriptionally modified to form HBeAg. HBeAg has an N-terminal extension of 10 amino acids (aa) and a C-terminal truncation of 34 aa as compared to HBcAg. 3.5-kb pgRNA transcribes HBcAg and HBV polymerase. In HBc, its N-terminal assembly structural domain (NTD) contains 140 aa and is sufficient for capsid self-assembly, the C-terminal arginine-rich structural domain (CTD) consists of 34 aa and is known to be critical for viral replication and mediating the pgRNA/RT encapsidation. HBV polymerase contains four domains, including an N terminal protein (TP) domain, a spacer domain, a reverse transcriptase (RT domain) domain, and a carboxy-end located RNase H (RH) domain.

1.2.5 Encapsulation and nucleocapsid assembly

The formation of progeny virions begins with the self-assembly of the icosahedral pgRNA-containing nucleocapsid, which requires the incorporation of pgRNA together with polymerase (P) into newly forming capsid (**Figure 5, step 7**). Encapsidation of pgRNA into the nucleocapsid initiates with the formation of ribonucleoprotein complex formation, in which the terminal protein (TP) domain [125] of the polymerase is recruited to the interior loop of the packaging signal epsilon (ε) near the 5' terminus of the pgRNA [126–128]. The ε forms a conserved stem-loop structure with an apical loop and two stems separated by an internal bulge (**Figure 7**). Both the internal bulge and the apical loop are required for the function of ε packaging RNA, and the internal bulge is also required for the formation of the pgRNA-P ribonucleoprotein complex [129–134]. The second ε copy existing at the 3' terminus of pgRNA (**Figure 7**) does not have any role in encapsulation or rcDNA synthesis [135]. The cap structure at the 5' terminus of the pgRNA and additional host factors like Hsp90, Hsp70 also appear to be involved in this encapsidation process [129, 136, 137].

The specific pgRNA-P ribonucleoprotein complex triggers the assembly of nucleocapsid, but also initiates the reverse transcription of rcDNA. HBc subunits are recruited to initiate nucleocapsid assembly, and meanwhile, the nucleocapsid acts as a replication compartment where pgRNA is reverse transcribed into rcDNA. The core protein has 183 or 185 aa, according to the genotype [138], and has two separate domains connected by a linker consisting of 9 or 11 aa (**Figure 7**). The first N-terminal assembly domain (NTD) contains 140 aa, which is sufficient for self-assembly of the capsid shell [34, 139]. The C-terminal arginine-rich domain (CTD) consists of 34 aa and is considered critical for viral replication and mediating pgRNA/P encapsidation [34]. Deficiency of the CTD of HBc suppresses the encapsidation of pgRNA-P [140].

Once translated, the core protein is rapidly dimerized by the disulfide-bridge (SS-bond) between the 61-cysteine residue [141–143]. But the current studies also suggest that the dimerization of core proteins is caused by hydrophobic and electrostatic interactions [144]. The dimers start to aggregate and form capsid after reaching a certain threshold concentration [141, 142], hydrophobic interactions are considered to be the main driving force for this assembly [145, 146]. The HBc can either self-assemble into empty icosahedral capsid, 30 nm or 35 nm in diameter, or package viral pgRNA-P to form nucleocapsids. It is not clear how the pgRNA-P complex is recognized by the assembled HBc dimer. Studies have found that strategically dynamic phosphorylation/dephosphorylation in the CTD structural domain permits selective packaging of the pgRNA/polymerase complex [147, 148]. The arginine rich CTD of core protein is intrinsically active in RNA binding (non-specific). Phosphorylation of all sites of the CTD (hyperphosphorylation) can inhibit its ability to bind RNA, while one or more latter dephosphorylation events facilitate the specific packaging of pgRNA-P complex [149, 150]. Meanwhile, it has also been reported that specific motifs of pgRNA interact with the CTD of core protein (sequence-specific interactions) to facilitate the assembly of nucleocapsid [151].

1.2.6 rcDNA synthesis/nucleocapsids maturation

The process of reverse transcription of pgRNA into rcDNA is also defined as nucleocapsids maturation (**Figure 5, step 8**). Since initiation of rcDNA synthesis does not require HBc proteins, this process can take place before, during or after the assembly of nucleocapsids [152]. The HBV polymerase (P) has 4 domains (**Figure 7**), and except for the spacer domain, the other 3 functional domains play key roles in rcDNA synthesis [153]. As previously mentioned, the TP domain at the amino-end, which initiates the encapsidation of pgRNA; the reverse transcriptase (RT) domain, which contains the polymerase activity; and the carboxy-end located RNase H (RH) domain, is essential for degradation of pgRNA.

The initiation of viral minus-strand DNA occurs through a unique protein priming mechanism. When the TP domain binds to the interior loop of the ε near the 5' terminus of the pgRNA, the sequence 5'-UUCA-3' on the interior loop acts as a template to synthesize a short DNA primer 5'-TGAA-3', which is able to covalently link to the TP domain via a phosphodiester bond between the dGTP residue and the hydroxyl group of the tyrosine residue at position 63 in the TP domain [132, 154–157] (**Figure 8A**). To proceed with DNA synthesis, the produced P-primer complex is next translocated to the direct repeat 1 (DR1) sequence at the 3' end of pgRNA, where it base-pairs to a complementary sequence located in DR1 [154, 157, 158] (**Figure 8A**). It was found that two elements, ϕ and ω, play a role in translocating the P-primer complex to the correct position [159, 160]. After translocation, the minus-strand DNA is synthesized by reverse transcription as progressing toward the 5' end of the pgRNA and a terminal redundancy of about 10 nucleotides is formed at its end (**Figure 8B**). This terminal redundancy (r) has been found to facilitate the synthesis of plus-stranded DNA and the circularization of the viral genome [16, 161]. Meanwhile, the pgRNA template is degraded by the HBV polymerase RH domain, except for its capped 5' terminal DR1 region [162] (**Figure 8B**). Then, this undegraded RNA sequence is transferred to the 5' terminal of the newly synthesized minus-strand DNA by base-pairing with the complementary sequences located in DR2 [163] (**Figure 8C**). This translocation prompts the circularization of the viral genome. Following the translocation, synthesis of the plus-strand DNA then proceeds to the terminal redundancy (r) at 5' terminal of the minus-strand DNA (**Figure 8D**). Afterwards, the 3' terminal of the nascent plus-strand anneals to the terminal redundancy (r) at the 3' terminal of the minus-strand DNA (**Figure 8E**), thereby using the 3' terminal of the minus-strand DNA as a template to proceed toward the 5' terminal of the minus-strand DNA to synthesize the plus-strand and form rcDNA (**Figure 8F**) [164, 165]. Synthesis of the plus-strand stops after the nucleocapsid is enveloped via budding into the multivesicular bodies. At this point the nucleotide reservoir within the nucleocapsid is depleted, leaving an incomplete plus-strand DNA, this gives the HBV genome a partially double-stranded relaxed circular property [166, 167].

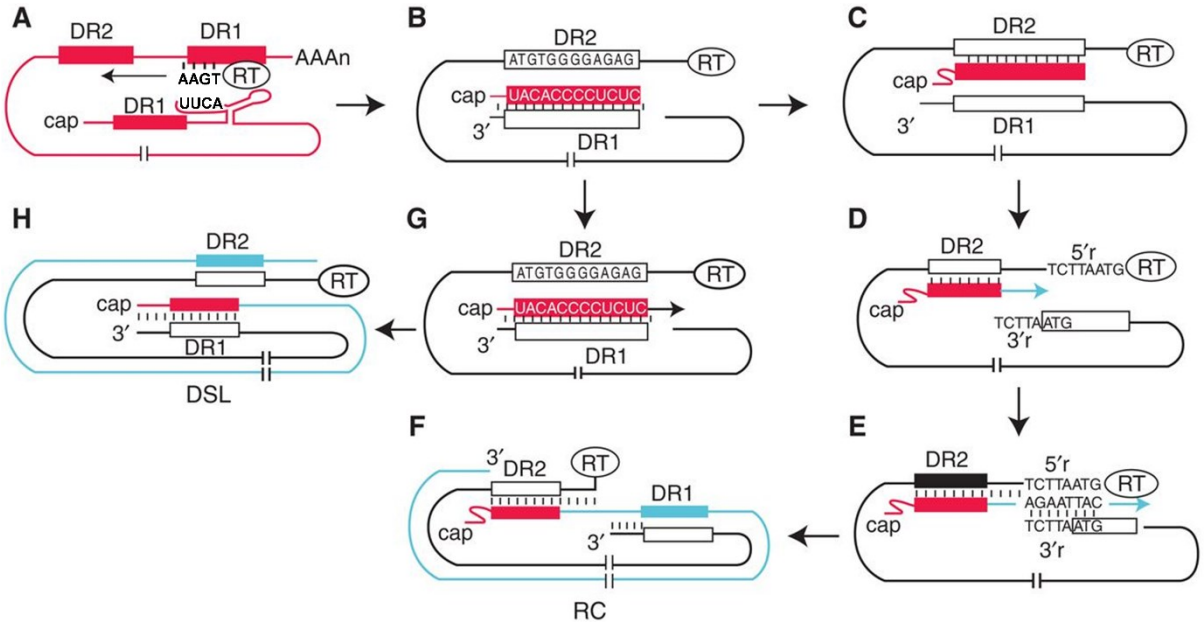

Figure 8. Schematic illustration of the formation of rcDNA and double-stranded linear DNA (dslDNA) from pgRNA. (A) The TP domain of HBV polymerase is recruited to the ε near the 5' terminus of pgRNA, the DNA primer from ε is transferred to DR1 at the 3′ end of pgRNA. **(B)** Minus-strand DNA is synthesized and the pgRNA template is degraded except for its capped 5' terminal DR1 region. **(C)** In the second translocation, the undegraded RNA sequence is base-paired with the complementary sequences located in DR2 of the minus-strand. **(D)** Synthesis of plus-strand DNA to the 5' terminus of minus-strand DNA. **(E)** The third translocation, the template of synthesis nascent plus-strand DNA switches to the 3′ end of negative-strand DNA, resulting in circularization of the genome. **(F)** Synthesis of the plus-strand DNA. **(G)** No second translocation and in situ priming of plus-strand DNA. **(H)** Formation of double-stranded linear DNA (dslDNA). Image retrieved and modified from [135].

In the case of the second translocation failing to occur, the caped RNA primer derived from the 5' terminal of the pgRNA could move along the 3' end of the minus-strand DNA (**Figure 8G**), thus synthesizing the plus-DNA (in situ priming) and eventually forming a double-stranded linear DNA (dslDNA) in the mature nucleocapsid [167] (**Figure 8H**). This dslDNA is a minor form of the genomic DNA and occurs at a frequency of approximately 5%-20% relative to the rcDNA formed by translocation event [168, 169]. The dslDNA could be integrated into the host chromosomes by nonhomologous recombination, which can occur in the early stages during acute infection or accumulate gradually during the chronic infection [168, 170, 171]. Since it cannot transcribe viral pgRNA, the integrated dslDNA is unable to contribute to viral replication, but it can synthesize viral proteins [152]. It has been shown to have oncogenic potential by activating host cell genes and producing truncated surface proteins [152, 172].

1.2.7 Nuclear Recycling of rcDNA and cccDNA amplification

To complete the viral life cycle, the progeny nucleocapsid containing the viral genome is either assembled into an enveloped virus to be released or, alternatively, is re-transported to

the nucleus to amplify and maintain the cccDNA reservoir (**Figure 5, step 9**). It has been shown that viral LHBs directly regulate this recycling of the nucleocapsid through a negative feedback mechanism [173, 174]. In the early phases of infection, the levels of LHBs are low and the progeny nucleocapsids are re-delivered to the nucleus, resulting in the formation of more cccDNA. Subsequently, more LHBs produced in the cytoplasm during infection due to increased cccDNA levels block this recycling pathway and inhibit cccDNA amplification, the maturing nucleocapsids are released from the cell after acquiring their viral envelope. It was also found that mature rcDNA-containing nucleocapsids are unstable (destabilization) as compared to immature ones, which could facilitate the uncoating of mature nucleocapsids and release of rcDNA into the nucleus, thus promoting the formation of cccDNA [175, 176].

1.2.8 Nucleocapsids envelopment and secretion of virions and subviral particles

To release the Dane particles, the rcDNA-containing mature nucleocapsids need to be encapsulated by the viral envelope (**Figure 5, step 10**). Many enveloped and non-enveloped viruses are known to complete their replication cycle either directly or by formation of vesicles budding from the host plasma membrane. The current study reveals that HBV envelope proteins are being trafficked out of the ER/Golgi complex to the endosomal system and ultimately to multivesicular bodies (MVBs) with the involvement of host factors, like ɣ2-adaptin, Rab GTPase and Rab33B [90, 177, 178]. The autophagic pathway probably also facilitates this trafficking [179, 180]. The LHBs, with their preS1+preS2 domain disposing in the topology to the cytosolic side (corresponding to the virion inside, i-preS), and the cytosolic loop between TM1 and TM2 of SHBs can thereafter interact with the mature nucleocapsids [53, 55, 181–183]. This interaction prompts a tight arrangement of envelope proteins at the membrane of MVBs and drives the process of inward budding [184]. It was found that α-taxilin could be involved in the recruitment of capsid to LHBs through interaction with LHBs and ESCRT I component tumor susceptibility gene 101 (Tsg101) [185]. Subsequently, the infectious viruses bud into MVBs during membrane fission, and afterwards exit the host cell via the exosome release pathway when the membrane of the MVBs fuses with the cell membrane (**Figure 5, step 11**). The endosomal sorting complex required for transport (ESCRT) machinery, ɣ2-adaptin, Nedd4, Vps4, CHMP3/4, and α-taxilin are all utilized by virus involved in regulating this secretion process [177, 185–188].

In addition to Dane particles, the DNA-free empty virions (enveloped capsids without viral genome or pgRNA inside) and RNA-containing particles (enveloped capsids with HBV RNA or pgRNA inside) are probably released in a MVBs-dependent manner [184]. Also, it was shown that the subviral particle, filament, is being released through the MVB/ESCRT pathway like infectious viral particles [189], whereas the spheres are secreted via a distinctly different pathway, the constitutive secretory pathway [190–193] (**Figure 5, step 12**).

Furthermore, the release of naked capsids in HBV-replicating cells is thought to be mediated by an ESCRT independent mechanism [188, 194]. The detailed mechanism of this pathway has not yet been elucidated, Alix (apoptosis-linked gene-2 (ALG-2)-interacting protein X) and hepatocyte growth factor-regulated tyrosine kinase substrate (HRS, also known as HGS) were found to be involved in mediating this release [194, 195].

1.3 Exosomes in virus infection

1.3.1 Exosome biogenesis and function

Besides viral particles, the host cells also release a large number of extracellular vesicles at the same time, exosomes are one sub-type of these lipid bilayer-enclosed vesicles with a size range of ~30 to 150 nm and share the same budding pathway with many virions [196]. Concretely, internalized cargoes are sorted into intraluminal vesicles (ILVs) that are formed by inward budding inside an intracellular endosome, this causes the appearance of late endosomes and is known as MVBs [197] (**Figure 9, step 4, 5**). The fate of ILVs can be degraded if MVBs mature into lysosomes [197]. Alternatively, MVBs could then fuse with the plasma membrane, which allows the release of their ILVs to the extracellular milieu as exosomes [197] (**Figure 9, step 6-8**). Thus, unlike the formation of microvesicles (100-1000 nm) through outward budding from the plasma membranes [198], exosomes are generated by the exocytosis of MVBs carried with ILVs. Cells from many types have been shown to release exosomes into the extracellular environment, and they can also be detected in a variety of body fluids, including plasma, saliva, and urine [199, 200].

Once released, the property of being a multi-component transport unit makes exosome-associated bioactive material functionally transferable from one cell to another. The entry strategies utilized by exosomes depend on the distribution of proteins and lipids on both the membrane of exosome and the target cell [201]. Uptake of exosomes seems to be mediated by endocytosis or membrane fusion, which partially overlaps with the entry pathways of some viruses [201, 202]. The content carried by exosomes can be released directly into the cytosol of recipient cells upon fusion, or it can travel with exosomes into the endosomal recycling system to be transported to the endoplasmic reticulum, or to the nucleus, or targeted to lysosomes to be degraded. Exosomes are now considered as an additional carrier for local or distant intercellular communication, this kind of exosome-mediated transmission plays important roles in various physiological events [203, 204].

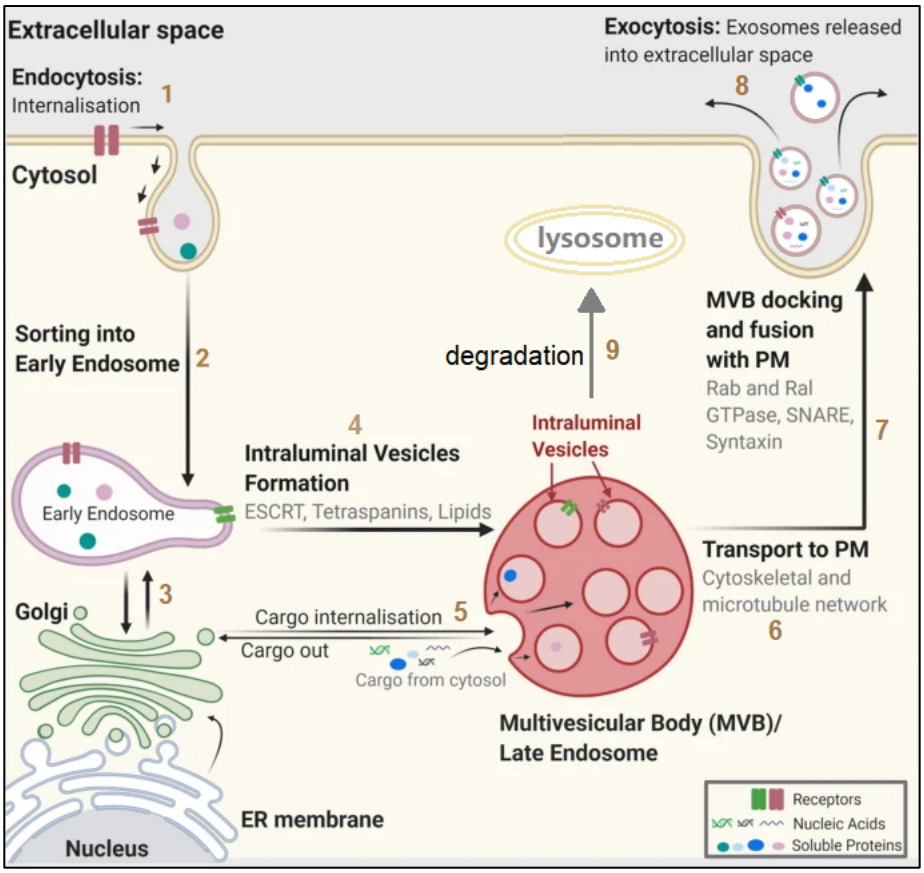

Figure 9. Exosome biogenesis. (1-3) Early endosome is maintained by the continual fusion of vesicles formed by invagination of the plasma membrane (PM) and budding from the trans-Golgi network. **(4-5)** Early endosome matures into multivesicular body (MVB)/late endosomes, where intraluminal vesicles (ILVs) are formed by inward budding of the limiting endosomal membrane. **(6-8)** MVBs release ILVs into extracellular space by fusion with the PM, namely the release of exosomes. **(9)** Alternatively, MVBs are degraded by being fused with lysosomes/autophagosomes. Image retrieved and modified from [201].

Several sorting machineries are engaged in the discrete steps needed to generate exosomes. It is now clear that different types of secreted exosomes co-exist (heterogeneity), this is probably due to the presence of different modes of regulating the formation of exosomes. The currently considered mechanisms are mainly divided into ESCRT-dependent and independent.

In the ESCRT-dependent system, internalized cargo is recruited and clustered to the budding site of endosome by ESCRT-0 complex in an ubiquitination-dependent manner [205] (**Figure 10A**). The two subunits of ESCRT-0 (HRS and signal transducing adaptor molecule 1/2 (STAM1/2) in mammals) interact as a 1:1 heterodimer [206], recognizing cargoes through its multiple ubiquitin-binding domains and reaching the phosphatidylinositol-3-phosphate (PI3P) enriched endosomal membrane via the FYVE domain of HRS [207, 208]. Through the interaction of PSAP domains of HRS with the ESCRT-I subunit Tsg101, ESCRT-0 also recruits ESCRT-I complex [209] (**Figure 10A**). In mammalian cells, ESCRT-I is composed of

Tsg101, vacuolar protein-sorting-associated protein (VPS) 28, VPS37 (VPS37A, B, and C), and MVB12 (MVB12A and B) subunits in a heterotetramer with a length of 20 nm [210–212]. Subsequently, ESCRT-I along with another Y-shaped heterotetramer, ESCRT-II, appear to function as a 1:1 supercomplex to facilitate the inward budding of the limiting endosomal membrane to shape the initial bud [212–214] (**Figure 10A**). The subunits EAP30 (VPS22), EAP45 (VPS36) and EAP20 (VPS25) form ESCRT-II in 1:1:2 [215–217]. ESCRT-III begins to be recruited after high-affinity binding of charged multivesicular body proteins-6 (CHMP6) to the ESCRT-II subunit EAP20 (VPS25) [217] (**Figure 10A**). The proteins that constitute ESCRT-III in mammals include CHMP6, CHMP4A-4C, CHMP3, CHMP2A-2B, which do not form stable complexes [218]. When ESCRT-III subunits, mainly CHMP4, aggregate around the neck of the bud to form a loop, after the incorporation of CHMP3, the bud is cleaved to form ILV into MVBs (**Figure 10A**). Then, after completing its scission function, ESCRT-III is disassembled in an ATP-driven reaction catalyzed by Vps4-Vta1 complex (accessory ESCRT protein), after which it moves to the next cycle [219–221] (**Figure 10A**).

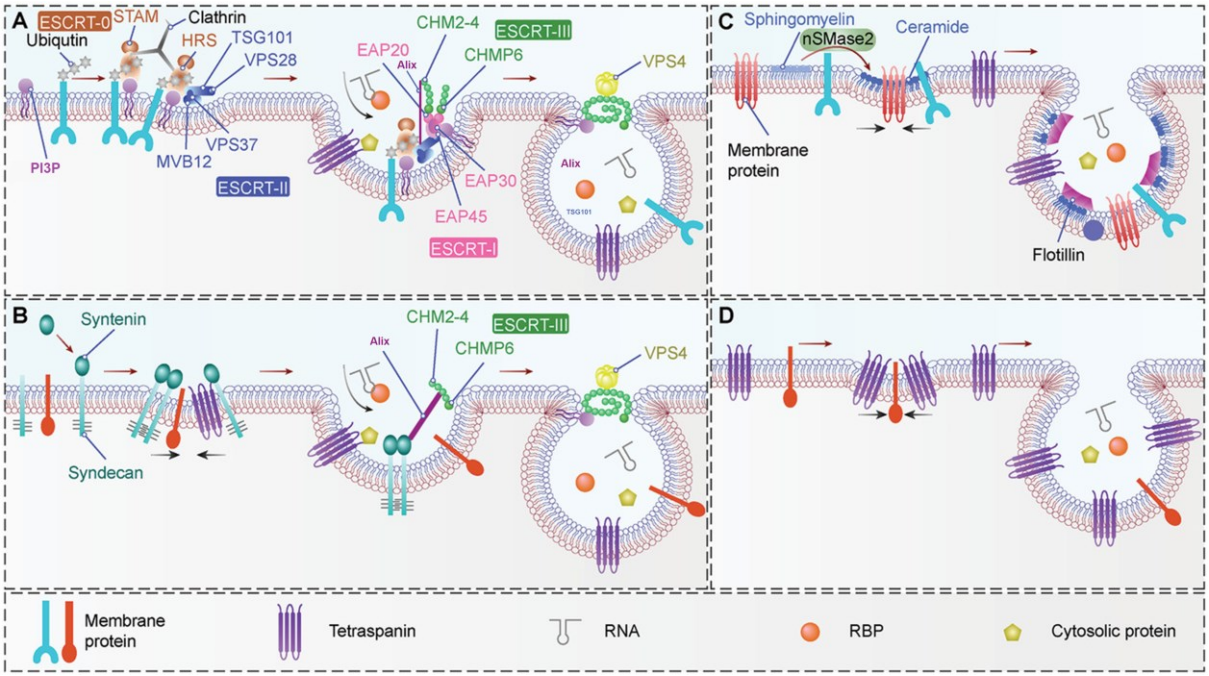

Figure 10. Generation mechanism of ILVs (exosomes) in MVB. (A) ESCRT mediated canonical pathway. Ubiquitinated cargoes is recognized by ESCRT-0 and recruited to the endosomal membrane by binding with phosphatidylinositol 3-phosphate (PI3P). Subsequent clustering into microdomains by binding of ESCRT-0 to clathrin. Then ESCRT-0 recruits ESCRT-I and ESCRT-II is recruited by ESCRT-I. ESCRT-I along with ESCRT-II facilitate the inward budding of the limiting endosomal membrane to shape the initial bud. Following the aggregation of ESCRT-III subunits in the neck of the bud forming a loop, the bud is cleaved to form ILVs into MVBs. Alix can stabilize the assembly of ESCRT and bind to the subunit Tsg101 of ESCRT-I. **(B)** Syndecan-syntenin-Alix-driven membrane budding and cargo clustering, ESCRT-III and Vps4-dependent ILV formation model. **(C)** Ceramide triggers budding of ILVs into MVBs. Phosphatidic acid (PA) induced budding is like this. **(D)** Tetraspanins cluster in the microdomains of endosomal membrane and trigger inward budding of ILVs into MVBs. Image retrieved and modified from [222].

Alix (ALG-2-interacting protein X), as another accessory ESCRT protein, being recruited by CHMP4B through its Bro1 domain [223], stabilizes the assembly of ESCRT-III [201, 224] and has a prominent role in facilitating the formation of ILV during budding and abscission (**Figure 10B**). The proline-rich domain (PRD) of ALIX also contains multiple sites that bind to the ubiquitin E2 variant (UEV) domain of the ESCRT-I subunit Tsg101 [225]. In addition, Alix functions as an ubiquitin receptor for sorting cargo into ILVs and MVBs through the ubiquitin binding domains of its central V structural domain [226, 227]. Recently, syntenin and syndecans have also been shown to be involved in ESCRT-III-dependent, but ubiquitin- and ESCRT-0-independent, exosome formation. Syntenin interacts directly with Alix via the LYPX(n)L motifs and with Syndecans (single transmembrane domain protein) to drive the inward curvature of endosomal membranes [228, 229] (**Figure 10B**). E3 ubiquitin-protein ligase NEDD4 and Nedd4 family interacting protein 1 (Ndfip1) were also found to be involved in regulating the levels of ubiquitinated and total protein in exosomes [230].

Along with the ESCRT-dependent processes, lipid rafts, tetraspanins and other protein-related pathways are also involved in the generation of exosomes. The lipid rafts dependent exosome formation is cell type dependent. The type of exosome carrying proteolipid proteins requires ceramide to induce inward curvature at the limiting MVBs membrane to form ILVs, the ceramide is converted from sphingomyelin by sphingomyelinase enzymes [231] (**Figure 10C**). Phospholipase D2 (PLD2), by participating in the hydrolysis of phosphatidylcholine to phosphatidic acid (PA), is required for the biogenesis of exosomes in some cells [232]. Like ceramide, PLD2- and PA-rich exosomes are thought to form ILVs by promoting the inward budding of vesicles via PA [228, 233]. Endosomal cholesterol accumulation also potentiated the secretion of exosomes in a Flotillin-2-dependent manner [234]. Tetraspanins have four transmembrane domains and are highly enriched in exosomes, among them CD63, CD81 and CD9 are often used as specific markers of exosomes. By interacting with other related proteins, tetraspanins cluster in the microdomains of endosomal membrane and perhaps trigger inward budding of endosomal membrane and the formation of exosomes through their cone-shaped conformation [235, 236] (**Figure 10D**). In addition, CD63 and CD81 have been shown to sort target proteins into ILVs [235, 237].

1.3.2 The role of exosome pathway on virus spread

Emerging evidence is revealing that exosomes play various roles in viral pathogenesis and transmission. The pathway of exosome formation overlaps significantly with the assembly of many viruses, as the host factors that regulate exosome generation are also employed for viral assembly. Meanwhile, encapsulating of viral components or even intact virions within exosomes facilitates the viral evasion from immunological surveillance and transmission intercellularly through the “free ride” of exosomes.

Most enveloped viruses acquire their outer lipid envelope and exit host cells by budding through the limiting plasma membrane [238]. But some, such as HBV, acquire their viral envelope by budding into the MVBs system as exosomes and are being released subsequently by membrane fusion [239–241]. In both cases, trafficking of the host ESCRT pathway is required to complete budding and fission steps. The traditional non-enveloped viruses have also recently been found with the ability to leave host cells in a non-lytically manner by utilising host vesicles [238, 242–248]. This requires them to access the endosomal system to acquire the host-derived lipid membrane.

Containing virus within vesicles of exosomal origin has been found in several viruses. Quasi-enveloped HAV viruses (picornaviruses) circulate in the blood as exosome-like vesicles were revealed recently which were presumed to assemble into exosomes and budded to MVBs via the YPX_nL motif in their VP2 capsid protein (and possibly also the pX protein) interacting with the central V domain of Alix [242]. The HEV particles were individually wrapped to exosome-like lipid membranes were also revealed by electron microscopy [243]. It is likely that the PSAP late domain motif situated in the ORF3 protein C-terminus interacts with the ESCRT-I subunit Tsg101 to bud HEV into MVBs [244–246]. HAV and HEV shed their host-acquired envelopes when passing through the biliary tract, producing more stable non-enveloped particles that are better adapted to the harsh environment [249]. HCV-RNA-containing exosomes derived from infected cells and plasma from infected patients are likely regulated by ESCRT-III component CHMP4B [250]. Moreover, vesicles cloaked rotaviruses and noroviruses clusters are shown to be highly virulent in transmission between organisms [251].

Thus, it is clear that many viruses hijack the host vesicle system by interacting with factors that mediate exosome formation, such as the ESCRT machinery, to complete self-assembly and dissemination. The late assembly domains [252, 253], conserved motifs (P(T/S)AP, YPX_nL/YXXL, and PPXY) in viral structural proteins, function by mimicking similar cellular interactions [238, 239]. Briefly, the P(T/S)AP motif recruits Tsg101 by binding directly to its N-terminal UEV domain [254], the YPX_nL late domain interacts with the central V domain of Alix [255], and the PPXY motif could bind WW domains as present in the E3 ubiquitin-protein ligase NEDD4 to utilize the MVBs pathway by ubiquitination [256–258]. Moreover, an non-canonical L-domain sequence, the FPIV structure, is also used by viruses for budding, which implies that some different components of the host ESCRT can be recognized and utilized by some viruses [259–261]. It is also interesting to note that, ubiquitin could sometimes relate to viral budding, functioning as a late domain [238]. Alix could also interact with viral proteins via the Bro1 domain [262–265], which lacks the YPX_nL late domlain binding activity, and NEDD4 family members could also stimulate the release of viral proteins that do not have the PPXY motif [266–270]. In spite of the fact that HBV is not a late assembly domain enriched

virus, it can complete its maturation and budding process by interacting with ESCRT-III, Vps4, γ2-adaptin, NEDD4, α-taxilin, Tsg101, and Alix [177, 185, 186, 194, 271, 272]. Meanwhile, the overlap with the exosome biogenesis, using MVBs as the release platform, raises the possibility for the release of exosomal HBV particles.

1.3.3 Methods for separating viruses and exosomes

A prerequisite for studying its characteristics is relying on practical methods to isolate highly purified exosomes. With the understanding of exosomes morphology, 6 commonly used and reliable methods have been derived (**Figure 11**). As the gold standard method for exosome isolation, differential ultracentrifugation (**Figure 11A**) has been applied to many pioneering studies [273]. The principle is that cells, cell debris and larger vesicles are first removed from the supernatant by several cycles of centrifugation with gradually increasing force (300 - 10,000 × g), and then the exosomes are obtained by centrifugation in speed spins at 100,000 - 200,000 × g for 70 min [274]. The method is easily extended to large-scale preparation, but it has low efficiency for viscous biological fluids. In addition, there are microsomes contaminations due to the ER membrane remaining in the supernatant is disrupted by centrifugation.Another common method is density gradient centrifugation (**Figure 11B**) based on media such as sucrose or iodixanol [275], and since it facilitates the separation of exosomes from larger vesicles, it is often used in combination with differential ultracentrifugation to help obtaining more pure exosomes [276]. The substances are effectively separated in this method by their differential sedimentation in gradients. Also, it was found that iodixanol-based density gradient centrifugation can separate exosomes and viruses, such as HIV particles [277, 278]. But this approach is time consuming and requires long running hours to reach equilibrium. Another size-based separation tool is size exclusion chromatography (**Figure 11C**), which is characterized by the ability to separate the majority of soluble components from exosomes [279]. Due to its mild conditions, no aggregation of exosomes is induced, and the structure and biological activity of exosomes are protected [280, 281]. The exclusion matrix is reproducible and customizable [282]. This method is also scalable, but the low resolution of similarly sized molecules will co-isolate to some contents and therefore is not suitable for the separation of viruses and exosomes.

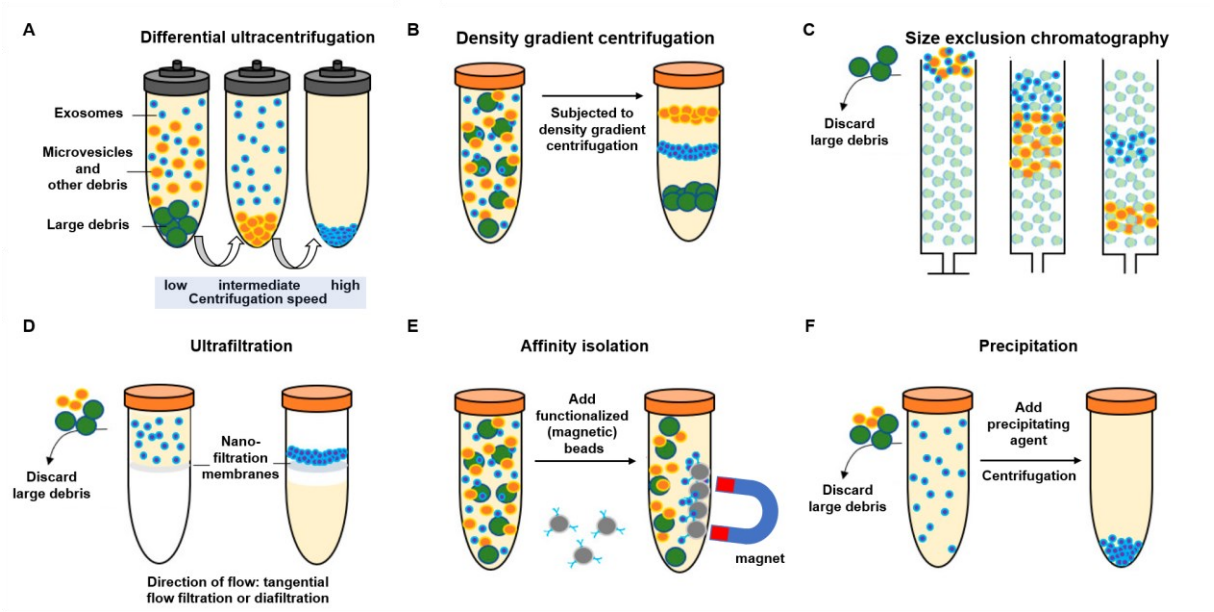

Figure 11. Commonly used methods for exosomes isolation. (A) Differential ultracentrifugation separation. **(B)** Density gradient centrifugation separation. **(C)** Size exclusion chromatography-based separation. **(D)** Ultrafiltration-based separation. **(E)** Immunoaffinity isolation. **(F)** Precipitation separation. Image retrieved and modified from [279].

Ultrafiltration-based separation offers the potential for industrial-scale preparation of exosomes and other extracellular vesicles (**Figure 11D**) [283]. By easily using nano-membranes of different pore diameters multiple times, exosomes can be separated from a large volume in a relatively shorter time [284, 285]. In addition to removing soluble proteins, this method also allows the exclusion of smaller size aggregates. Basically, ultrafiltration for the separation of exosomes by liquid flow direction is divided into tangential flow filtration and diafiltration [286]. While both can lose exosomes in varying degrees, diafiltration is more prone to membrane plugging and loss of morphology [287, 288]. Therefore, it is not favorable for small-scale volume exosome purification.

Immunoaffinity isolation is based on the strong binding affinity of antibodies to exosomal surface specific antigens resulting in highly specific and purified exosomes [283] (**Figure 11E**). It is suitable for small scale samples studies and often used in an additional step after differential ultracentrifugation to obtain purer exosomes. Also, it can isolate specific subsets of exosomes [275, 283]. But for the overall isolation of exosomes, it is necessary to target substances that are universally presented on the exosomal surface [283]. Besides, how to maintain the native state of exosomes during elution is the main issue to be considered [289].

The precipitation separation method is performed by changing the solubility or sedimentation rate of exosomes through incubation with agents, such as water-excluding polymers, then exosomes are enriched by low-speed centrifugation or filtration [279] (**Figure 11F**). This method is easy to perform and low in equipment demands, but the specificity is highly

questionable and unable to separate exosomes from lipoproteins, protein aggregates, and viruses.

For virus-related exosome isolation, samples are often enriched from large scale to reach the target detection threshold. Therefore, the first step of purification using differential ultracentrifugation, size exclusion chromatography, or ultrafiltration is particularly necessary. But, due to the extremely similar size, density and sedimentation rate of them, these preliminary methods co-isolate many viruses along with the exosomes. For this reason, to study their respective functions, a further step such as density gradient centrifugation or specific immunoaffinity isolation, depending on the situation, could help to efficiently separate each one of them.

2 Aim of this study

Over the past 50 years, fundamental principles of Hepatitis B virus (HBV) life cycle and morphogenesis have been revealed. Growing evidence demonstrates that the release of HBV virions as well as of filaments depends on the endosomal sorting complex required for transport (ESCRT) machinery and host membrane trafficking systems. To efficiently releasing from the host cell, multivesicular bodies (MVBs) are assumed to be the platform for HBV budding and egress, where mature nucleocapsid is encapsulated by the viral envelope and then escape from cells by means of exosomal release pathway as the MVBs fuse with the plasma membrane.

Exosomes have been increasingly shown to play multiple roles in viral pathogenesis and transmission. Cloaking viral components or even intact virions within exosomes facilitates viral evasion of immunological surveillance and spreads viruses intercellularly through the "free ride" of exosomes.

Therefore, the close intertwining of exosome biogenesis and HBV egress raises the hypothesis of this study as to whether intact HBV progeny viruses in HBV-producing cells can be released by being encapsulated in exosomes. If this hypothesis holds true, then, like the previously detected quasi-enveloped HAV and HEV viruses, HBV could usurp the pre-existing exosome biogenesis for its own assembly and propagation. This currently undiscovered type of HBV particle that utilizes the exosomal pathway to acquire a host membrane covering would blur the classical definition of HBV as an enveloped particle and potentially change the conventional understanding of the HBV life cycle.

3 Material

3.1 cells

3.1.1 Prokaryotic cells

Strain	Genotype	Source
E. coli DH5α Competent Cells	F⁻φ80*lac*ZΔM15 Δ(lacZYA-argF)U169 recA1 endA1 hsdR17(r_K^-, m_K^+) phoA supE44 λ⁻*thi*-1 gyrA96 relA1	Invitrogen, Karlsruhe

3.1.2 Eukaryotic cells

Strain	Description	Source
HepG2	Human Hepatoblastoma-derived cell line	Originally established in 1979 by Aden, D P et al [290]. The patent was filed in 1980 by researchers at the Wistar Institute in Philadelphia [291].
HepAD38	HepG2 derived cell line and can replicate HBV stably from a single integrated 1.1 copies of HBV genome under the control of the tetracycline responsive promoter (genotype D ayw serotype)	Established in 1997 by Ladner, S K et al [292].
HepAD38-Alix KO	Stable Alix knockout cell line generated by CRISPR/Cas9 system derived from HepAD38	Generated by this work
HepAD38-SDCBP KO	Stable SDCBP knockout cell line generated by CRISPR/Cas9 system derived from HepAD38	Generated by this work
HepAD38-NT	non-target HepAD38 cells from off-target sgRNA generated by CRISPR/Cas9 system	Generated by this work
HepaRG	Isolated from a hepatic tumor of a female patient with hepatocellular carcinoma and HCV infection, susceptibility to HBV after differentiation	Gripon, P et al [293]

3.2 Reagents for cell culture

Reagent	Manufacturer
RPMI-1640 Medium (R0883-500ML)	Sigma-Aldrich, Hamburg, Germany
DMEM (Dulbecco's Modified Eagle's Medium) (4.5 g/L glucose) (D6546-500ML)	Sigma-Aldrich, Hamburg, Germany
William's E growth medium (BS.F 1115)	Bio & Sell GmbH, Feucht, Germany
L-glutamine (BS.K 0283)	Bio & Sell GmbH, Feucht, Germany
Streptomycin	Paul-Ehrlich-Institut, Langen, Germany
Penicillin	Paul-Ehrlich-Institut, Langen, Germany
Trypsin/EDTA (0.05% Trypsin)	Paul-Ehrlich-Institut, Langen, Germany
Fetal bovine serum (FBS.S 0615)	Bio & Sell GmbH, Feucht, Germany
Hydrocortisone 21-hemisuccinate (sc-250130)	Santa Cruz Biotechnology, Heidelberg, Germany
Insulin (I6634-100MG)	Sigma-Aldrich, Hamburg, Germany
Dimethyl sulfoxide (DMSO) (M6323.0250)	Genaxxon, Biberach, Germany

3.3 Plasmids

Name	Description	Source
pJO19 plasmid	Containing 1.2-fold HBV genome (subtype ayw, genotype D)	Generated by J.Lupberger
pX459 (pSpCas9(BB)-2A-Puro V2.0) plasmid	Mammalian expression vector type; genome engineering used for CRISPR-Cas9 system; Cas9 from S. pyogenes with 2A-Puro; cloning backbone for sgRNA; suitable for puromycin selection	Addgene, #62988
pX459-hAlix-sgRNA	Plasmids for knockout of human Alix protein expression	Generated by this work
pX459-hSyntenin-sgRNA	Plasmids for knockout of human Syntenin protein expression	Generated by this work
mCherry-hALIX plasmid	containing human full-length Alix with its N-terminal in-frame mCherry fusion	Addgene, #21504

3.4 Oligonucleotides

Name	Gene ID (NCBI)	Sequence
HBV S-domain	944569	Forward: 5'-GCACCTGTATTCCCATCCCA-3' Reverse: 5'-CGAACCACTGAACAAATGGC-3'
Human-RPL27	6155	Forward: 5'-AAAGCTGTCATCGTGAAGAAC-3' Reverse: 5'-GCTGCTACTTTGCGGGGGTAG-3'
Human Alix sgRNA (target exon 8)	10015	5'-CGGGGTAGATTTCACAAGTG-3'
Human Syntenin sgRNA (target exon 7)	6386	5'-ACAGAATGTCATTGGATTGA-3'
non-target sgRNA	/	5'-GCACTACCAGAGCTAACTCA-3'
Sequencing of pX459 (CRISPR)	/	5'-ACTATCATATGCTTACCGTAAC-3'

3.5 Antibodies

3.5.1 Primary antibodies

Antibody	Species and clonality	Dilution	Manufacturer
Anti-human-Alix	Mouse, monoclonal	WB: 1:500	SantaCruz (sc-271975)
Anti-human-Tsg101	Mouse, monoclonal	WB: 1:300	SantaCruz (sc-7964)
Anti-human-CD63	Mouse, monoclonal	WB: 1:2000 Immunolabeling: 1:50 and 1:100	Abcam (ab59479)
Anti-human-syntenin	Rabbit, polyclonal	WB: 1:1000	Proteintech Europe (22399-1-AP)
Anti-human-β-Actin	Mouse, monoclonal	WB: 1:10,000	Sigma-Aldrich (A5316)
Anti-HBV-LHBs, MA18/7 [294]	Mouse, monoclonal	WB: 1:1000	kindly provided by Dr. Glebe Giessen
Anti-HBcAg, K46	Rabbit, polyclonal	WB: 1:5000	a gift from Reinhild Prange, Department of Medical Microbiology and Hygiene, Johannes Gutenberg-Universität Mainz, Mainz, Germany

Anti-HBV-LHBs preS1/preS2 domain, K112-4 (antiserum)	Rabbit, polyclonal	Immunolabeling: 1:50 and 1:100	Dr. Sami Akhras

3.5.2 Secondary antibodies

Antibody	Dilution	Manufacturer
Amershan ECL HRP-linked sheep anti-mouse IgG	WB: 1:3000	GE Healthcare (NA931-1ML)
Amershan ECL HRP-linked donkey anti-rabbit IgG	WB: 1:3000	GE Healthcare (NA934-1ML)
goat anti-mouse IgG conjugated with 10-nm gold	Immunolabeling: 1:50	BBI Solutions (EM.GMHL10)
goat anti-rabbit IgG conjugated with 5-nm gold	Immunolabeling: 1:50	BBI Solutions (EM.GAR5)

3.6 Enzymes and related buffers

Name	Manufacturer
RQ1 RNase-Free DNase	Promega GmbH (M610A)
RQ1 RNase 10 × reaction buffer	Promega GmbH (M198A)
Stop solution (for RQ1 DNase)	Promega GmbH (M199A)
T4-Polynucleotide kinase	New England Biolabs (M0201)
Bbs1 restriction endonuclease	New England Biolabs (R3539)
T7 DNA ligase	New England Biolabs (M0318)
10 × Tango buffer	Thermo Scientific™ (BY5)
10 × T4 DNA ligation reaction buffer	New England Biolabs (B0202S)

3.7 Chemicals

Name	Manufacturer
OptiPrep™ (Iodixanol, 60% (w/v))	ProgenBiotechnik (1114542)
D(+)-sucrose	Carl Roth (4621.2)
Nonidet P-40 (NP-40)	Fluka (74385)
Triton X-100	Sigma-Aldrich (T9284-500ML)
U18666A	Sigma-Aldrich (U3633-5MG)

Manumycin A (MA)	Cayman Chemical (52665-74-4)
GW4869	Sigma-Aldrich (D1692)
Dithiothreitol (DTT) solution (0.1 M)	Invitrogen (Y00147)
Adenosine-5'-triphosphate (ATP) solution (10 mM)	Invitrogen™ (AM8110G)
Ampicillin	Carl Roth (K029.2)
Kanamycin	Carl Roth (T832.2)
Puromycin	Sigma-Aldrich (P9620)
Polyethyleneimine	Polysciences (9002-98-6)
Phosphotungstic acid hydrate (PTA)	Sigma-Aldrich (P4006-100G)
Formaldehyde (FA) solution	Sigma-Aldrich (F8775-25ML)
Glutaraldehyde (EM grade)	Sigma-Aldrich (G5882)
Agarose	Sigma-Aldrich (A6877-25G)
Lonza SeaPlaque Agarose (Low gelling temperature agarose)	SeaPlaque™ (LZ50101)
Methylcellulose	Sigma-Aldrich (M7027-100G)
Uranyl acetate	Merck (8473)
Bovine Serum Albumin (BSA) Fraction V	Applichem (A1391, 0100)
Aprotinin (serine proteases inhibitor)	Applichem (A2132,0025)
Leupeptin hemisulfate salt (serine and cystein proteases inhibitor)	Applichem (A2183,0010)
Peptastin A (acidic proteases inhibitor)	Applichem (A2205,0010)
Phenylmethylsulfonyl fluoride (PMSF) (serine proteases inhibitor)	Applichem (APA0999.0005)
N,N,N',N'-Tetramethylethylenediamine (TEMED)	Applichem (APA1148.0100)
Rotiphorese Gel 40 (29:1)	Carl Roth (A515.1)
Ammonium peroxydisulphate (APS)	Carl Roth (9592.2)
Bromophenole blue sodium salt	Sigma-Aldrich (B8026)
Sodium dodecyl sulfate (SDS)	Carl Roth (CN30.3)
Skim milk powder	Carl Roth (T145.4)
Glycerol 99.5%	Gerbu Biotechnik GmbH (2006.1)

Tween-20	Carl Roth (9127)
ddH_2O containing 0.1% Diethyl pyrocarbonate (DEPC)	Paul-Ehrlich-Institut
EDTA 0.5 M (pH 8.0)	Paul-Ehrlich-Institut
Trichloromethane/Chloroform	Carl Roth (Y015.1)
Methanol (96% v/v)	Carl Roth
Isopropanol	Carl Roth
β-mercaptoethanol	Carl Roth (4227.1)
Ethanol (96% v/v, nondenatured)	Carl Roth

3.8 Reagents and Kits

Name	**Manufacturer**
Bradford reagent	Sigma-Aldrich (B6916-500ML)
BSA solution standard	New England Biolabs (B9000S)
CD63-coated Dynabeads™	Invitrogen (10606D)
DNA Gel Loading Dye (6 ×)	Thermo Scientific™ (R0611)
dNTP Mix (10 mM each)	Thermo Scientific™ (R0192)
Dynabeads™ M-280 Sheep Anti–Rabbit IgG	Invitrogen (11203D)
Enzygnost® HBsAg 6.0 ELISA kit	Siemens Healthcare GmbH (OPFM07(Q)
Enzygnost®/TMB	Siemens Healthcare GmbH (OUVP17)
Epoxy Embedding Medium kit	Sigma-Aldrich (45359-1EA-F)
FuGENE® HD Transfection Reagent	Promega (PRE2311)
GeneRuler 1 kb DNA Ladder	Thermo Scientific™ (SM0314)
Immobilon western Chemiluminescent HRP Substrate	Merck Millipore (WBKLS0100)
Maxima SYBR green qPCR kit	Thermo Scientific™ (K0221)
peqGold TriFast reagent	Peqlab Biotechnologie GmbH (30-2010P)
PrestoBlue™ Cell Viability Reagent	Invitrogen (A-13261)
PageRuler™ Prestained Protein Ladder	Thermo Scientific™ (26616)

QIAGEN Plasmid Maxi Kit	QIAGEN (12162)
QIAprep Spin Miniprep Kit	QIAGEN (12125)
QuickTiter™ HBV Core Antigen ELISA Kit	Cell Biolabs (VPK-150)
Random Hexamer Primer	Thermo Scientific™ (SO142)
RevertAid H Minus reverse transcriptase	Thermo Scientific™ (EP0451)

3.9 Buffers and solutions

Buffer	Composition
Lysogeny broth (LB) medium	1% Trypton (w/v) 1% Sodium chloride (w/v) 0.5% Yeast extract (w/v)
LB agar medium	1% Trypton (w/v) 1% Sodium chloride (w/v) 0.5% Yeast extract (w/v) 1.5%-2% Solid agar (w/v)
Phosphate Buffered Saline (PBS) without Mg^{2+} and Ca^{2+} (1 ×)	137 mM NaCl 2.7 mM KCl 8.1 mM Na_2HPO_4 pH 7.1
RIPA lysis buffer	50 mM Tris/HCl 150 mM NaCl 0.1% SDS (w/v) 1% Sdium deoxycholate (w/v) 1% Triton X-100 (v/v) pH 7.2
RIPA lysis buffer with protease inhibitors	10 µg/mL Aprotinin 1 mM PMSF 25 µg/mL Leupeptin 20 µg/mL Pepstatin 2.5 mM EDTA
SDS-running buffer (10 ×)	0.25 M Tris 2 M Gycine 1% SDS (w/v) pH 8.3
SDS-separating gel buffer	1.5 M Tris 0.4% SDS (w/v) pH 8.8
SDS-tacking gel buffer	0.5 M Tris 0.4% SDS (w/v) pH 6.7
Anode buffer I	20% Ethanol (v/v) 0.3 M Tris

Anode buffer II	20% Ethanol (v/v) 25 mM Tris
Cathode buffer	20% Ethanol (v/v) 40 mM 6-aminohexanoic acid
TBS-T (1 ×)	20 mM Tris 150 mM NaCl 0.05% Tween-20 (v/v) pH 7.8
TAE buffer (50 ×)	2 M Tris base 1 M NaAc 50 mM EDTA pH 8.0
PHEM buffer (1 ×)	60 mM PIPES 21 mM HEPES 10 mM EGTA 2 mM $MgCl_2$ 685 mM NaCl pH 7.5 (adjust with KOH)
2% (w/v) Methylcellulose	2 g methylcellulose in 100 mL ddH_2O, heat at 95°C until milky turbid, centrifuge for 1 h at 28,000 rpm, collecting the supernatant

3.10 Devices

Type	Device	Manufacturer
Centrifuge	Beckman Avanti® J-26 XPI Centrifuge	Beckman Coulter
	Heraeus Fresco 21R Refrigerated Microcentrifuge	Thermo Scientific™ Heraeus™
	Heraeus Multifuge 1S-R	Thermo Scientific™ Heraeus™
	Mini centrifuge ROTILABO®	Carl Roth
	Mini centrifuge ROTILABO® with butterfly rotor	Carl Roth
	Optima L-80 XP Ultracentrifuge	Beckman Coulter
	Optima™ Max XP Ultracentrifuge	Beckman Coulter
	Optima XPN-80 Ultracentrifuge	Beckman Coulter
Centrifuge rotor	JA25.50	Beckman Coulter
	SW32-Ti	Beckman Coulter
	SW41-Ti	Beckman Coulter

	TLS-55	Beckman Coulter
PCR cycler	LightCycler® 480 Instrument II	Roche
	Mastercycler® gradient	Eppendorf
	Thermal cycler	VWR International
Electrophoresis and blotting system	Electrophoresis power supply EPS 301	GE Healthcare
	HE33 Mini Horizontal Agarose Electrophoresis Unit	Hoefer
	Mighty small multiple gel caster SE 200	Hoefer
	SE250 Mighty Small II Mini Vertical Protein Electrophoresis Unit	Hoefer
	Standard power pack P25	Biometra
	TE77 PWR semi dry transfer unit	GE Healthcare
Microscopy	Axiovert 40C	Carl Zeiss AG
	EM-109 Transmission Electron Microscope	Carl Zeiss AG
	Jeol JEM-1400 Transmission Electron Microscope	Jeol Ltd
Sectioning system	Cryo-Ultramicrotome EM FC7	Leica
	Ultracut FC4E Ultramicrotome	Reichert-Jung
Imaging system	AGFA Curix60 film developer	AGFA
	Hypercassette™	Amersham
	ImageQuant800™ system	Cytiva Europe GmbH
	INTAS imaging system (gel documentation)	INTAS
	LI-COR Odyssey imaging system	LI-COR
Other devices	BBD 6220 CO_2 Incubator	Thermo Scientific™ Heraeus™
	BINDER™ Series B Standard Incubator	BINDER™
	Hemocytometer	Carl Roth
	IKAMAG® universal hot plate magnetic stirrer	IKA
	Infinite® M1000 Microplate Reader	Tecan
	Innova® 44/44R Incubator Shaker	New Brunswick Scientific
	MagRack™ 6 (Magnetic Rack)	Cytiva

NanoDrop™ One^{C} Microvolume UV-Vis Spectrophotometer	Thermo Scientific™
NanoSight NS300 instrument	Malvern Panalytical
PELCO easiGlow™ Glow Discharge Cleaning System	TED PELLA, INC.
Pipettes	Eppendorf
Pipette Controller	BrandTech™ accu-jet™
Refractometer	Bausch & Lomb
Satorius Cubis® Precision Balances MCE2202S	Satorius
Shakers and Mixers Promax 1020	Heidolph
Sonopuls HD 2200 ultrasone homogenisator	Bandelin/Sonorex
SterilGARD III Advance biological safety cabinet	The Baker Company
Stuart® roller mixer SRT9	Bibby Scientific Limited
S20-SevenEasy™ pH	Mettler Toledo
Thermomixer Comfort	Eppendorf
Vortex-Genie™ 2	Scientific Industries
Captair® Smart ductless fume hood	Erlab
Water bath 1228-2F	VWR International

3.11 Softwares

Software	Manufacturer
Citavi 5	Swiss Academic Software
GraphPad Prism 9.2.0	GraphPad Software
ImageQuant™ TL	Cytiva Europe GmbH
Image Studio Lite	LI-COR Biosciences
LightCycler® 480 Software version 1.5	Roche
MS Office	Microsoft
NTA 3.3 software	Malvern Panalytical

Photoshop CS6	Adobe
TECAN iControl	Tecan
iTEM	OLYMPUS
Vector NTI Advance 11.5	Thermo Scientific™

3.12 Consumables

Consumable	**Manufacturer**
Cell culture flasks (T25, T75, T175)	Greiner bio-one
Cell culture plates (6, 12, 96 wells)	Greiner bio-one
Cytiva Amersham™ Hyperfilm™ ECL	Amersham (28-9068-37)
Developer type E 1-3	C & L GmbH (ADE38)
Falcon tubes (15 mL, 50 mL)	Greiner bio-one
Filtered pipette tips (10 µL, 100 µL, 1mL)	Sarstedt
Fixer type F 1-2	C & L GmbH (ADF38)
Formvar/carbon-coated Nickel 200-mesh grids	Plano GmbH (S162N)
LightCycler® 480 Multiwell plate 96	Roche (04729692001)
5Prime Phase lock gel heavy, 2 ml	QuantaBio (2302830)
Pipette tips (10 µL, 100 µL, 1mL)	Sarstedt
polypropylene ultracentrifuge tube	Beckman (331372), (326823)
polyvinylidene difluoride membrane (PVDF)	Carl Roth (P667.1)
RotiLabo® syringe filters (0.22 / 0.45µm)	Carl Roth
Safe-Lock micro test tubes	Sarstedt
Serological pipettes (1, 5, 10, 25 mL)	Greiner bio-one
Whatman filter papers, D=32 mm, Grade 1	GE Healthcare (1001-032)

4 Methods

4.1 General cell culture

HepG2 cells were cultivated in RPMI-1640 Medium supplemented with 2 mM L-glutamine, 100 µg/mL streptomycin, 100 IU/mL penicillin and 10% (v/v) fetal bovine serum.

HepAD38 cells and all knockout cell lines generated based on HepAD 38 cells were maintained in DMEM supplemented with 2 mM L-glutamine, 100 µg/mL streptomycin, 100 IU/mL penicillin and 10% (v/v) fetal bovine serum, and with 50 µM hydrocortisone 21-hemisuccinate and 5 µg/mL insulin in addition.

HepaRG cells were seeded in 6-well plates with a cell density of 3×10^5 cells/well and cultivated for 2 weeks in growth medium with medium changes every 2 to 3 days, the growth medium is composed of William's E growth medium supplemented with 2 mM L-glutamine, 100 µg/mL streptomycin, 100 IU/mL penicillin, 10% (v/v) fetal bovine serum, 50 µM hydrocortisone 21-hemisuccinate and 5 µg/mL insulin. After this, these HepaRG cells were cultivated in differentiation medium for 2 more weeks, also with medium changes every 2 to 3 days. The differentiation medium was constituted by the addition of 2% (v/v) DMSO to the growth medium. After two weeks of differentiation, HepaRG cells are susceptible and available for HBV infection experiments. The above cells all grew at 37°C, 95% humidity and 5% atmospheric CO_2.

4.2 Exosome isolation

4.2.1 Differential ultracentrifugation-based isolation

To purify sufficient exosomes for detection, HepG2 cells or HepAD38 cells were cultivated at density of 25×10^6 in T175 cell culture flasks with 30 mL media for 3 - 4 days. Subsequently, exosomes were isolated from these cell culture supernatants by differential ultracentrifugation according to the established method [274] with some modifications. The detailed steps were as follows: from 30 - 35 mL of supernatant was first removed the cell debris, shedding vesicles and apoptotic bodies by centrifugation at 10,000 × g for 40 minutes using a SW 32 rotor. Then, the supernatant was proceeded to ultracentrifugation at 100,000 × g for 70 minutes to pellet the exosomes and 1 mL PBS was used to resuspend the exosomal pellet.

4.2.2 Density gradient ultracentrifugation-based isolation

The exosomes obtained by ultracentrifugation were further purified by discontinuous density gradient ultracentrifugation. A six-layer gradient, consisting of 1.5 mL of 10%, 20%, 30%, 40%, 50% and 60% (w/v) iodixanol or sucrose solution from up to low, was established in a

13 mL polypropylene ultracentrifuge tube, and 1 mL of resuspended exosomes was gently overlaid onto the uppermost layer of the gradient solution. The 10%-50% iodixanol or sucrose solutions were prepared by diluting 60% (w/v) iodixanol or 60% (w/v) sucrose/PBS stock solutions with PBS. The gradient samples were further centrifuged at 125,000 × g for at least 18 hours at 4°C with SW 41 rotor for separation. After centrifugation, the samples were fractionated from top to bottom with 0.5 mL fractions. An OptimaTM XPN-80 ultracentrifuge or was used for all centrifugation procedures at 4°C. The distribution of exosome markers, viral genomic DNA, HBsAg, HBcAg in the gradient was further analyzed by western blot, qRT-PCR and ELISA. The refractive index of each fraction was assessed using a refractometer and converted to density according to the instructions provided by the supplier of Iodixanol.

4.2.3 CD63-coated magnetic beads-based immunoaffinity isolation

Exosome fractions from the iodixanol gradient were further incubated with Dynabeads™ coated with CD63 or unassociated Dynabeads™ M-280 sheep anti-rabbit IgG and mixed at 4°C for 18 to 22 hours. The next day, the Dynabeads™ conjugated samples were washed at least four times with isolation buffer under a magnetic rack and eventually suspended with an appropriate amount of isolation buffer. The isolation buffer was PBS containing 0.1% (w/v) BSA, filtered through a 0.22 μm filter. Afterwards, the exosomes on magnetic beads were ready for western blot analysis after protein denaturation by boiling with 4 × SDS-loading buffer at 95°C for 10 minutes.

4.3 Size and morphology analysis of exosomes

4.3.1 Nanoparticle tracking analysis (NTA)

The NTA method provides a quick measurement of the size distribution and concentration of vesicles in liquid suspension [295]. It uses light scattering to capture each particle in suspension under Brownian motion and calculates the hydrodynamic diameter of each particle using the Stokes-Einstein equation. Here, the exosome pellet derived from the supernatant of HepAD38 or HepG2 cells was diluted to the appropriate concentration in filtered PBS (0.22 μm filter membrane) and then was slowly and uniformly pushed through a syringe into the laser chamber. A 60-second video of the Brownian motion of exosomes in suspension was recorded using the NanoSight NS300 instrument according to the manufacturer's instructions four times. Data were automatically analyzed with the NTA 3.3 software with a detection threshold of 5.

4.3.2 Whole-mount exosome negative staining

Whole-mount exosome morphology was visualized by transmission electron microscopy. Negative staining with 1% (w/v) phosphotungstic acid (PTA)/ddH_2O was prepared as described in a published protocol [274]. Briefly, a drop of 20 µL of 4% (v/v) formaldehyde/ddH_2O fixed exosome was immobilized with carbon-coated, glow-discharged formvar grid for 20 minutes at room temperature (RT). After two washing steps with 100 µL ddH_2O, grids were stained with 1% PTA for 10 seconds at RT and air-dried. Grids by negative staining were analyzed using a Zeiss EM-109 or Jeol JEM-1400 transmission electron microscope.

4.4 Western blot analysis

4.4.1 Sample preparation and bradford assay

To lyse the proteins from the cells, the culture media were aspirated, and cells were washed twice with cold PBS. After which the appropriate amount of RIPA lysis buffer with protease inhibitors was added and incubated on ice for 10 minutes. Cell lysates were collected and centrifuged at 16,000 × g for 20 min at 4°C, subsequently the protein lysate supernatant was collected and used for further analysis.

Protein quantification was performed by Bradford assay according to the manufacturer's protocol. It is based on the principle that a color change occurs after the acidified Coomassie Brilliant Blue G-250 in the Bradford reagent binds to the proteins, with the light absorbance maximum shifting from 465 to 595 nm. In brief, 2 µL of protein extract supernatant was placed in a 96-well plate along with 100 µL of Bradford reagent and mixed. After incubation for 5 minutes at RT, the absorbance of the sample was analyzed in a Tecan Microplate Reader. The protein concentration was calculated by reference to a standard curve generated from different concentrations of BSA solution.

Exosomal pellet, fractions after density gradient centrifugation or proteins extracted from cells were supplemented with appropriate amount of 4 × SDS-loading buffer and denatured at 95°C for 10 minutes, then these samples are ready for gel electrophoresis. For the detection of CD63, samples were boiled with 4 × non-reducing SDS-loading buffer.

4.4.2 SDS-PAGE electrophoresis

SDS-PAGE is a discontinuous electrophoretic system used as a method to separate proteins depending on their molecular weight. Here, vertical electrophoresis system was used. The polymer density of the separation gel is selected according to the molecular weight of the target protein. For stacking gel, a polymer density of 4% is used to concentrate all proteins in one band. Afterwards, the SDS-PAGE-gel was submerged with 1 × SDS running buffer, with

samples and protein marker loaded on the gel. Electrophoresis was performed for 120 minutes at 80 - 100 V.

4.4.3 Protein transfer and detection

The proteins were transferred onto a methanol activated polyvinylidene difluoride membrane at 1.5 mA/cm^2 for 1 hour in a semi-dry blot procedure and discontinuous buffer system [296]. After blotting, the membrane was blocked in 10% (w/v) skim milk powder/TBS-T dissolved in 1 × TBS-T for 1 hour at RT. For detection of blotted proteins, membranes were incubated overnight at 4°C with primary antibodies appropriately diluted in blocking buffer, followed by washing with 1 × TBS-T at RT. Membranes were further incubated with horseradish peroxidise-linked secondary antibodies diluted in blocking buffer for 1 hour at RT and followed by 1 × TBS-T final washing step at RT. Bound antibodies were visualized using peroxidase substrate reagent (ECL reagent, Immobilon western Chemiluminescent HRP Substrate) and an Amersham ImageQuant800^{TM} western blot imaging system. Quantification of band intensities was performed using ImageQuant^{TM} TL software.

4.5 Quantification of HBV DNA and RNA

4.5.1 Extracellular viral DNA quantification

HBV genomic DNA in each density-gradient fractions or harvested cell culture supernatants was measured by quantitative real-time PCR (qPCR) based on the Maxima SYBR green qPCR kit and a LightCycler® 480 instrument. Primers targeted HBV S-domain (SHB-F, SHB-R) were used with a working concentration of 10 µM. The qPCR was performed in a 10 µL reaction mixture consisting of: 3 µL sample from fractions or supernatants as template, 5 µL SYBR green 2x Master Mix, 0.25 µL for each primer, and 1.5 µL nuclease-free water. The amplification conditions were set as follows: initial denaturation for 10 minutes at 95°C, followed by 45 cycles of amplification (denaturation 15 seconds at 95°C, annealing 30 seconds at 56°C and elongation 30 seconds at 72°C. After this, the final PCR product was exposed to a temperature gradient from 56°C to 95°C while fluorescence readouts were collected continuously to obtain the melt curves. The Cp values (quantification cycle) were calculated automatically by the LightCycler480 software using the “Second Derivative Maximum” method. Absolute genomic DNA in samples was converted based on the Cp values and the standard curve described below.

4.5.2 SHBs primer standard curve plotting

Linearized pJO19 plasmid containing 1.2-fold HBV genome but only one copy of SHBs (subtype ayw, genotype D) were used as the template to create a standard curve of the SHB primers. The copy number per µL was calculated based on the plasmid concentration and

molecular weight. 0.3 ng of template was subjected to five 10-fold serial dilutions and then qPCR was performed on these serially diluted templates by the same reaction system and amplification conditions described above. A standard curve is created by plotting the measured Cp values against the log of the copy number of the diluted templates.

4.5.3 Intracellular HBV total RNA quantification

To detect the replication of HBV in the presence of inhibitors and in the targeted knockout HepAD38 cells, intracellular HBV total RNA was relatively quantified. Total RNA was isolated from the corresponding HepAD38 cells using the peqGold TriFast reagent and resuspended in ddH_2O containing 0.1% (w/v) DEPC according to the manufacturer's instructions. Afterwards, one unit of RQ1 RNase-free DNase was used to remove DNA contaminations from the isolated RNA. cDNA synthesis was performed in the presence of 4 µg DNase treated RNA using 1 µL (0.2 µg/µL) random hexamer primer, 1 µL (10 mM) dNTPs and 200 Units RevertAid H Minus reverse transcriptase. After 10-fold dilution of cDNA with ddH_2O containing 0.1% (w/v) DEPC, the cDNA was available for qPCR. Primers targeted HBV S-domain (SHB-F, SHB-R) and primers targeted housekeeping gene 60S ribosomal protein L27 (RPL27-F, RPL27-R) were used for intracellular HBV total RNA relative quantification. The qPCR was performed under the Maxima SYBR green qPCR kit and a LightCycler® 480 instrument according to the system and amplification conditions described above. The expression levels of total HBV RNA were analyzed using the ΔΔCT method with normalization to RPL27. Fold change compared with untreated cells or non-target cells was plotted.

4.6 Detergent treatment of exosomes

4.6.1 RIPA buffer combined with ultrasonication treatment

After density gradient, an appropriate amount of RIPA buffer was added to each fraction and incubated for 15 minutes at 4°C, followed by disruption of the exosome membrane with the facilitation of sonication. Subsequently, the HBsAg amount in each fraction was measured by an Enzygnost® HBsAg 6.0 ELISA kit prior to membrane disruption, and afterwards, as suggested by the manufacturer's instructions.

4.6.2 NP-40 treatment

Exosome fractions and free virus fractions obtained by iodixanol density gradient centrifugation were further subjected to NP-40 treatment to remove the exosomal membrane or viral envelope. For free virus fractions, treatment with 0.5% (v/v) NP-40 at 37°C for 40 minutes was used to expose their encapsulated nucleocapsids. The purified exosome fractions were then subjected to treatment with 0.25% (v/v) NP-40 at 30°C for 20 minutes or

0.5% (v/v) NP-40 at 37°C for 1 hour, separately. Both treatments were designed to disrupt the exosome membrane and thereby release the enveloped virus, as well as to destroy a portion or entire of the released envelope of the virus resulting in the exposure of the nucleocapsid. Thereafter, all treated groups and the untreated group serving as a control were again subjected to iodixanol- or sucrose-based density gradient centrifugation, as described above. After centrifugation, the samples were fractionated from top to bottom with 0.5 mL fractions. The corresponding analyses were performed by western blot, qRT-PCR and HBcAg ELISA. For quantification of HBcAg, a QuickTiter™ HBV Core Antigen ELISA Kit was performed to capture the nucleocapsid as suggested by the manufacturer's instructions.

The HBV virions fractions and nucleocapsid fractions obtained by treating exosomes with NP-40 were concentrated by ultracentrifugation at 42,000 rpm for 2.5 hour and resuspended in TNE buffer. Subsequently, these two fractions were immobilized on grids by the negative staining method with 1% (w/v) phosphotungstic acid (PTA) described above and observed under an electron microscope TEM Zeiss EM-109.

4.7 Interference with MVB or exosome production with specific inhibitors

4.7.1 Cell viability assay

HepAD38 cells were seeded in 96-well plates with a cell density of 5×10^4 cells/well and cultivated overnight. The next day, after aspirating the supernatant, the cells were cultured with media containing serial dilutions of U18666A (1 - 10 µg/mL) manumycin A (1 - 50 µM,) and GW4869 (1 - 50 µM), respectively, at 37°C. After 48 hours, the cell viability was monitored using a PrestoBlue™ Cell Viability Reagent according to the manufacturer's instructions and the fluorescence was measured at 560/590 nm using Tecan Microplate Reader. To standardize percent viability, fluorescence measured from untreated cells (cultivated with media containing the corresponding concentration of DMSO) was calculated as 100% survival and that from 0.5% (v/v) Triton X-100 treated samples as a qualitative cytotoxicity control was calculated to be nearly 0% survival.

4.7.2 Detection of the influence of inhibitors on HBV replication

HepAD38 cells were cultivated at a density of 1.5×10^6 in 6-well plates with 2 mL media overnight. The next day after the change of media, the cells were treated with media containing indicated concentrations of inhibitors and maintained for 48 hours. Afterwards, the effect of inhibitors on HBV replication and HBsAg production was assessed by western blot for intracellular LHBs (MA18/7 antibody) and HBsAg (K46 antibody), and by qPCR for intracellular total HBV RNA levels with the above described procedure. Fold changes with untreated cells were plotted.

4.7.3 Inhibitors treatment in HepAD38 cells

HepAD38 cells were plated into T175 cell culture flasks at a density of 25 × 10^6 with 30 mL media and cultivated overnight. The next day after the change of media, the cells were cultured with either media containing indicated concentrations of inhibitors or DMSO and maintained for 48 hours. Thereafter, exosomes were isolated from the cell culture supernatant by differential ultracentrifugation and discontinuous iodixanol gradient centrifugation as described above. Alix, Tsg101 and HBcAg in each fraction were detected by western blot. HBV genomic DNA distribution across the gradient was measured by qPCR.

4.8 Generation of HepAD38 cells with stable Alix or Syntenin knockout

4.8.1 Construction of sgRNA expression plasmid

Single guide RNAs (sgRNAs) targeting Alix or Syntenin were chosen from GenScript gRNA database, and a non-target sgRNA that do not recognize any sequence in the human genome was designed from Origene scrambled sequence, and the complementary strand sequence of all sgRNAs was transcribed. Then add a ‘CACCG’ to the 5’ end of each sgRNA sequence, an ‘AAAC’ to the 5’ end and a ‘C’ to the 3’ end of each complementary strand and proceed to oligo synthesis. Subsequently, each pair of synthesized forward and reverse oligos was phosphorylated and annealed to duplexed DNA oligos. For this purpose, a 10 µL reaction mixture was prepared, which included 1 µL of each oligo, 0.5 µL of T4-Polynucleotide kinase, 1 µL of 10 × T4 ligation buffer and 6.5 µL of nuclease-free ddH_2O. Annealing was performed in a thermocycler using the following parameters: first being at 37°C for 30 minutes, followed by 95°C for 5 minutes and then ramp down to 25°C by 5°C per minute. Annealed oligo duplex was diluted 250-fold.

Following digestion with BbsI restriction endonuclease, the CRISPR/Cas9 system was generated by complementary base pairing of the sticky ends of pX459 plasmid (pSpCas9(BB)-2A-Puro V2.0) with the designed each annealed oligo duplex. The digestion-ligation reaction was proceeded simultaneously by the following system: 100 ng pX459, 2 µL of 250-fold diluted annealed oligo duplex, 2 µL of 10 × Tango buffer, 1 mM of DTT, 1 mM of ATP, 1 µL of high fidelity BbsI, 0.5 µL of T7 DNA ligase and filled up to 20 µL with ddH_2O. The ligation reaction was completed in the thermocycler by first proceeding at 37°C for 5 min, then at 23°C for 5 min, and conducting 6 cycles of both steps.

Subsequently, pX459 plasmids carrying different sgRNAs were separately transformed into E. coli DH5α competent cells by heat shock method. Briefly, gently mix 10-50 ng of the sgRNA-carrying pX459 plasmid into 100 µL of competent cells and incubate the mixture on ice for 30 minutes. After a subsequent heat shock at 42°C for 45 seconds, the cells were then incubated on ice again for 5 minutes. Afterwards, 500 µL of non-antibiotic LB liquid media

was added to the mixture and grown in 37°C shaking incubator for 45 minutes. Then 100 µL of the amplified E. coli was plated onto LB agar plates containing the appropriate antibiotic (ampicillin, 100 µg/mL) and plates were incubated at 37°C overnight. The following day, suitable single colonies were picked and grown in 5 mL of LB-media (ampicillin, 100 µg/mL) at 37°C shaking incubator for 12-16 hours. The plasmids were then isolated from the bacterial cultures using the QIAprep Spin Miniprep Kit according to the manufacturer's protocol, and positive clones were identified by DNA sequencing. Bacteria containing positive plasmid were further cultured overnight in 300 mL LB media (ampicillin, 100 µg/mL) at 37°C shaking incubator, and sufficient plasmids were isolated for subsequent transfection experiments by using the QIAGEN Plasmid Maxi Kit according to the instructions. The isolated plasmids were stored at -20°C with a concentration of 1 µg/µL in ddH_2O.

4.8.2 Knockout clonal cell lines

HepAD38 cells were seeded into 6-well plates with a density of 1.5×10^6 and reached 80% confluency before transfection. Cells were then transfected with the pX459 plasmids containing sgRNA using FuGENE® HD transfection reagent. 48 hours post-transfection, cells were treated with media containing 2.5 µg/mL puromycin for two weeks to select monoclones. Subsequently, monoclones were isolated and endogenous expression of target proteins was detected by western blotting after culture amplification. Clones in which endogenous protein expression could not be detected were stable KO cell lines and can be used for follow-up experiments.

In addition, similar to the inhibitor treatment experiments, the effect of knockout on HBV replication and HBsAg production was performed as described above.

4.9 Rescue of Alix in stable knockout cells

For Alix-rescue experiment, DH5α strain containing human full-length Alix with its N-terminal in-frame mCherry fusion expression vector was obtained from Addgene and amplified by incubation in 300 mL LB medium (Kanamycin, 50 µg/mL) overnight in a 37°C shaking incubator. The next day, plasmids were extracted according to the instructions of the QIAGEN Plasmid Maxi Kit for the subsequent transfection experiments.

HepAD38 cells were seeded into 150 mm dishes with a density of 22×10^6 and were available for transfection after reaching 60 - 80% confluence. The transfection solution was prepared as follows: 20 µg of the mCherry-hAlix plasmid prepared above was added to 2 mL of PBS (pH 7.1, suitable for cell culture) and mixed well. Subsequently, a 6-fold (w/v) polyethyleneimine was also included and immediately mixed the solution with a vortex mixer for about 10 seconds. After incubation at RT for 20 minutes, the plasmid/polyethyleneimine polyplexes was added to the cell culture in a drop-wise manner and mixed gently by shaking

the dish in a “cross-like pattern”. The medium was refreshed 12 hours post-transfection. After a further 48 hours, cell supernatants were collected, and exosomes were isolated by the differential ultracentrifugation and discontinuous iodixanol gradient centrifugation methods described above. The amounts of HBV genome, HBcAg and exosomal marker Alix in each fraction were analyzed according to the methods described above.

4.10 Exosome ultrathin section preparation and immunolabeling-TEM

4.10.1 Sectioning of Epon-embedded exosomes

Visible exosome pellets enriched by differential ultracentrifugation were fixed with 0.1 M PHEM buffer containing 4% (v/v) formaldehyde (FA) plus 0.1% (v/v) glutaraldehyde (EM grade) at RT for 30 min [297, 298]. The pellets can be stored in 0.1 M PHEM buffer containing 4% (v/v) FA at 4°C until use. After subsequent careful washing of the fixed pellets with 0.1 M PHEM buffer, the pellets were gently mixed with 3% (w/v) agarose, then centrifuged to form pellets and trimmed into cubes. The cubes were rinsed with PBS and embedded in epoxy resin according to standard preparation protocols, followed by cutting into ultrathin sections with a thickness of 70 nm by Ultracut FC4E Ultramicrotome [299, 300]. The Epon sections were transferred to 300-mesh copper grids and stained with 0.2 % (v/v) uranyl acetate.

4.10.2 Exosome cryo-sectioning and immuno-gold labeling

A mixture of 3% (w/v) low gelling temperature agarose with fixed exosomes was infiltrated with 2.3 M sucrose, after which it was frozen in liquid nitrogen and then processed with Cryo-Ultramicrotome EM FC7 for 100 nm cryo-sections [297]. Afterwards, the sections were picked up on a drop of cold 2.3 M sucrose and transferred onto the formvar surface of nickel grids [298]. The grids with the sucrose drop on its surface can be stored at 4°C for two weeks.

The immunolabeling procedure of cryo-sections was first performed by incubating the grids in a 6 cm petri dish filled with PBS for 15 minutes, followed by incubation in a 35 mm petri dish filled with PBS twice for 3 minutes each. These steps are designed to remove sucrose residues. Afterwards, the grids were incubated for 15 min in a 6 cm Petri dish filled with 1 % (w/v) milk for blocking. Primary antibody incubation was performed by floating the grids on a drop containing the indicated dilution of mouse anti-CD63 primary antibody or antiserum against the preS1/preS2 structural domain of LHBs (K112-4, from rabbits) for 1 to 3 hours at RT. After washing with PBS 5 times of 3 minutes each, the grids were floated on secondary goat anti-mouse IgG conjugated with 10-nm gold or goat anti-rabbit IgG conjugated with 5-nm gold at RT with 50-fold dilution. A final wash was performed by incubating with PBS five times with 3 minutes each to remove the non-specific binding. After labeling, the grid was washed twice with distilled water for 3 minutes each to remove PBS and incubated with a

drop of 2% (w/v) methylcellulose containing 0.4% (v/v) uranyl acetate on ice for 10 minutes. Later, the grid is hooked up through a loop and dried in air [301]. All samples were examined using a Zeiss EM-109 transmission electron microscope.

4.11 Inoculation and neutralization assays of HBV hijacked exosomes

As described above, exosomes were isolated from 400 mL HepAD38 cell culture supernatant with differential ultracentrifugation and iodixanol gradient method. Gradient purified HBV-loaded exosome fractions or free HBV virus fractions were used for infection. The same volume of fractions was used instead of an identical multiplicity of infection to exclude that infection could be caused by a contamination of free HBV virions.

HepaRG cells differentiated according to the above method were used for infection. First, an RBD-binding anti-preS1 antibody (MA18/7) or an unrelated monoclonal anti-hexa-His antibody was mixed with the purified HBV exosomal fractions or free HBV virus fraction at a concentration of 1 µg/mL and kept at 37°C for 2 hours. The mixtures were then inoculated into differentiated HepaRG cells and incubated at 37°C for 20 hours. Alternatively, purified HBV exosomal fractions or free HBV viral fractions along with or without 500 nM Myrcludex B were also plated with differentiated HepaRG cells at 37°C for 20 hours.

In parallel, HepG2 cells and HepG2-NTCP cells were also used here. Cells were seeded in 6-well plates at a density of 3 x 10^5 the day before inoculation. Same amount of exosomes or free HBV was inoculated with the cells at 37°C for 20 hours.

At the end of incubation, the supernatant was collected, cells were washed four times with PBS and maintained in their respective culture media. Thereafter, medium was collected and refreshed every other day till 14 days after inoculation. Analysis of infection was performed by measuring HBsAg levels in the supernatants collected at the indicated time points by an Enzygnost® HBsAg 6.0 ELISA kit as suggested by the manufacturer's instructions.

4.12 Statistical analysis

Results are presented by at least 3 independent replicate experiments unless otherwise stated. The quantified data are shown as mean value and corresponding standard errors of the mean (SEM). The statistical significance between each of the two groups was tested by unpaired parametric t-tests. For multiple comparisons, two-way ANOVA followed by Sidak’s multiple comparison test was used. All statistical analyses were performed in GraphPad Prism 9.2.0.

5 Results

5.1 Characterization of exosomes isolated from culture supernatants of HepAD38 or HepG2 cells

To clarify the potential role of exosomes on HBV release and spread, the profiles of exosomes purified from the culture supernatants of human hepatoma cell lines were investigated. Exosomes were purified from the culture fluids of HepG2 cells (HBV negative) or of the HBV-inducible HepAD38 cell line using differential ultracentrifugation (**Figure 12A**). Western blot analyses of the precipitates confirmed the presence of exosomes markers Alix and CD63 in the exosomal pellet (**Figure 12B**). In addition, LHBs and HBcAg proteins were banded in exosomal pellet isolated from HepAD38 cells (**Figure 12B**). To characterize the hydrodynamic diameter distribution of exosomes derived from these two cell lines, nanoparticle tracking analysis (NTA) was performed. The NTA showed a peak diameter of approximately 134 nm for exosomes isolated from HepAD38 cell line, with a significant difference compared to exosomes derived from HepG2 cells, which had a peak size at 119 nm (**Figure 12C**).

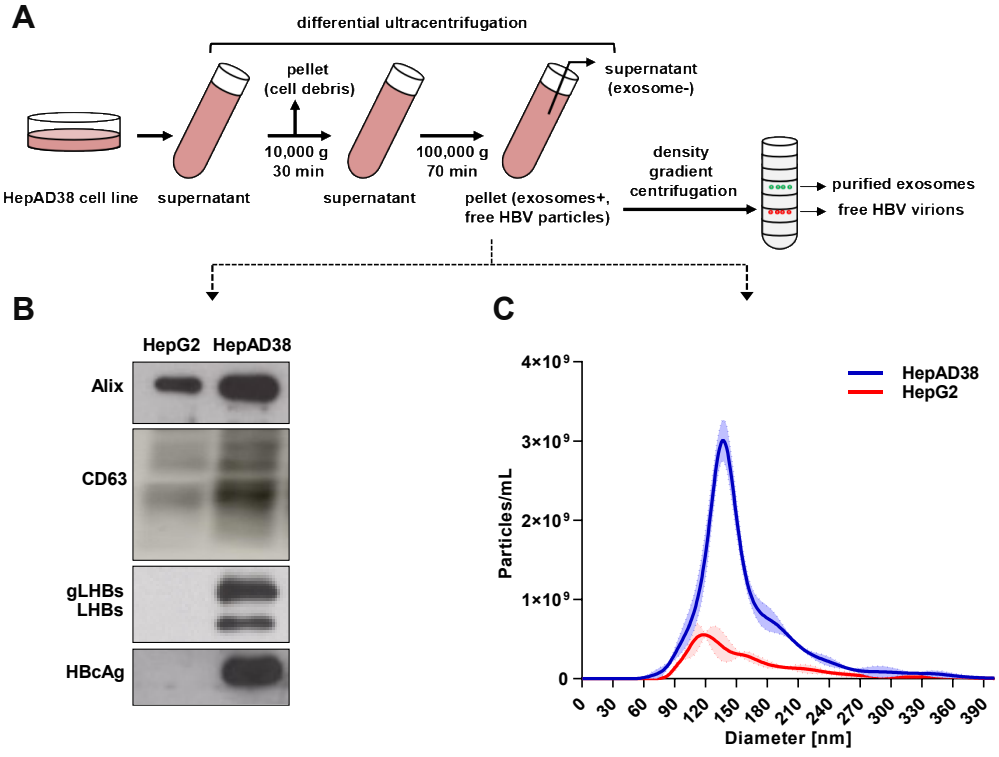

Figure 12. Characterization of exosomes purified from HBV-negative HepG2 cells and from the HBV expressing stable cell line HepAD38. (A) Depiction of the procedure for purification of exosomes from cell culture fluids. **(B)** Exosomes were purified from the supernatant of HepG2 cells or HepAD38 cells by differential ultracentrifugation as shown in Figure 12A. The purified exosomal pellet was analyzed by western blot with antibodies against Alix, CD63, LHBs, and HBcAg. **(C)** The size

distribution of the exosomes derived from HepG2 cells or HepAD38 cells. The analysis was performed by NanoSight NS300. The error bars were shown as dotted lines with fill areas.

Many methods for isolating exosomes involve a differential ultracentrifugation step. However, this gold standard step of isolating exosomes leads to co-sedimentation of exosomes and HBV viruses because of their similar sedimentation properties. Therefore, an iodixanol density gradient centrifugation method was extended in the isolation procedure to efficiently separate exosomes and viruses (**Figure 12A**). Western blot analyses revealed the presence of both LHBs and HBcAg in fractions with higher density that were separated from exosomes which were characterized by the markers -Alix, -Tsg101 and -CD63 (**Figure 13A**). The distribution profile of HBV genomic DNA and HBcAg over the gradient showed two peaks. In the lower density peak of viral DNA and HBcAg positivity, including fractions 6 to 9 (densities corresponding to 1.06-1.10 g/cm^3), exosomes were present as characterized by Alix, Tsg101 and CD63 (**Figure 13A-B**). The higher HBV DNA and core antigen positive peak was observed in fraction 12 (density of 1.18 g/cm^3), which is expected to be HBV intact virions, and was further featured by the absence of exosome markers (**Figure 13A-B**).

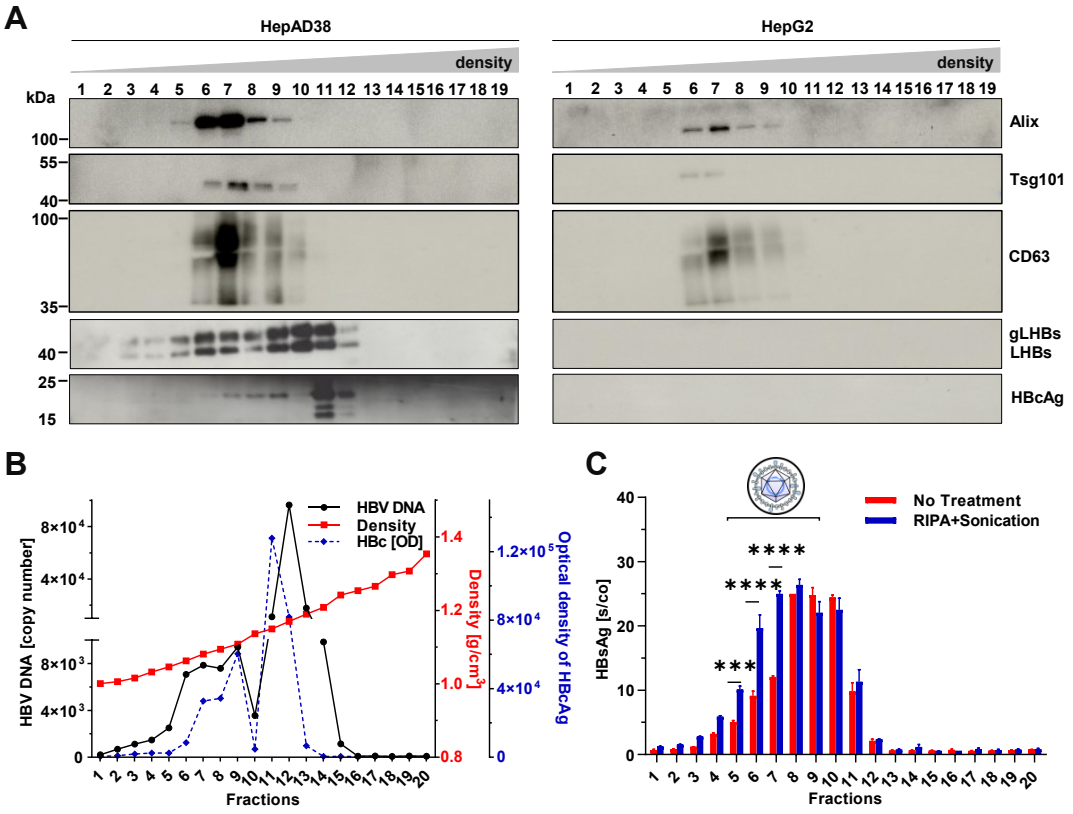

Figure 13. Density gradient centrifugation analysis of exosomes derived from HepG2 cells and from HepAD38 cells. (A) Exosomes isolated by differential centrifugation from the supernatant of HepAD38 or HepG2 cells were subjected to iodixanol density gradient centrifugation, as shown in Figure 12A. The fractions of the gradient were analyzed by western blot with antibodies against Alix, Tsg101, CD63, LHBs and HBcAg. **(B)** Absolute quantification of the distribution of HBV DNA

(indicated with black line) and of HBcAg (**Gray** values of the western blot in Figure 13A; indicated with blue dotted line) in fractions of the iodixanol gradient. The red line indicated the density. **(C)** HBsAg in each fraction of the iodixanol gradient was quantified by ELISA. The left untreated fractions were shown with red bars. The fractions pretreated with RIPA buffer and ultrasound sonication were indicated with blue bars. Two-way ANOVA followed by Sidak's multiple comparison test for all panels; *** $P < 0.001$.

Due to the positivity of HBV DNA and HBcAg in the exosomal fraction, a further analysis was performed to determine whether these fractions are also HBs antigen positive. For this reason, radioimmunoprecipitation assay buffer (RIPA buffer) combined with ultrasonication was used to disrupt the membrane of exosomes. The non-treated fractions and RIPA buffer pretreated fractions were subjected to HBsAg-specific ELISA. The data showed that RIPA buffer treatment resulted in a distinct increase of HBsAg signal in fractions F5 to F7 (**Figure 13C**), and these fractions were characterized by exosomal markers. This suggests that disruption of the membrane of exosomes permits the HBsAg harbored within exosomes to be captured by the HBs antigen specific antibodies.

To further confirm the presence of HBV antigens within the exosomes, anti-CD63-coated magnetic beads were used to perform an immunoprecipitation assay on the exosomal fractions isolated by the method as described in **Figure 12A**. The input, unbound supernatant and immunoprecipitated targets from the fractions were analyzed by western blotting (**Figure 14A**). A remarkable reduction of Alix, LHBs and HBcAg levels was observed in the unbound supernatant as compared to the input (**Figure 14A**). Meanwhile, Alix, LHBs and HBcAg appeared at the same density after immunoprecipitation from the exosomal input with anti-CD63 coated magnetic beads (**Figure 14A**).

Immunoprecipitation with an irrelevant Dynabeads™ Sheep anti-Rabbit IgG from exosomal input showed no detectable HBV antigen signal or exosome marker Alix on magnetic beads, and the weak LHBs signal on magnetic beads probably derived from non-specific binding (**Figure 14A**).

The percentage of exosome-associated HBV genomic DNA and HBcAg was found to be approximately 1.76% (**Figure 14B**) and 2.04% (**Figure 14C**) of the total input of the gradient by qPCR quantification of DNA and ELISA quantification of HBcAg, respectively.

In conclusion, these findings indicate that exosomes released from HBV-expressing cell lines can be separated efficiently from HBV free virus. Moreover, HBV-specific DNA and viral proteins are present in exosomes released from these HBV producing cells.

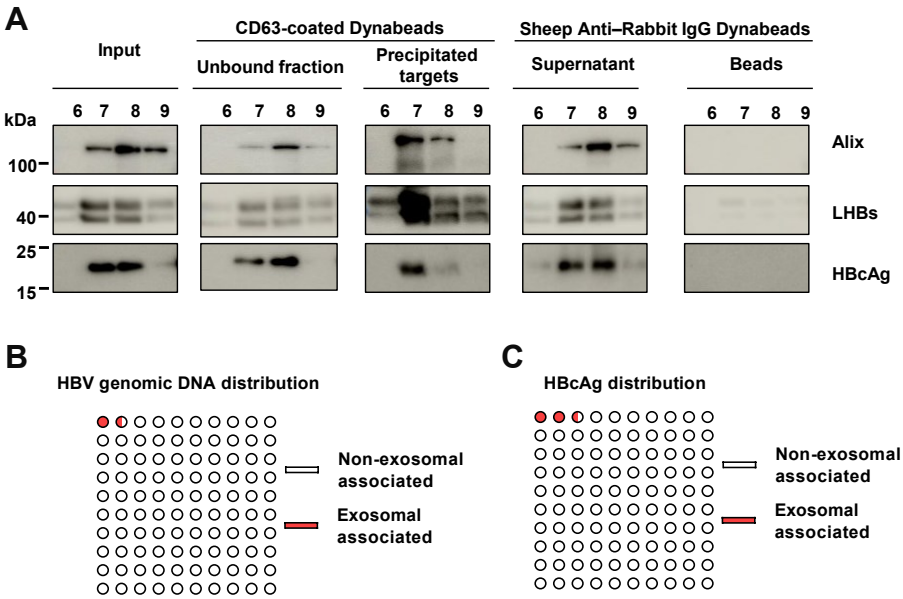

Figure 14. Exosome-associated HBV genome and viral proteins identification. (A) Iodixanol-gradient isolated exosomes were further separated by CD63-coated magnetic beads. The input, unbound fraction and bead-bound exosomes were analyzed by western blot using anti-Alix, -LHBs, and -HBcAg antibodies. An unrelated Dynabeads® M-280 sheep anti-rabbit IgG was used as a control. **(B/C)** The percentage of exosome-associated HBV genomic DNA and HBcAg to the total input were quantified by qPCR for DNA (B) and by ELISA for HBcAg (C).

5.2 Identification of HBV particles in exosomes derived from HBV-producing cells

The above data show that viral DNA, HBs antigen, and HBc antigen can be detected in exosomes derived from HBV-producing cells. This raises the question about the possibility of discovering fully assembled HBV virions within the exosomes.

The outer envelope of HBV virions is detergent-sensitive, a core particle is able to be released from the Dane particles after treatment with mild nonionic detergents [302]. The same conditions can also cause partial or complete disruption of the exosomal membrane [303]. Therefore, exosomes derived from HBV-expressing cells were processed in a limited treatment with the mild detergent NP-40 to explore whether intact virus could be released after the exosomal membrane was disrupted.

As shown in **Figure 15A**, exosomal fractions 6-9 purified by iodixanol gradient were incubated with 0.5% of the nonionic detergent NP-40 at 37 °C for 2 hours and were then centrifuged again with iodixanol density gradient. Non-treated exosomes were used as control. qPCR quantification over the gradient fractions revealed that the HBV genomic DNA in the non-treated input was present in the 7 - 9 fractions having a density of 1.064 to 1.105 g/cm^3 (**Figure 15B**). However, the viral DNA migrated to 11 - 14 fractions in the NP-40 treated input, with a peak fraction 12 corresponding to a density of 1.185 g/cm^3 (**Figure 15B**).

The iodixanol gradient fractions of the non-treated and the NP-40 treated input were also characterized by western blot. In the non-treated groups, the results showed that the exosomal marker Alix, LHBs and HBcAg were distributed around 7 to 9 fractions (**Figure 15C**).

In the case of NP-40 treated input, the HBcAg-containing fraction shifted to a higher density (1.185 g/cm^3) (**Figure 15C**), where the viral DNA loading was also at its peak there. This suggests the presence of free intact HBV virions and naked nucleocapsid in these fractions, and they are released by the detergent-dependent disruption of the exterior exosomal membranes and/or viral envelope. This was corroborated by the dispersion of Alix and LHBs across the gradient fractions reflecting the destruction of the membrane, as shown in **Figure 15C**.

In addition, fraction 8 of the gradient in the case of non-treated input and fractions 11, 12 in the case of NP-40 treated input were analyzed by HBcAg-specific ELISA. Compared to fractions 11 and 12 (NP-40 treated fractions), significant lower values were observed in fraction 8 (untreated input) (**Figure 15D**). In this case, the intensive treatment with NP-40 has stripped away the masked exosomal and viral membranes, therefore, the nucleocapsid is accessible for the HBcAg-specific antiserum.

When processing fraction 8 (untreated input) with Triton X-100, the membranes of exosomes and virus were consequently destroyed, thereby exposing the nucleocapsid and a distinctly significantly elevated specific signal of HBcAg was obtained (**Figure 15D**).

These data suggest that exosomal membrane destruction with mild detergent relates to partial disruption of the viral envelope. Viral particles can be detected in the exosomes derived from the cells expressing HBV.

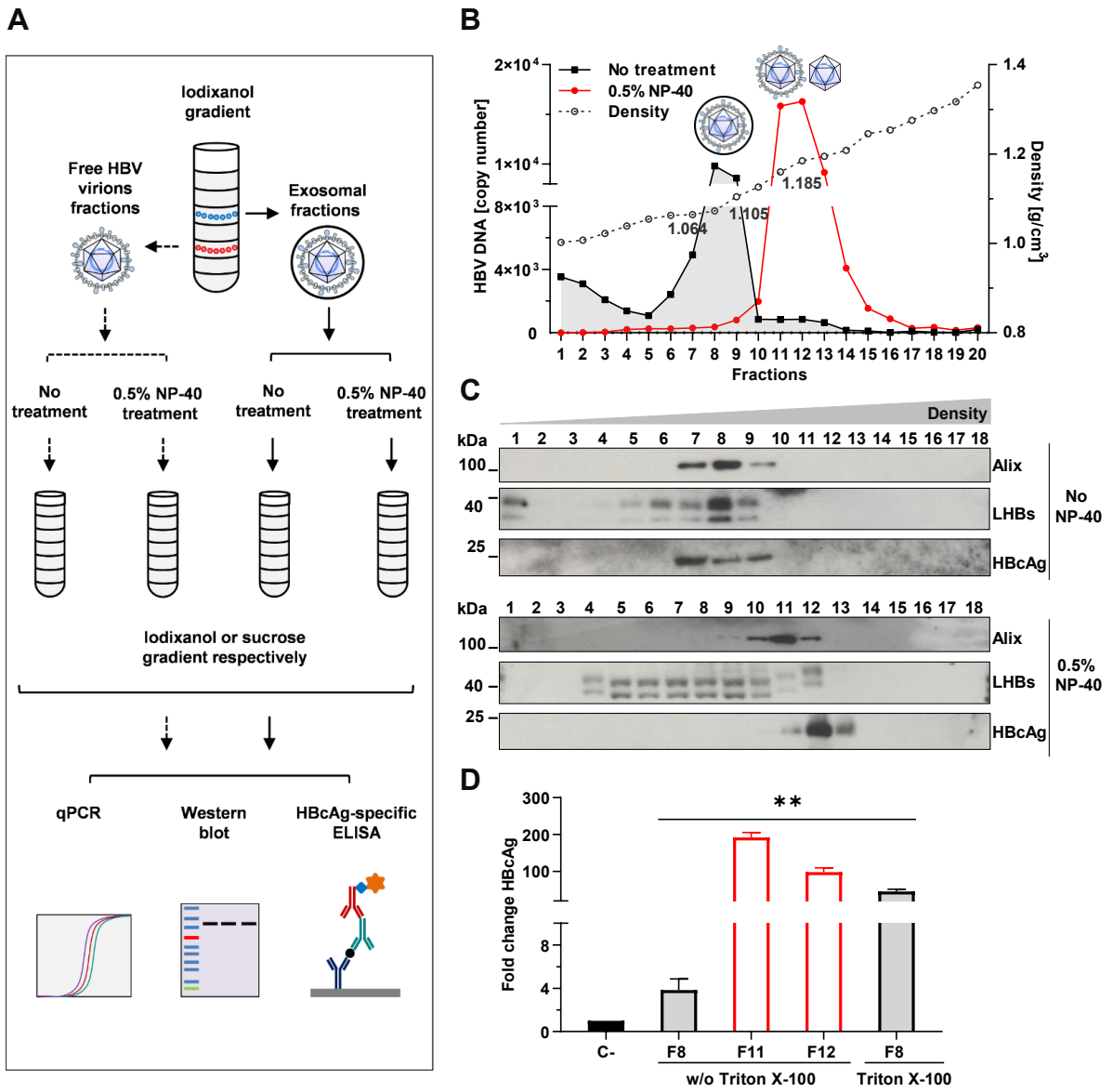

Figure 15. Exosomal HBV and free HBV particles were separated by iodixanol and sucrose density gradient centrifugation. (A) Schematic description of NP-40 treatment: Iodixanol gradient purified exosomal fractions or free HBV viral fractions were collected and then subjected to 0.5% NP-40 and incubated at 37 °C for 2 hours. Subsequently, re-centrifugation of the NP-40 treated input or non-treated input was performed on an iodixanol or sucrose density gradient. **(B)** The HBV genome distribution in each fraction of the iodixanol gradient was absolutely quantified by qPCR. The non-treated input was represented with black lines. The NP-40 treated input was displayed by red lines. The grey line indicated the density. **(C)** Western blot analysis was performed on fractions of iodixanol gradient centrifuged from the non-treated input and from the NP-40 treated input. LHBs and core-specific antibodies as well as Alix-specific antibody were used. **(D)** HBcAg was quantified by HBcAg-specific ELISA for fraction 8 (from NP-40 non-treated input) and fractions 11 and 12 (from NP-40 treated input) of the iodixanol gradient (Figure 15B) in the absence or presence of detergent Triton X-100. Unpaired parametric t-tests for all panels. ** $P < 0.01$.

5.3 Intact HBV virus was found to be harbored in exosomes derived from HBV-producing cells

The above results show that treatment of exosomes with NP-40 mild detergent results in the release of HBV-genome containing particles, these particles probably represent a mixture of HBV virions and naked nucleocapsid.

To investigate whether intact HBV virions and naked nucleocapsid could be effectively separated based on iodixanol gradient centrifugation, purified intact HBV virions, and purified intact HBV virions processed with NP-40 were submitted to iodixanol density gradient centrifugation. Viral DNA in the fractions of the gradient was quantified by qPCR. As presented in **Figure 16A**, the distribution of intact HBV virions and NP-40 treated virions over the gradient showed no obvious difference, there was a peak of viral DNA in both cases, with a corresponding density of around 1.18 - 1.20 g/cm^3.

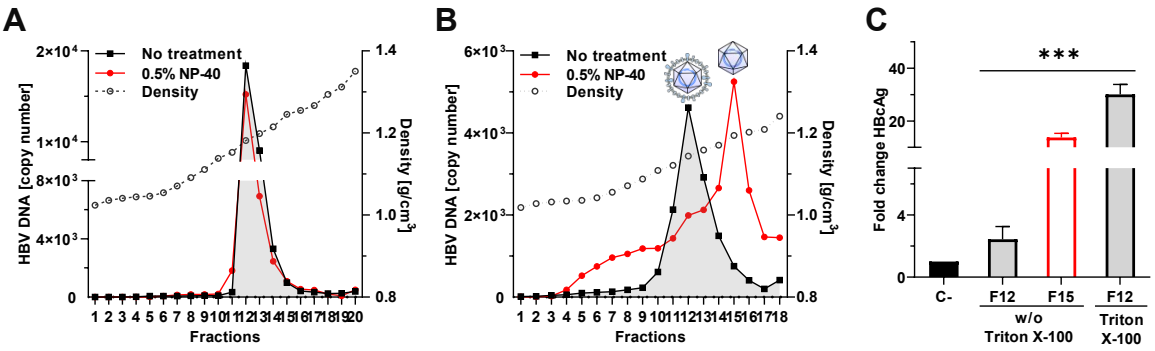

Figure 16. Separation of naked nucleocapsid from free HBV virions by sucrose density centrifugation. (A) The iodixanol gradient isolated free HBV viruses (see schematic representation in Figure 15A) treated with 0.5% NP-40 at 37°C for 40 min (red line) or without NP-40 pretreatment (black line) were being re-centrifuged in iodixanol density gradient. Quantification of HBV genome copy number in the gradient fractions was performed by qPCR. The grey dashed line shows the density value. **(B)** The iodixanol gradient purified free HBV viruses were treated with or without 0.5% NP-40 for 40 min at 37°C and then subjected to sucrose based gradient centrifugation. The copy number of HBV genomic DNA was quantitatively analyzed by qPCR in the gradient fractions. The black line, the red line and the gray dashed line respectively represent the input without NP-40 processing, the input with NP-40 processing, and the gradient density value. **(C)** Sucrose gradient fraction 12 from the NP-40 untreated input and fraction 15 from the NP-40 treated input (Figure 16B) were quantified by ELISA for core antigen with or without Triton X-100 prior treatment. Unpaired parametric t-tests for all panels. *** P < 0.001.

However, when purified intact HBV virions and purified intact HBV virions treated with NP-40 were subjected to a sucrose-based gradient, a distinct separation of the virion-specific peak from the specific naked nucleocapsid peak was acquired when the centrifuged fractions were analyzed by qPCR (**Figure 16B**).

The analysis of the corresponding peak fractions of the sucrose gradient fraction 12 from the untreated input and fraction 15 from the NP-40 treated input by HBcAg specific ELISA further confirmed this (**Figure 16C**). There was a significant lower HBcAg-specific signal observed in case of fraction 12 compared to fraction 15, although in both fractions equivalent amounts of HBV genomic DNA were identified (**Figure 16C**). However, the HBcAg specific signal increased drastically when processing fraction 12 with Triton X-100 to remove the protective viral envelope (**Figure 16C**).

Therefore, these data suggest that HBV naked nucleocapsid can be separated effectively from intact virions at these NP-40 treatment and sucrose gradient-based conditions.

Considering the above results, the same sucrose density gradient centrifugation system was introduced for the analysis of the exosomal fractions obtained from the iodixanol gradient (**Figure 15B**). Half of the fraction was subjected to 0.25 % NP-40 treatment at 30 °C for 20 min, the other half was left untreated **(Figure 17A)**. Then, the untreated or treated input was re-centrifuged on a sucrose density gradient. The HBV genome was quantified in each fraction of the sucrose gradient by qPCR. The qPCR quantification showed for the untreated exosome fraction there was one peak of HBV genomic distribution (fractions 7-9) after sucrose gradient centrifugation (**Figure 17A**). However, a clear separation of intact virions (fraction 11-12) and naked nucleocapsids (fraction 14-15) by sucrose density gradient was obtained for the NP-40 treated exosome fraction (**Figure 17A**).

Subsequently, the distributions of Alix, LHBs and HBcAg in the sucrose gradient fractions were analyzed by western blotting (**Figure 17B**). In case of NP-40 untreated input, detecting Alix as a marker of exosomes confirmed in fractions 7 to 9 the existence of exosomes (**Figure 17B**). Meanwhile, HBcAg was found in the same fractions and the strongest specific signal of LHBs was obtained (**Figure 17B**). Corresponding analysis of the NP-40 treated inputs showed that the Alix-specific signal spread across almost the entire gradient, while the core-specific signal was transferred to fractions 10 - 12 and 14 - 16 (**Figure 17B**). Under these conditions, as the envelope of partial HBV is disrupted, the LHBs-specific signal was diffused in fractions 2 to 14 (**Figure 17B**).

The corresponding peak fractions of the sucrose gradient fraction 8 from the untreated input and fractions 11 and 12, 14 and 15 from the NP-40 treated input (shown in **Figure 17A**) was further analyzed by HBcAg specific ELISA (**Figure 17C**). The results revealed that for fractions 8 and 11 and 12 of the gradients, pretreatment with Triton X-100 caused a strong increase of the HBc antigen specific signal (**Figure 17C**). This reflects the fact that due to the treatment with Triton X-100, the exosomal membranes in fraction 8 and viral envelope in fraction 11-12 were stripped and the core signal in these fractions became detectable by the HBcAg-specific antibody.

In contrast, the non-significantly different HBcAg signals in fractions 14 and 15 with and without Triton X-100 treatment reflected that the HBcAg signals in here were exposed (**Figure 17C**).

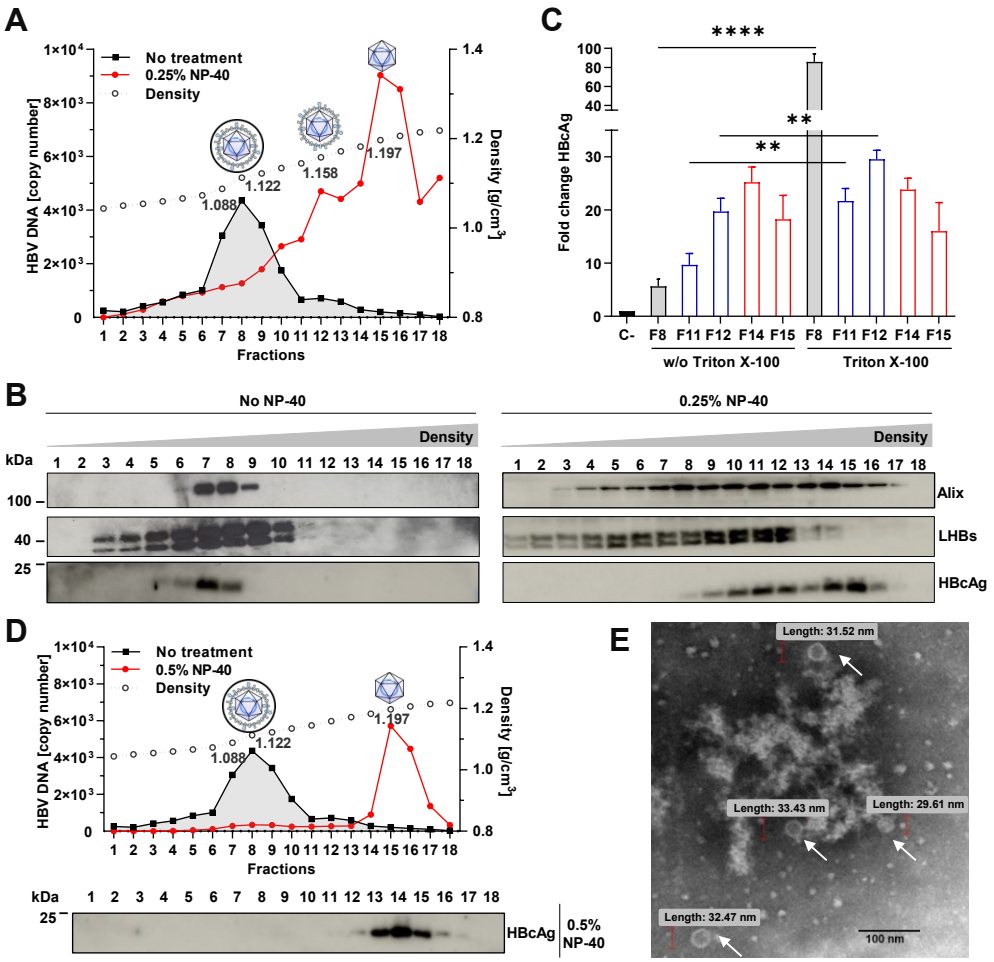

Figure 17. Intact HBV virus and naked nucleocapsids can be separated from exosomal HBV. (A) The iodixanol gradient purified exosomes in the absence (black line) or pretreatment with 0.25% NP-40 (red line) at 30°C for 20 min was followed by a sucrose density gradient. Quantification of the HBV genome copy number in the gradient fractions was performed by qPCR. The gray line indicates the density. **(B)** Western blot analysis of sucrose gradient centrifuged fractions shown in Figure 17A was performed with specific antibodies anti-LHBs and anti-HBcAg as well as anti-Alix. **(C)** Core antigen quantification by HBcAg-specific ELISA was performed on untreated and Triton X-100 pretreated fraction 8 (NP-40 untreated input), and fractions 11, 12, 14 and 15 (NP-40 treated input) of the sucrose gradients shown in Figure 17A. Unpaired parametric t-tests were used, * $P < 0.05$; *** $P < 0.001$. **(D)** The iodixanol gradient purified exosomes were re-subjected to a sucrose density gradient in the absence (black line) or pretreatment with 0.5 % NP-40 (red line) for 1 hour at 37 °C. The gray line shows the density. The HBV genome copy number was quantified in the gradient fractions by qPCR and is displayed in the upper panel. The HBcAg profiles in the 0.5 % NP-40 treated gradient were identified by western blot and are displayed in the lower panel. **(E)** Transmission electron microscopy analysis of the naked capsids found in fractions 14 and 15 of the sucrose gradient (NP-40 treated input (Figure 17D)) after phosphotungstic acid staining (arrow highlighted).

Thereafter, by increasing the NP-40 treated concentration to 0.5% and treating for more than 1 hour at 37°C, it was revealed by qPCR that for the NP-40 treated input, the viral genomic

DNA was completely moved to the naked nucleocapsid fraction (fractions 14, 15) (**Figure 17D**). Visual analysis by transmission electron microscopy was also performed on the naked nucleocapsid fractions 14, 15 of sucrose gradient (NP-40 treated) in **Figure 17D**. Through negative staining, in these fractions only naked capsids lacking any HBV envelope were identified (**Figure 17E**).

In summary, sucrose-based gradients indicate that following mild and limited NP-40 processing, complete HBV virions can be released from the HepAD38 cells-derived exosomes and be separated from the naked nucleocapsis. It is further confirmed by these data that intact HBV particles are present in the exosomal fractions.

5.4 Impairment of MVB- or exosome-generation with specific inhibitors impairs the release of host membrane-cloaked HBV particles

The above data suggest that intact HBV virus can be detected in exosomes. To investigate the implications of interference with MVB function and exosome biogenesis on the generation of encapsulated HBV, a variety of inhibitors was used.

U18666A directly suppresses the NPC1/2 protein, thereby impairing cholesterol intracellular trafficking. This can lead to the dysfunction of multivesicular bodies and consequently influences the release of exosomes [304]. The concentrations of U18 used in this study were obtained from a cell viability assay (**Figure 18A**) as well as earlier results [189, 304].

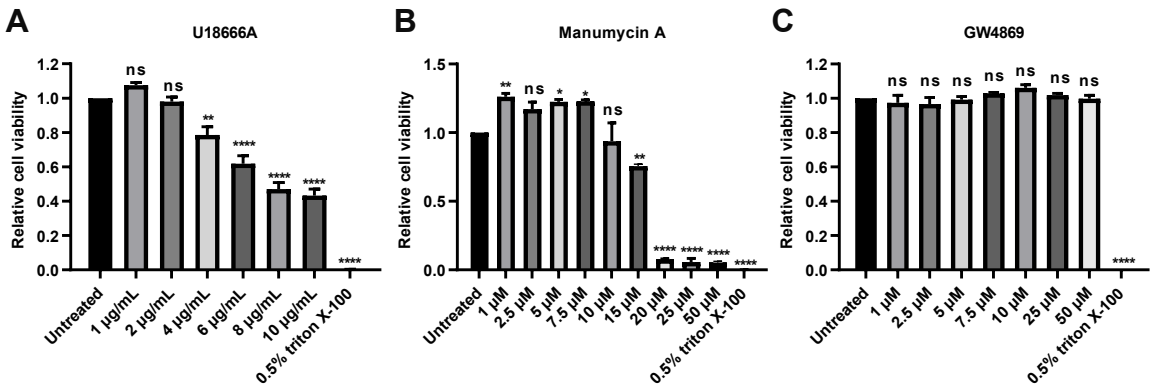

Figure 18. Cell viability of persistently HepAD38 cells treatment with multiple concentrations of U18666A (A), Manumycin A (B) or GW4869 (C) upon 48 hrs. As assessed via PrestoBlue assays, 2 µg/mL, and 4 µg/mL of U18666A were chosen to modulate exosomes generation. Manumycin A is intolerable at high concentrations, here 10 µM and 15 µM were selected. GW4869 has no significant cytotoxicity effect in HepAD38 cells. 25 µM and 50 µM were used to inhibit exosomes generation. Dunnett's Multiple Comparisons tests for all panels. * P < 0.05; ** P < 0.01; **** P < 0.0001; ns, not significant.

HepAD38 cells were incubated with 2 or 4 µg/mL U18666A for 48 hours. Subsequently, the supernatants were analyzed to isolate the exosomes using the method described in **Figure**

12A. Quantification of the viral genome by HBV-specific qPCR was performed on the fractions of the iodixanol gradient (**Figure 19A**), and the fractions were also analyzed by western blotting by using Alix-specific and HBcAg-specific antibodies (**Figure 19B**). As shown in **Figure 19B**, U18666A treatment was associated with changed distribution of Alix as compared to untreated control. After treatment with U18666A, the levels of Alix and Tsg101 in the exosome fractions 6-8 were reduced (**Figure 19B**). Following U18666A treatment, the viral DNA (**Figure 19A**) and HBcAg (**Figure 19B**) present in fractions 6-8 nearly disappeared completely, and instead were concentrated in fractions 10, 12 (viral DNA) and in fractions 10 and 11 (HBc antigen).

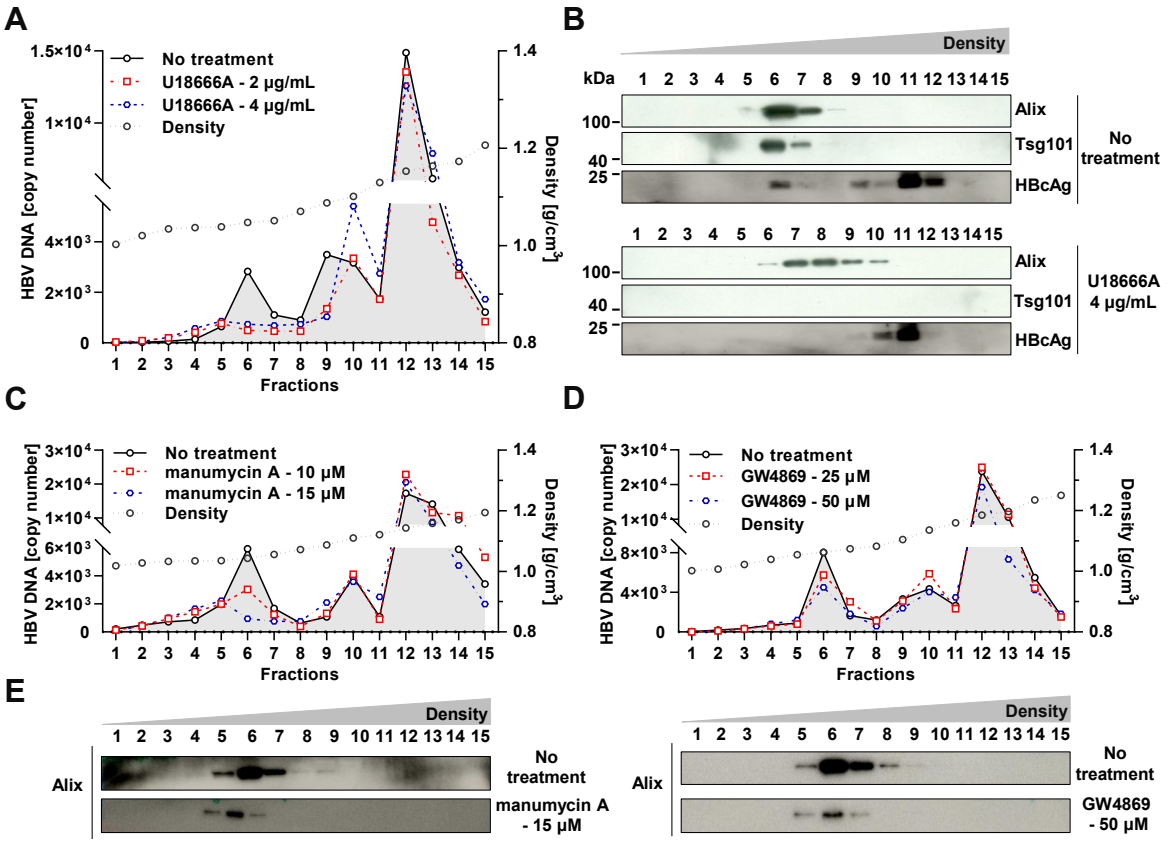

Figure 19. The release yield of membrane-encapsulated HBV virus was impaired by suppression of MVB or exosome formation. (A) Treatment of HepAD38 cells with 2 µg/mL (red dashed line) or 4 µg/mL U18666A (blue dashed line) for 48 hours or without treatment (black line). Exosomes enriched from the supernatants of these cells were subjected to iodixanol density gradients. HBV genome distribution in the gradient was quantified by qPCR. **(B)** The density gradient fractions shown in Figure 19A were analyzed by Western blotting with Alix and Tsg101-specific antibodies and HBcAg-specific antibody. The input from untreated is shown in the upper panel. The input treated with 4 µg/mL U18666A is shown in the lower panel. **(C)** Exosomes enriched from the supernatants of HepAD38 cells with 10 µM (red dashed line) or 15 µM of manumycin A (blue dashed line) treatment for 48 hrs or non-treated (black line) were subjected to iodixanol density gradients. HBV genomic distribution in the gradient was shown by qPCR quantification. **(D)** Exosomes enriched from the supernatants of HepAD38 cells with 25 µM (red dashed line) or 50 µM GW4869 (blue dashed line) treatment for 48 hrs or non-treated (black line) were subjected to iodixanol density gradients. HBV

genomic distribution in the gradient was shown by qPCR quantification. **(E)** The distribution of Alix in the iodixanol density gradient in Figure 19C and D. Treatment from Manumycin A is shown in the left panel and treatment from GW4869 is shown in the right panel.

Comparable inhibition results were achieved by using Manumycin A (**Figure 19C**), which represses the ESCRT-dependent biogenesis of exosomes, and GW4869 (**Figure 19D**), which damages exosome secretion by inhibiting neutral sphingomyelinase (nSMase). Dose response cell viability assay was performed with these two inhibitors to assess the non-cytotoxic doses (**Figure 18B, C**). The number of HBV genomic DNA in the exosome fractions in both cases was dose-dependently reduced (**Figure 19C, D**). Meanwhile, the efficacy of Manumycin A or GW4869 processing on exosome formation was assessed by the amount of Alix in the exosome fractions (**Figure 19E**). In both cases, the abundance of Alix in the exosomal fractions was decreased (**Figure 19E**).

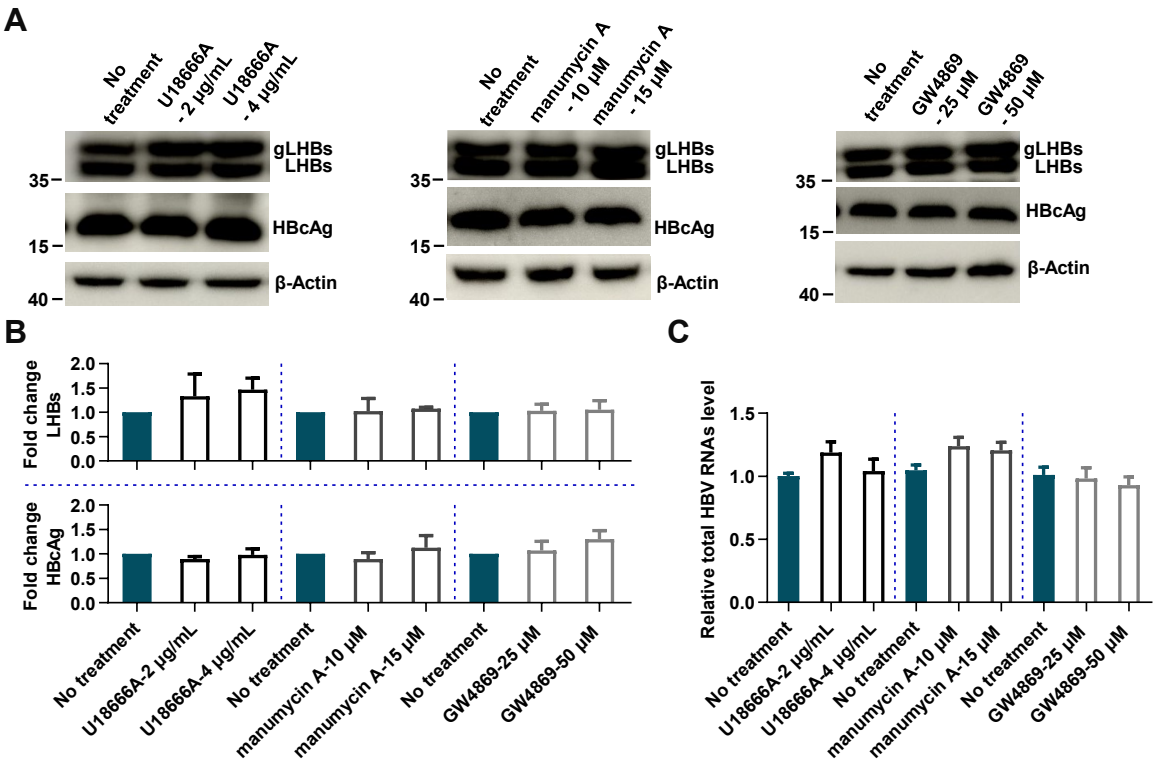

Figure 20. The impact of several MVB/exosome inhibitors on HBV replication and HBsAg production. (A) Western blot analysis of LHBs and HBc antigen in HepAD38 cells treated with inhibitors for 48 hours or untreated cells. The left panel showed cells treated with U186666, manumycin A treated cells were shown in the middle, and the right panel indicated cells treated with GW4869. β-actin detection was used as a load control. **(B)** Quantification of the relative amounts of intracellular LHBs (upper panel) and HBcAg (lower panel) signals in Western blot analysis of Figure 20A. Unpaired parametric t-tests was used for all panels. The fold change is displayed compared to the untreated cells. **(C)** Expression levels of HBV total RNAs in untreated HepAD38 cells or cells treated with indicated concentrations of U18666A or Manumycin A or GW4869 for 48 hours. The relative expression levels against RPL27 mRNA of HBV total RNAs were quantified by reverse

transcription (RT)-qPCR and were plotted as a change in fold compared to untreated cells. Unpaired parametric t-tests were performed for all panels.

To further identify that the observed suppression of the exosomal wrapped HBV virus is mediated by the specific compromise of exosome formation, the impact of these inhibitors on the replication of HBV and the production of HBsAg was confirmed by detecting the levels of intracellular LHBs and HBcAg by western blot (**Figure 20A, B**) and the intracellular amount of the total HBV RNAs by qPCR (**Figure 20C**). In the groups of cells treated with different inhibitors for 48 hours almost the same levels of intracellular LHBs and HBcAg were detected compared to the untreated cells (**Figure 20B**). At the same time, the intracellular levels of total HBV RNAs were not significantly changed by the inhibitor treated cells and the untreated cells (**Figure 20C**). All of these demonstrated that compared to untreated cells, the replication of HBV and HBsAg production were not impacted in the cells treated with these inhibitors.

Consequently, these data suggest that suppressing the biogenesis/release of exosomes with these inhibitors can specifically damage the generation of membrane covered HBV virions.

5.5 Release of exosome packaged HBV requires exosome-related proteins

The previous studies showed that MVBs and exosomes have an essential function in regulating the maturation and trafficking of exosome-wrapped HBV particles.

To elucidate the mechanism through which HBV enters into the exosome, specific proteins with critical roles in the biogenesis of exosomes and in the sorting of MVB/exosome cargo were targeted. The ESCRT-related protein Alix (PDCD6IP) has been demonstrated in several evidence mediating the generation of host membrane cloaked viruses. To evaluate the direct effect of Alix on the biogenesis of exosomal HBV particles, an Alix-deficient HepAD38 cell line (Alix-KO) was produced by using CRISPR/Cas9 mutagenesis. Western blot analysis of cell lysates from Alix-KO cells confirmed the absence of endogenous Alix protein (**Figure 21A**). The replication of HBV and the formation of HBsAg were also investigated in the Alix-deficient HepAD38 cells. Intracellular LHBs analysis by western blot showed that the number of N-glycosylated species of LHBs was lower in these Alix-KO cell lines compared to the non-target cells (NT) (**Figure 21C**), but the intracellular amount of HBcAg stayed unchanged (**Figure 21C**). Intracellular quantification of total HBV RNAs showed comparable amounts in Alix-deficient HepAD38 cells compared to non-target cells (NT) (**Figure 21D**). Furthermore, qPCR analysis of HBV genomic DNA levels in the supernatant revealed a slight impact on HBV release in Alix gene-deficient cell lines as compared to non-target cells (**Figure 21E**).

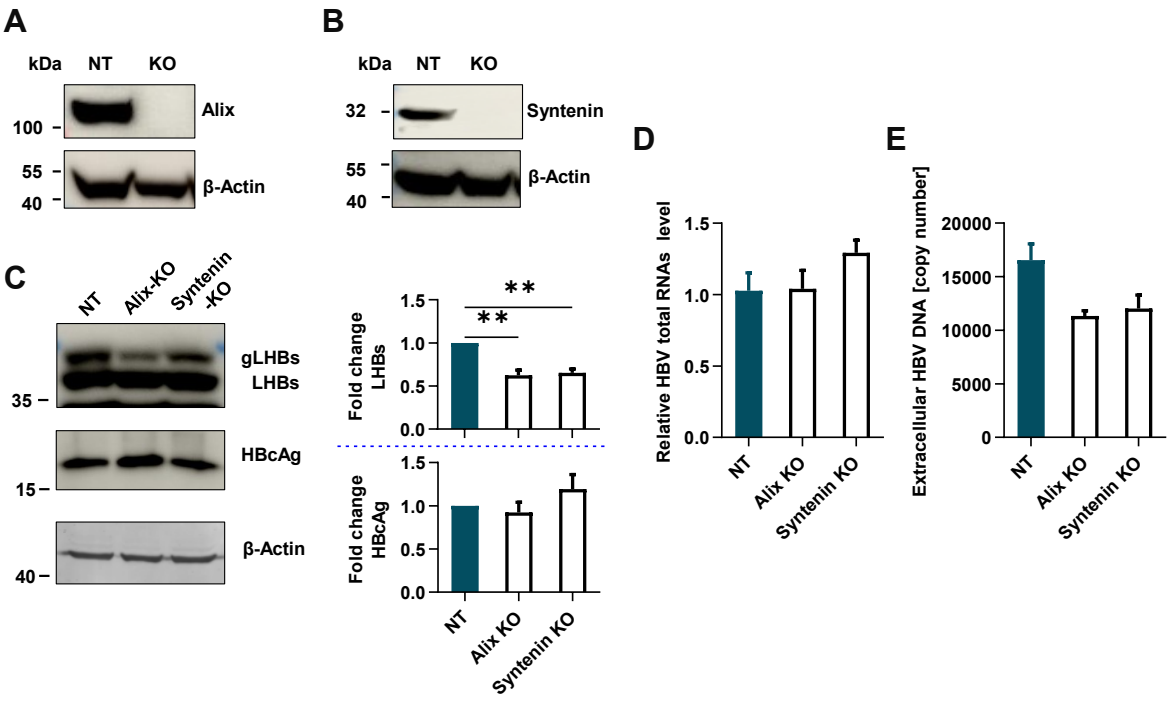

Figure 21. Impact of CRISPR/Cas9-mediated knockout of Alix or Syntenin on HBV replication and HBsAg production in HepAD38 cells. (A/B) Western blot analysis of the endogenous Alix or Syntenin in cell lysates from Alix-deficient (A) or Syntenin-deficient HepAD38 cells (B). Loading control was the detection of β-actin. **(C)** Relative amounts of intracellular LHBs and HBcAg from Alix- or Syntenin-knockout HepAD38 cells. In the left panel showed the typical western blots of LHBs, HBcAg and β-Actin. Relative quantitative analysis was shown in the right panel for fold change compared to non-target cells (NT). ** $P < 0.01$. **(D)** Expression levels of HBV total RNA in Alix- or Syntenin-knockout HepAD38 cells. Quantification was performed by reverse transcription qPCR. Relative levels to RPL27 mRNA were compared with non-target cells (NT), the fold change was plotted. **(E)** The absolute quantification of extracellular HBV DNA was performed by qPCR from non-target (NT) or Alix- or Syntenin-knockout HepAD38 cells. Unpaired parametric t-tests were used for all panels.

Afterwards, the supernatants collected from these cell lines were submitted to differential centrifugation and then subjected to iodixanol gradients, as indicated in **Figure 12A**. Quantification of HBV genomic DNA distribution in iodixanol gradients of Alix- silenced HepAD38 cells and non-target cells was performed by qPCR (**Figure 22A**). Since in the Alix-deficient HepAD38 cell line the release of HBV was mildly affected and the number of HBV was decreased both in the exosome- and the free HBV viral-fractions compared to the non-target cells (NT) (**Figure 22A**), the fold changes of each fraction compared to HBV virions fraction 12 in gradients was analyzed and displayed in **Figure 22B**.

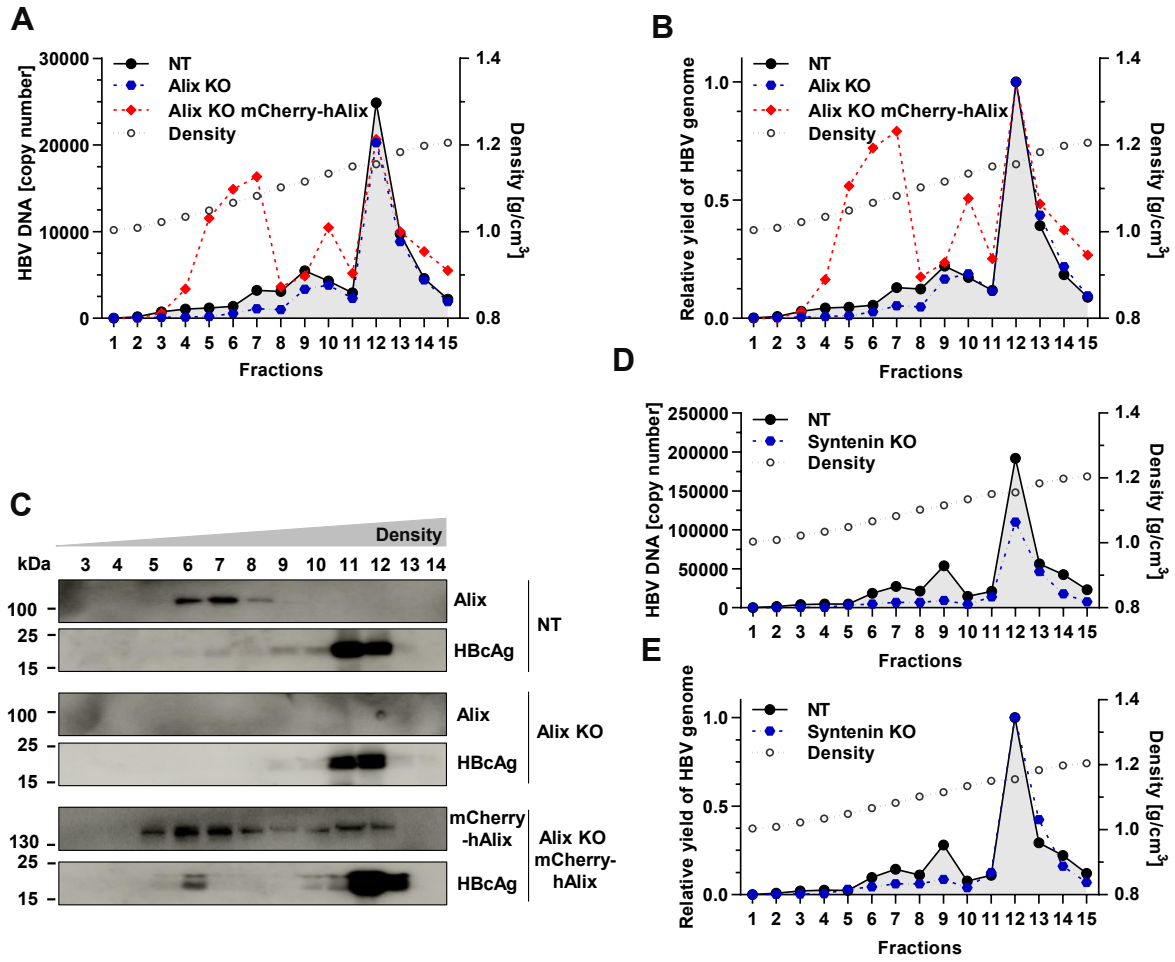

Figure 22. CRISPR/Cas9 mediated knockout of Alix or Syntenin in HepAD38 cells impairs the release of exosomal HBV virions. (A/B) HBV genomic DNA profiles over iodixanol gradients of exosomes enriched from the culture fluid of non-targeted HepAD38 cells (NT, black line), of Alix gene **silencing** HepAD38 cells (blue dotted line) and of Alix gene silencing HepAD38 cells rescued by mCherry-Alix over-expression (red dotted line). Quantification of the viral genome was performed by qPCR. At Figure 22A the absolute quantification was shown. Figure 22B showed the fold change of each fraction in the gradients against fraction 12. **(C)** Western blot analysis of fractions from the iodixanol gradient in Figure 22A/B with Alix-specific and HBcAg-specific antibodies. **(D/E)** HBV genomic DNA distributions over iodixanol gradients of exosomes enriched from the culture fluid of non-targeted HepAD38 cells (NT, black line) or of Syntenin gene knockout HepAD38 cells (blue dotted line). Quantification of the viral genome was performed by qPCR. At Figure 22D the absolute quantification was shown. Figure 22E showed the fold change of each fraction in the gradients against fraction 12.

Quantitative analysis of the viral genome for the gradients by qPCR revealed a significant reduction in the number of HBV genomes at the exosome peaks (fractions 6 and 7) in Alix-deficient cells (**Figure 22A/B**). Using western blot analysis of Alix- and HBc antigen-specific antibodies showed that Alix and HBcAg were co-present in fractions 6 and 7 in the case of non-target cells (NT) (**Figure 22C**). However, in KO cells, Alix-specifc signals were

undetectable, and signals of HBcAg in the exosomal fraction (fractions 6 and 7) were also not detectable (**Figure 22C**).

As demonstrated by qPCR (**Figure 22A/B**) and HBcAg-specific western blotting (**Figure 22C**), rescuing Alix-deficient cells by overexpression of mCherry-hAlix, nevertheless, restored the release of exosomal HBV from these cells. The detection of protein mCherry-hAlix in the exosomal fraction of the gradient demonstrated the effectiveness of the rescue (**Figure 22C**). In addition, it appears that Alix overexpression altered the size or the subtypes of exosomes, as the exosomal HBV was shifted marginally to a lower density. Alternatively, Alix overexpression could lead to excessive exosome release, which could also potentially lead to an altered distribution over the density gradient compared to non-target cells (**Figure 22A/B**).

Furthermore, the influence of knockout Syntenin on exosomal HBV release has been studied. Syntenin interacts with Alix through the motif-LYPXnL and contributes to the generation of intraluminal vesicles which constitute the main source of exosomes. HepAD38 cell-based stable Syntenin-deficient cell lines were generated by CRISPR/Cas9 system. The effective elimination of endogenous Syntenin in HepAD38 KO cells was demonstrated by western blotting (**Figure 21B**). HBV replication and HBsAg production were investigated in the Syntenin-deficient HepAD38 cell line, and the results revealed comparable amounts of intracellular HBcAg (**Figure 21C**), total intracellular HBV RNA levels (**Figure 21D**) and HBV genomic DNA in the supernatants (**Figure 21E**) in comparison to non-target cells. In addition, like the silencing of Alix, in Syntenin knockout HepAD38 cell lines a lower number of N-glycosylated species of LHBs was detected (**Figure 21C**). Similarly, qPCR of the iodixanol gradient fractions found a reduced number of HBV genomes in the exosome fractions from Syntenin-KO cells (fractions 6 and 7) when compared to the exosome fractions from non-target cells (NT) (**Figure 22D/E**).

Taken together, these data suggest that diminishing exosome formation/release prevents the release of membrane-encapsulated HBV-particles.

5.6 Visualization of exosome encapsulated HBV particles by transmission electron microscopy

The method of visualizing exosomes most widely utilized is to negative stain them and then perform imaging analysis via transmission electron microscopy (TEM) [274]. However, because of the fact that negative staining is restricted to the surface and is unable to penetrate the phospholipid bilayer [305], this approach is not sufficient to characterize the inner structure of exosomes. Therefore, ultrathin sections of 4 % paraformaldehyde fixed exosomes were observed to visualize the presence of HBV particles inside of the exosomes.

TEM imaging of Epon-embedded exosomal sections and exosomal cryo-sections with methylcellulose/uranyl acetate staining revealed that virion particle structures of approximately 45 nm in diameter were detected frequently within exosomal membrane structures (**Figure 23A**). Furthermore, in exosomal cryo-sections, the dense viral envelope around the nucleocapsid could be observed at membrane concealed viral particle structures (**Figure 23A**, asterisk).

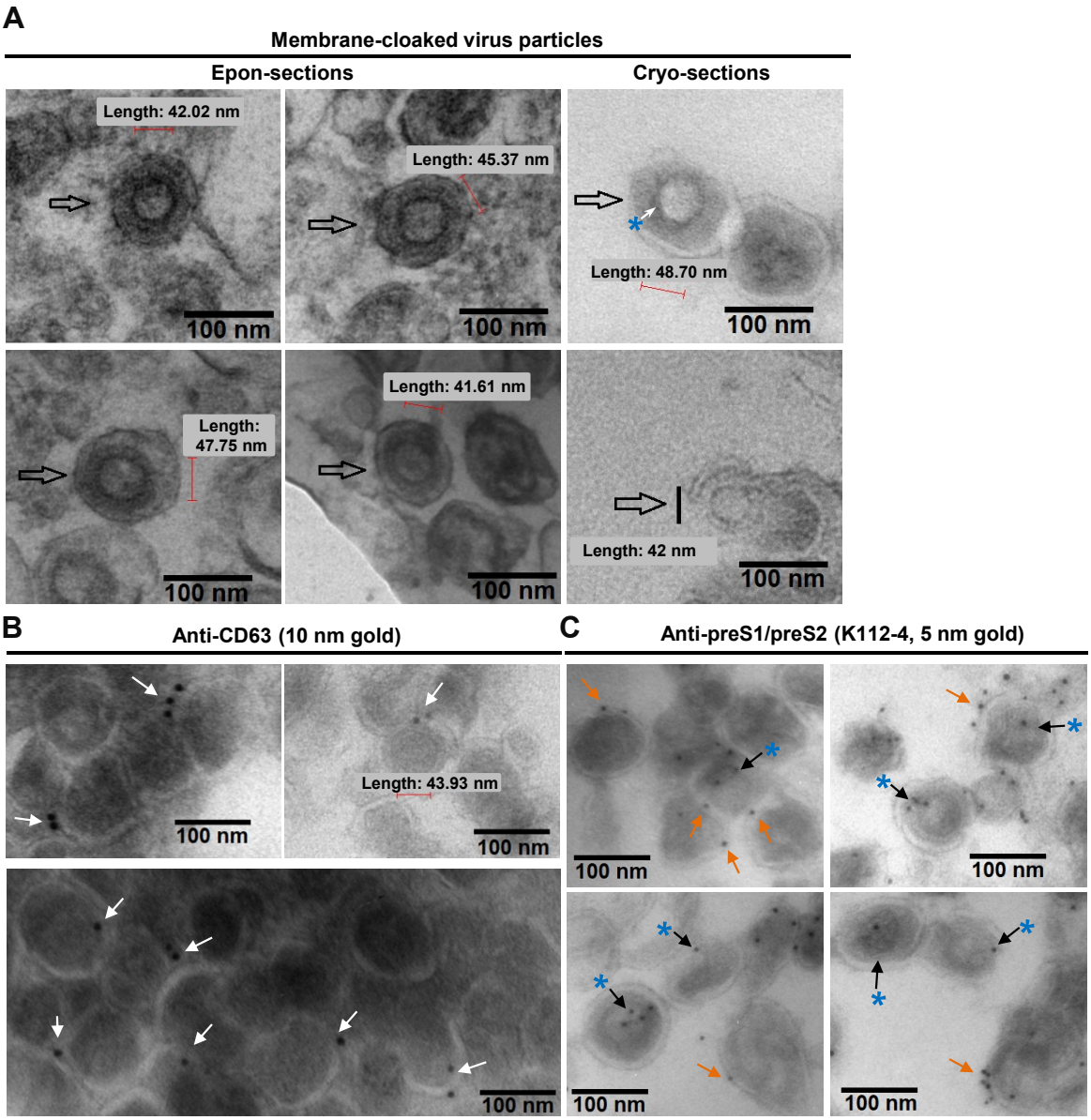

Figure 23. Ultrathin section of exosomes released from HepAD38 cells visualized by transmission electron microscopy. (A) TEM images of ultrathin sections of 4 % paraformaldehyde plus 0.1 % glutaraldehyde fixed exosomes revealing virions surrounded by a membrane-based structure (highlighted by arrows). Epon-embedded exosomal sections were shown on the left and exosomal cryo-sections were shown on the right. An asterisk shows that within the membrane structure, the dense envelope of virion stands out from its encapsulated nucleocapsid. **(B/C)** The ultrathin thawed exosomal cryo-sections were immunogold labeled with an antibody anti-CD63 (exosomes marker, 10 nm gold particles) or an anti-preS1/preS2 domain specific serum (designated as K112-4) (5 nm gold particles). The specific colloidal gold labeling was indicated with arrows. The

asterisks denoted that anti-LHBs gold particles were localized at identifiable membrane closed virus like particles (5 nm). The membrane surface of exosomes from cryo-sections was also tagged with anti-LHBs gold particles (shown by orange arrows).

To further confirm the discovery that indeed complete HBV virions were discovered in the exosomal structures, the ultrathin thawed exosomal cryo-sections were immunogold labeled with either an antibody anti-CD63 or a specific antiserum targeting the LHBs preS1/preS2 domain. As shown in **Figure 23B**, the specific colloidal gold labeling of CD63 was discovered to be located on the membrane surface of these sectioned vesicles. The specific tagging of LHBs was observed towards the lumen of some vesicular exosomes, in some cases clearly identifiable sequestered viruses were found (**Figure 23C**, asterisk). Furthermore, as further demonstrated in **Figure 23C** (orange arrows), specific labeling of LHBs could also be detected on the surface of some exosomes.

Collectively, the electron microscopic imaging and immunogold labeling analysis support the finding that exosomes generated from HBV-producing cells carry intact HBV virions.

5.7 Infectious ability of the HBV hijacked exosomes

To study if the exosomes generated from HBV-producing cells are infectious, the iodixanol gradient separated exosomal fractions (fractions 8 and 10) and the fractions that represent free viruses (fractions 13, 14) were prepared and applied to infect HepG2 cells (non-susceptible for HBV infection) or differentiated HepaRG cells (dHepaRG, susceptible to HBV infection) (**Figure 24A**).

Here, instead of inoculating with the equivalent multiplicity of infection (MOI), the identical volume of each fraction from the same gradient was used in the inoculum. This was designed to control the possible influences caused by free virions contaminations, as the number of free virions was expected to be higher in the later exosome fractions.

HBsAg-ELISA analysis of the supernatant obtained from inoculated HepG2 cells showed neither the exosomal HBV particles (fraction 8) nor the virions (fraction 13) could establish infection in HepG2 cells (**Figure 24B**).

Nevertheless, in the case of inoculation with dHepaRG cells, a productive infection by using the exosomal HBV fraction (fraction 8) pre-incubated with an anti-His control antibody could be obtained (**Figure 24C**). The infection was blocked by the monoclonal anti-preS1 antibody MA18/7 that binds to the receptor binding domain (RBD) (**Figure 24C**).

Compared to the pure exosome fraction (fraction 8), the posterior fraction 10, more closely to the free viral fraction, had not initiated productive infection (**Figure 24C**). This demonstrates implicitly that infections founded by pure exosome fraction were exclusively triggered by exosome carried intact HBV virion and argument for the possibility of being contaminated by

free viruses. Because in case of the presence of free virus contamination, there should be more free virus available in fraction 10.

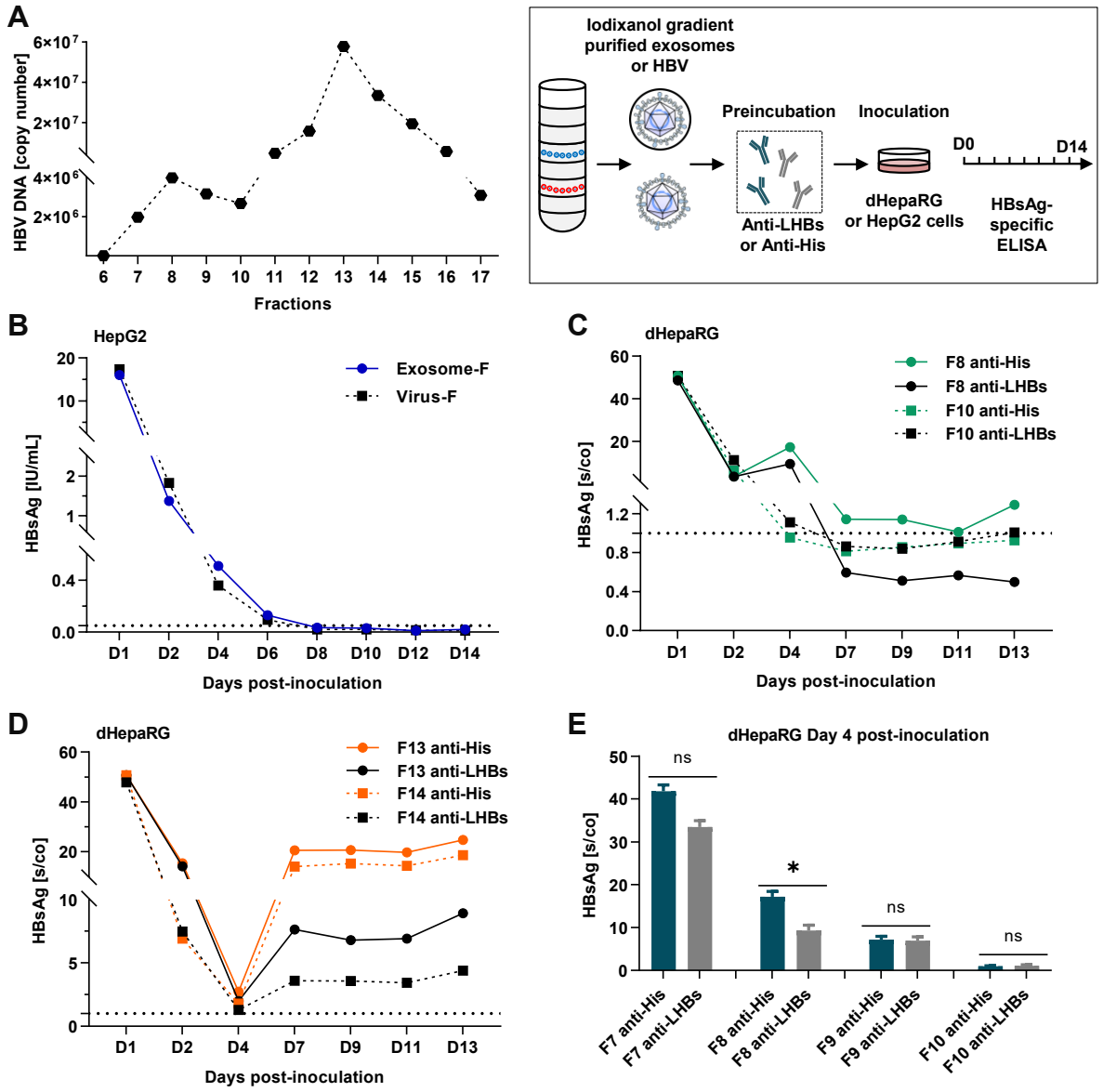

Figure 24. Density gradient separated exosomal HBV and free HBV inoculated with HepG2- and differentiated HepaRG cells. (A) Absolute quantification of HBV genomic DNA copy number in exosomal inoculum and free viral inoculum separated by density gradient and shown on the left. The right panel shows a schematic description of the infection procedure. **(B)** Detection by HBsAg-ELISA of HepG2 cell supernatants that were inoculated with exosomal HBV virus or free HBV virus. The culture medium was replaced at the designated time-points and subjected to HBsAg ELISA analysis. **(C)** HBsAg-ELISA analysis of the supernatant obtained from the inoculated differentiated-HepaRG cells. The cells were inoculated with either fraction 8 representing purified exosomal HBV or the later less pure exosomal fraction 10, and the inoculum was derived from the same iodixanol gradient. Before inoculation, the inoculum was pre-incubated with antibody MA18/7 (specific anti-LHBs, 1 µg/mL) or a control anti-His specific antibody (monoclonal, 1 µg/mL). The culture medium was changed at the designated time-points and subjected to HBsAg ELISA analysis. **(D)** HBsAg-ELISA analysis of the supernatant obtained from the free HBV viral fractions 13 and 14 inoculated differentiated-HepaRG cells. The inoculum was pre-incubated with antibody MA18/7 (specific anti-LHBs, 1 µg/mL) or a control

anti-His specific antibody (monoclonal, 1 µg/mL). The culture medium was changed at the designated time-points and subjected to HBsAg ELISA analysis. **(E)** HBsAg-ELISA analysis of the supernatant obtained from the inoculated differentiated-HepaRG cells. The inoculums were from the same iodixanol gradient fraction 8 representing purified exosomal HBV or the later less pure exosomal fraction 9 and 10. Before inoculation, the inoculum was pre-incubated with antibody MA18/7 (specific anti-LHBs, 1 µg/mL) or a control anti-His specific antibody (monoclonal, 1 µg/mL). The culture medium was changed at the designated time-points and subjected to HBsAg ELISA analysis. Here the HBsAg levels at day 4 of samples preincubated with different antibodies were compared. Nonpaired parametric t-tests was used, ns, not significant. ** P < 0.01. *** P < 0.001. The horizontal dashed line in Fig. B-D represents the cut-off value. S/CO in Fig. B-E represents the signal of sample to cut-off value.

The effective infection resulting from incubation with purified virus fractions (part 13/14) is evidenced by the start of new HBsAg production after day 4. Preincubation with MA18/7 antibody that binds to the RBD compromised the infection (**Figure 24D**).

Regarding the release of HBsAg, there was a significant difference between cells infected by the exosome fraction and by the free virus fraction. The HBsAg input in the case of exosomal infection was not decreased as continuously as the free viral fraction until day 4. In the case of exosome incubation, an initial decline of HBsAg levels was interrupted by a re-emergence of HBsAg levels on day 4, and subsequently a further decline in HBsAg. Interestingly, the resurgence at day 4 of HBsAg release was influenced by preincubation with MA18/7 antibody, indicating that the LHBs-RBD might be required by this process (**Figure 24E**).

In differentiated HepaRG cells, the outcome of the infection indicated that the appearance of LHBs at the exosome membrane seems to be functional for the internalization/uptake of the exosomes that originate from HBV-producing cells. In this case, the exosome-encapsulated HBV virus can enter the host cells with the help of the NTCP interacting with LHBs.

With the aim of elucidating the potential contribution of NTCP in the infection initiated by exosome-wrapped virus, Myrcludex B, an HBV L protein-based synthetic peptide, was employed to prevent NTCP-LHBs mediated infection in differentiated HepaRG cells. As shown in **Figure 25A**, the productive infection generated by incubation with gradient-purified virus (part 13) was inhibited efficiently by Myrcludex B, demonstrating a robust resistance to NTCP-LHBs mediated entry. In parallel, exosomal HBV infection was impaired in differentiated HepaRG cells as the NTCP pathway was interrupted, showing a reduction in newly synthesized HBsAg in Myrcludex B incubated cells as compared to the untreated group (**Figure 25B**).

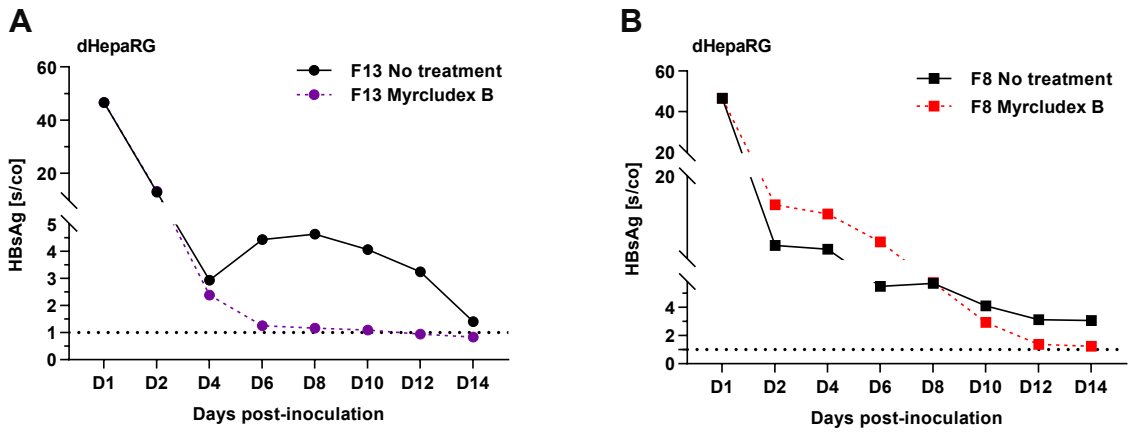

Figure 25. HBsAg-ELISA analysis of the supernatant obtained from the inoculated differentiated-HepaRG cells. The cells were inoculated with either free HBV virions fraction 13 **(A)** or fraction 8 representing purified exosomal HBV **(B)**, and the inoculum was derived from the same iodixanol gradient. During infection, 500 nM of Myrcludex B was added and the group without Myrcludex B was used as a control. The culture medium was changed at the designated time-points and subjected to HBsAg ELISA analysis. The horizontal dashed line represents the cut-off value. S/CO represents the signal of sample to cut-off value.

In summary, these data show that the exosome fraction derived from HBV-producing cells could trigger infection in HBV-susceptible differentiated HepaRG cells. The infection can be prevented both through anti-LHBs neutralizing antibody (MA18/7) and HBV entry inhibitor Myrcludex B. This suggests that the LHBs identified on the surface of exosomes are likely participating in the attachment/entry process in a LHBs/NTCP-mediated manner, or that the virus is released when exosome attachment to the cell surface and then enter the cell via the NTCP receptor complex. It appears in any case that infection in differentiated HepaRG cells is partially dependent on LHBs/NTCP, as the same input could not function in HepG2 cells. It does not eliminate the fact that exosome-dependent uptake of encapsulated virus is possible through exosome/cell surface interactions in the presence of a high number of exosomes that are absent of LHBs on the surface.

6 Discussion

Recent findings have shown that many viruses can hijack exosomes for their dissemination. The overlap between viral particle formation pathways and exosome biogenesis can be cleverly exploited by viruses to gain a host membrane coat, thereby facilitating their spread and survival. Previous results have shown that HBV components, including HBV protein, HBV nucleic acid and HBV RNA, can be detected in exosomes generated from HBV-positive hepatocyte [306]. The work in this study then revealed and visualized for the first time that intact infectious HBV particles can be identified in exosomes. The existence of LHBs on the surface of these exosomes confers them the potential to impair the ability of antibodies to neutralize HBV viruses and probably also be associated to the interaction with recipient cells.

Alterations in the quantity, size, content, and composition of the membrane structure of exosomes were detected when comparing exosomes from infected and uninfected cells. These changes probably are caused by the utilization of the endosomal network of the host cells during the propagation of the viral infection and by the impact on the activity of the host cells. In case of this study, significantly different secretion level and size distribution were observed when comparing the exosome characteristics in HBV-expressing stable cell line HepAD38 cells with those of HBV-negative HepG2 cells (**Figure 12B, 12C, 13A**).

The same impact of virus infection on increased exosome production was noted in ZIKA virus infected neuronal cells as well as in Enterovirus 71 infected human colorectal cell line (HT-29) and THP-cells (a human monocytic cell line derived from an acute monocytic leukemia patient) [307]. Meanwhile, expression of latent membrane protein 1 (LMP1), an Epstein-Barr virus (EBV) encoded oncoprotein, and HIV accessory protein negative factor (Nef) also enhanced the number of exosomes secreted from HEK293 cells [308] and HeLa.CIITA cells [309], respectively. It is interesting to note that the enhanced production of exosomes by viral particles infection or viral protein expression perhaps stimulates the egress of viruses being released through the same pathway.

Similarly, larger sizes of extracellular vesicles from Herpes simplex virus 1 (HSV-1) infected cells were detected as compared to that from uninfected cells [310], which could suggest a change of the cargoes within the extracellular vesicles. Many current studies on pathogenic infections have also confirmed significant changes in the content of the exosomes, in particular the presence of viral components within their lumen. In this case, an intriguing Trojan exosome hypothesis has been proposed, whereby retroviruses hijack the preexisting exosomal pathway for their own propagation [311]. The structural similarities between virions and exosomes are the prerequisite basis for this occurrence.

The incorporation of viral factors into exosomes from virus-infected cells accelerates the similarity between exosomes and viral particles, gradually blurring the defined boundary between exosomes and viral particles [312]. This provides an opportunity for viruses to tamper with the exosomal pathway for their own usage. In this perspective, the exosomes generated by virus-infected cells that carry only viral proteins and even fragments of genetic material are not infectious as they lack the ability to multiply progeny. However, the effect of this type of exosomes to enhance viral infection processes has been found in many studies. For example, hepatitis C virus envelope glycoprotein E2 coated exosomes serving as decoys can compromise antiviral immunity by binding neutralizing antibodies [313]. Extracellular vesicles released by HIV-infected cells could promote HIV infection by increasing the number of susceptible cells through their encapsulated HIV transactivation response element (TAR) RNA [314, 315].

In other cases, intact infectious virions have also been discovered to be wrapped in exosomes [238, 242–248]. These virus-carrying exosomes are assumed to be able to generate new infections in target cells through exosomes-cell interactions rather than receptor-mediated pathways. It has been shown in many studies that both enveloped and non-enveloped viruses can be detected in exosomes. Similar to previously detected quasi-enveloped hepatitis A virus and hepatitis E virus, the identification of these host exosomal membrane wrapped HBV particles in this study blurs the classical concept of enveloped HBV particles and potentially alters the traditional understanding on HBV life cycle [316].

There is increasing evidence suggesting that the release of HBV virions, as well as of filaments depends on the ESCRT machinery and host membrane trafficking pathways [186, 188, 189, 271]. Also, MVBs have been shown to be the platforms for the egress and budding of HBV virions and filaments. It is interesting because this implies that the budding of HBV is intimately intertwined with the biogenesis pathway of exosomes. Since “Dane particles” was first identified under the EM in 1970 [317], the complete HBV virion particle is known to be an enveloped virus, with three viral surface proteins (LHBs, MHBs and SHBs) and host lipid bilayer forming its envelope [306, 317, 318]. Here, this study found that the supernatant of HBV-expressing HepAD38 cells contains two infectious groups with significantly different buoyant density. The infectious population found at the low density was wrapped in exosomes. A prerequisite for this finding is the effective separation of exosomes and free viruses. In principle, the differential ultracentrifugation-based classical exosome enrichment process used here in fact co-sediments viral particles and exosomes at the same time [312]. However, further used iodixanol density gradient centrifugation demonstrated that exosomes and HBV virions can be adequately separated according to their different sedimentation in iodixanol gradient (**Figure 13A, B**). This made it possible to deeply analyze the exosomal

cargoes without the influence of free virus. The same method was also used to separate the enveloped HAV viruses from picornaviruses [242] and the exosomes from HIV particles [277, 278].

Limited detergent treatment of the exosome population resulted in the successive release of the intact HBV particles with the subsequent exposure of naked capsids under the influence of detergent (**Figure 15B, 17B, 17D**). These approaches were also successfully applied to identify additional host membrane enveloped viruses [243], to explore the types of exosomal cargoes [319] and to characterize the membrane stability of exosomes [303]. It is well known that the outer surface coat of HBV virions is detergent-sensitive, a core particle is able to be released from the Dane particles after treatment with mild nonionic detergents [302]. These conditions also cause a partially or complete disruption of exosomal membranes [303]. Therefore, the detergent sensitivity of exosomal membrane [303] and the outer envelope of HBV [302] together with their distribution properties in density gradient provided us an opportunity to demonstrate that complete HBV particles could be encapsulated in these highly purified exosomes.

Many pharmacological agents have been tried to inhibit the release of exosomes. To further determine the egress pathway of membrane-encapsulated HBV, three different MVBs/exosome inhibitors were chosen in this study, all of which compromised the release of exosomes and exosome-wrapped HBV in varying degrees. Recent studies have investigated the effect of U18666A on the dysfunction of MVBs by interfering with cholesterol and NPC1 protein trafficking in the endosomal/lysosomal system [189, 304, 320]. In the present study, the abnormal distribution of Alix and the almost undetectable Tsg101 in the exosome fractions resulting from U18666A treatment also demonstrated its effect on attenuated exosome formation (**Figure 19B**). As the MVBs system is associated with the release of infectious HBV particles and subviral filaments, the inhibitory effect of U18666A on the release of LHBs was observed in Huh 7.5 HBV-expressing cells [189], but the synthesis of LHBs was not obviously influenced. The U18666A concentrations used in this study were also found with no significant effect on the intracellular LHBs and HBcAg levels in HepAD38 cells as well as the total intracellular HBV RNA levels (**Figure 20A-C**). Meanwhile, the amount of released membrane-unassociated HBV particles that were found at high density was not significantly affected by U18666A treatment (**Figure 19A**).

The choice of Manumycin A and GW4869 two inhibitors is because the biogenesis of MVBs/exosomes is associated with two different mechanisms. Manumycin A can specifically inhibit ESCRT-dependent MVBs/exosomes biogenesis by blocking the Ras signaling pathway. It is therefore characterized as particularly affecting the trafficking of extracellular vesicles. A previous study also found that the use of 250 nM Manumycin A resulted in a 50-

60% reduction in exosome production in the prostate cancer cell lines [321]. GW4869 has been identified to inhibit exosomes by affecting lipid metabolism and is currently the more widely used exosome inhibitor. In this case, GW4869 prevents the secretion of ESCRT-independent exosomes by inhibiting the production of neutral sphingomyelinase and ceramide [322]. In fibroblasts, the effective blocking of exosome secretion using different concentrations of GW4869 has been extensively studied [323–325]. In other interesting studies on exosome uptake, it was found that the signal of substances delivered by exosomes was significantly reduced in recipient cells after pretreatment of donor cells with a certain concentration of GW4869 [326, 327]. In a similar manner, GW4869 has been used to explore exosome-mediated cell-to-cell transmission of hepatitis E virus [328] and porcine reproductive and respiratory syndrome virus [329]. Presently, there is no evidence suggesting that Manumycin A or GW4869 have a direct effect on HBV release, and this study also showed that the presence of these inhibitors did not interfere with HBV replication and HBsAg production in HepAD38 cells (**Figure 20A-C**). Thus, the reduction of HBV signals in the exosome fraction was indeed caused by specific inhibition of exosome production (**Figure 19C-E**).

The inhibition of exosome secretion was not accompanied by a remarkable change in the number of released membrane-unrelated free viral particles (**Figure 19A, 19C-D**). This indicates that there is no obvious flow between these two routes, or that the cells have saturated their capacity to release further free viruses. Furthermore, the data are against the likelihood that a portion of the free virus is formed by the disintegration of exosomes. If this was the situation, the reduction in the release of exosomes would be correlated with a decline in the amount of free virus. However, it cannot be strictly excluded that a decrease of exosomally derived free HBV virus is being compensated by an increase of the released free HBV particles.

In studies where exosomes are affected by inhibitors or related proteins, WB blot is mostly used to detect changes in the levels of exosome markers, in combination with density gradient distributions can then capture the effect on exosome size. But a further combination of nanoparticle tracking analysis or electron microscopy techniques would offer a more intuitive way of determining the impact on exosome characteristics.

The ability of exosomes to carry HBV out of host cells was also further confirmed by the establishment of Alix or Syntenin-deficient cells. Studies of gain and loss of function clearly demonstrated the correlation of Syntenin-Alix with the forming of intraluminal vesicles and the sorting of specific cargoes into exosomes [228, 330, 331]. Exhaustion of Syntenin impairs the turnover of exosomes, indicating an impact on the loading capacity of the cargoes [332]. Therefore, the decrease of exosome-associated HBV observed after knockout of Syntenin

(**Figure 22D-E**) in this study is insufficient to conclude that Syntenin is engaged directly in targeting HBV into exosomes. Nevertheless, following rescue of Alix-deficient cells through over-expression of the fusion construct mCherry-Alix, exosomal HBV release was dramatically elevated without affecting the release of membrane-unassociated HBV viruses, highlighting the importance of the Alix in correlating with exosomal HBV release (**Figure 22A-C**). In line with previous study, the deficient and rescue data obtained here provide additional evidence that Alix is dispensable for the egress of the free HBV particles [194].

The existing evidence points to a role for Alix functioning in HAV [242, 333], HIV and equine infectious anemia virus (EIAV) budding [334–338]. Generally, proteins that interact with Alix usually have one or more motifs, called late (L) domains (LYPx (n)L or YPx(n)L/I), that are specifically recognized by Alix protein. The VP2 protein of HAV is thought to interact with Alix through the two YPx(n)L/I motifs it contains [316]. Newly assembled HAV particles are assumed to bud into the MVBs by this interaction, thereby acquiring the host cell membrane and resulting in encapsulation [316]. Immunoprecipitated Alix can co-precipitate the intracellular HAV particles and exhaustion of Alix causes the release of HAV to be compromised [242]. Therefore, Alix is an essential protein for the encapsulation of HAV. Similarly, the LYPx (n)L motif in the EIAV p9 domain of Gag can mediate the interaction with the Alix host protein [334]. By interacting with the L domain present in HIV Gag p6, Alix becomes an element for the HIV viral budding machinery [334–338].

Interestingly, the HAV pX protein, which lacks the late (L) domains, is currently found to be also involved in quasi-enveloped HAV biogenesis and interacted to Alix through its C-terminus [333]. Due to the deficiency of late (L) domains, the mechanism of pX interaction with Alix remains unclear. However, it is noteworthy that the putative ubiquitination signals contained in pX are a common signal for the ESCRT sorting of cargo [339]. And Alix is available as a ubiquitin receptor that sorts ubiquitinated cargo to ILVs and MVBs through the ubiquitin-binding domain of its central V structural domain [226, 227].

HBV envelope proteins also naturally lack these motifs (LYPx (n)L or YPx(n)L/I). So far, whether HBV can hijack an Alix/ESCRT-associated pathway to sort HBV into exosomes remains unclear. Sequence analysis of HBV envelope proteins revealed an LPxF motif located in the HBV S domain, which is a conserved variant of canonical PY motif (L/PPxY) [340]. The PY motif was found to interact with the WW domains of the E3 ubiquitin ligase Nedd4 [340, 341]. Viral proteins possessing the PY motif recruit Nedd4 mediated ubiquitination to bud from the host cells [342]. More interestingly, Nedd4 mediated ubiquitination of Alix facilitates HIV-1 release through the LYPx (n)L Alix budding pathway [343]. The possibility that the LPxF motif in the S domain of HBV envelope protein affects the formation of exosomes encapsulating HBV requires further experimental demonstration.

However, as shown in the results of this study in **Figure 14B and 14C**, since membrane-encapsulated virus is not the predominant mode of hepatitis B virus release, the formation of exosome-encapsulated HBV cannot be excluded as an incidental possibility of long-term crosstalk between the virus and the host cells. If host factors are involved in the hitchhiking of HBV on exosomes, it remains an interesting but unknown challenge under which conditions the exosomal membrane-encapsulated virus is triggered and under which conditions it is released as free virus via the MVBs platform.

Two other interesting exosomal proteins, CD63 and Tsg101, were proven to be involved in the integration of LHBs in the HBV envelope [344] and in HBV release through interaction with α-taxilin [185], respectively. It is likely that these processes also facilitate the formation of exosomal HBV viruses, as they have both been shown to be essential for the biogenesis of MVB/exosomes [229, 345]. It would therefore be interesting to explore their functions in further detail. Previous study reported that depletion of Tsg101 by siRNA can inhibit the release of HEV from infected cells [244]. At the same time, Tsg101 was shown to bind specifically to HEV ORF3 via a late PSAP domain motif at its C-terminus [244, 245]. The third open reading frame, ORF3, encoded by the HEV genome is thought to mediate the envelopment of HEV [346–348]. Although it is still not completely clear how exactly ORF3 facilitates the envelopment and exit of HEV. But most evidence shows that ORF3 contributes to HEV budding through MVBs. The interaction of Tsg101 with ORF3 directly contributes to HEV egress via the MVB/exosomal pathway [244, 245, 328].

The existence of complete virus inside the exosome was further confirmed by electron microscopic analysis. Ultrathin sections are a useful method for visualising the inner luminal structure of exosomes [349–351]. In this method, the enrichment of a visible exosome pellet is a prerequisite for ultrathin sectioning. Based on this, the presence of HBV within the exosomal structure was directly demonstrated by the immunogold labeling of the exosomal ultrathin sections in this study (**Figure 23**). Ultrastructural appearance with exosomal shape and size characteristics was also presented in previous studies [305, 349–351]. A study of immunogold-staining EM combined with ultrathin sections of cryofixation-fixed exosome blocks also successfully detected lysyl-tRNA synthetase in the lumen of exosomes. An additional interesting point is that exosomes often show in negative staining the cup-like structure that is considered to be their typical shape. However, it was discovered in previous research that sections of block exosomes prepared by chemical fixation or cryofixation showed round structures rather than cup-shape in cryo-TEM, in this case enabling the observation of hydrated exosomes and reducing the dehydration defects [352]. TEM images of ultrathin sections of chemically fixed exosomes from this study also show the same structure of rounded exosomes. In addition, the labelling of anti-CD63 or anti-LHBs in this

study was specific but inefficient (**Figure 23B, C**). Higher concentrations of primary antibodies and increased incubation times were tried here to help improve efficiency, but no increase was seen, and the low labeling efficiency was probably due to some antigenic determinants being disrupted during fixation.

As we know, HBV viruses exploit a variety of strategies such as secreting large numbers of subviral particles to evade host immune system monitoring thereby enhancing their replication capacity, while the exact mechanisms involved are still elusive. Similar to the potential functionality of classical subviral particles (spheres and filaments) in HBV to deviate the immune system surveillance [353], it is likely that LHBs decorated exosomes are conferred with similar functions. In another study, extracellular vesicles were reported to transmit viral DNA into hepatocytes during HBV infection and indicated that this represents an alternative pathway of antibody-neutralizing resistance in HBV infection [354]. In addition to turning the exosome itself into a decoy to capture neutralizing antibodies, exosomes derived from virus-infected cells can also suppress the immune response in a variety of ways. A previous report claimed that exosomes from the serum of chronic hepatitis B patients could cause impaired proliferation and survival of NK cells [355]. Monocytes are induced to express programmed-death ligand-1 (PD-L1), a negative immunomodulatory molecule, after uptake of exosomes secreted by HBV-infected cells [356]. At the same time, this process is associated with the downregulation of the expression of CD69, a marker of activated immune cells [356, 357]. It is further speculated that these processes probably contribute to the depletion and inactivation of T cells in chronic HBV infection [306]. Furthermore, a study on the HBx protein indicated that HBx could export APOBEC3G, an antiviral substance, from HBx-expressing cells via exosomes, and this process was hypothesized to impair the inhibitory effect of APOBEC3G on HBV replication [358]. In other cases, exosomes released from virus-infected cells have been shown to inhibit the activation of $CD4^+$ and $CD8^+$ T cells, thereby enhancing infection [196]. An interesting study found that in Herpes simplex virus-1 infection, its encoded glycoprotein B could divert HLA-DR (a MHC class II cell surface receptor) into the MVBs or exosomes, thereby reducing the number of peptide-MHC complexes on the surface of its infected cells and thus evading the immune tracking system [359].

In HBV infection, a further function of subviral particles is to enhance viral infection [52]. The same function appears to be performed by exosomes from HBV-positive cells, and it is likely that by LHBs on the surface of the exosomes this enhancement is exerted. It has previously been found that microvesicles released by human cytomegalovirus-infected cells increase the susceptibility of recipient cells by delivering soluble DC-SIGN (a C-type lectin receptor) in a complex with viral glycoprotein B [360]. Exosomes and other extracellular vesicles released

from HIV infected cells (peripheral blood mononuclear cells (PBMCs) or megakaryocytes) could enhance susceptibility to HIV by transferring chemokine receptors, CCR5 and CXCR4, to target cells [361, 362]. Currently it has not been reported that exosomes released from HBV infected cells can influence the susceptibility of recipient cells by presenting relevant factors.

If exosomes carrying LHBs could attract neutralizing antibodies, this would require the virus to be able to escape from the antibody-decorated exosomes prior to opsonization, or as described in some reports, it might be an (inefficient) strategy for infecting non-liver tissues. Classically, HBV is a highly hepatotropic, non-cytopathic DNA virus. This high degree of species specificity and tissue tropism is thought to be due to the exclusively expressed hepatocyte-specific receptor NTCP or more as-yet unidentified, hepatocyte-specific co-receptors or host determinant(s) [81, 363, 364]. However, HBV antigens and DNA have been found in non-liver tissues, including gastric mucosa, PBMCs, and kidney, even though NTCP expression is lacking there [365–368]. This indicates that non-receptor-mediated (inefficient) viral uptake could occur in HBV transmission, like recent studies of HCV showing that spread of the virus can occur via exosomes [369, 370]. In the present study, it failed to produce efficient infection by exosomal HBV in non-permissive HepG2 cells (**Figure 24B**). It could be because the number of exosomes used for infection is relatively low, or that HBV as a cargo/LHBs embedded in exosomal membranes act as receptor-binding domain influencing the target specificity of these exosomes. If the uptake of exosomal HBV in non-hepatic target tissues is inefficient, this would be consistent with previous studies concerning the existence of HBV (infection) in non-liver tissues. Additionally, the inefficient infection in non-liver tissues could be due to the limited amount of simultaneously uptaken exosomal HBV. At the same time, there are some studies reporting that the kept low infection/replication of HBV in non-liver tissues is probably due to the high level of expression of HBV transcriptional repressors in these cells, like the defined Slug and Sox7, and/or due to the lack of liver-enriched transcription factors associated with HBV transcription in these non-liver tissues, as well as the inability to forming cccDNA [363, 371–374].

In addition, NTCP appears to play a role in the establishment of infection by exosomal HBV in differentiated HepaRG cells. Because in this study, anti-LHBs neutralizing antibody (MA18/7) and HBV entry inhibitor Myrcludex B could prevent infection in differentiated HepaRG cells (**Figure 24C, 25B**). Several modes of action could exist there. Interaction of hepatocytes with exosomes regulated by LHBs present on the surface of exosomes is prevented, which hinders the following internalization of exosomes. Alternatively, it is likely that exosomes disassemble in close vicinity to the target cell membrane to release viral particles, the released viruses are bound by the neutralizing antibody MA18/7, or its specific

NTCP mediated entry pathway is blocked by the presence of Myrcludex B. In this case, exosomal HBV entry could take place in the same way (via the HBV receptor NTCP) as for non-exosome associated viral particles. These hypotheses are in line with the widely acknowledged tissue tropism of HBV.

In summary, this study reveals the presence of complete HBV virus in exosomes. These HBV particle-carrying exosomes could transmit infection into differentiated HepaRG cells. This formerly unidentified strategy of encapsulating HBV particles within exosomes is likely as an evasion strategy for immune responses and keeping the particles targeted in hepatocytes surrounded by the protection of exosomal membranes. Also, this exosomal HBV probably contributes to the HBV DNA and antigens detected in non-liver tissues. This implies that exosomes potentially significantly contribute to the transmission of HBV.

7 Summary

As one of the most widespread infectious diseases in the world, it is currently estimated that approximately 296 million people globally are chronically infected with Hepatitis B virus (HBV), the consequences of HBV infection cause more than 620,000 deaths each year. Although safe and effective HBV vaccines have reduced the incidence of new HBV infections in most countries, there are still around 1.5 million new infections each year. HBV remains a major health problem because there is no large-scale effective vaccination strategy in many countries with a high burden of disease, many people with chronic HBV infection are not receiving effective and timely treatment, and a complete cure for chronic infection is still far from being achieved.

Since its discovery, HBV has been identified as an enveloped DNA virus with a diameter of 42 nm. For efficient egress from host cells, HBV is thought to acquire the viral envelope by budding into multivesicular bodies (MVBs) and escape from infected cells via the exosome release pathway. It is clear that HBV hijacks the host vesicle system to complete self-assembly and propagation by interacting with factors that mediate exosome formation. Consequently, the overlap with exosome biogenesis, using MVBs as the release platform, raises the possibility for the release of exosomal HBV particles. Currently, virus containing exosomal vesicles have been described for several viruses. In light of this, this study explored whether intact HBV-virions wrapped in exosomes are released by HBV-producing cells.

First, this study established a robust method for efficient separation of exosomes from HBV virions by a combination of differential ultracentrifugation and iodixanol density gradient centrifugation. Fractionation of the density gradient revealed that two populations of infectious viral particles can be separated from the culture fluids of HBV-producing cells. The population present in the low-density peak co-migrates with the exosome markers. Whereas the population that appeared in the high-density fractions was the classical HBV virions, which are rcDNA-containing nucleocapsids encapsulated by the HBV envelope.

Subsequently, the characterization of this low-density population was performed, namely the highly purified exosome fraction was systematically investigated. Relying on the detergent sensitivity of the exosome membrane and the outer envelope of the HBV virus, disruption of the exosome structure by treatment with limited detergent revealed the presence of HBsAg in the exosomes. At the same time, mild and limited NP-40 treatment of highly purified exosomes and a further combination of density gradient centrifugation resulted in the stepwise release of intact HBV virions and naked capsids from the exosomes generated by HBV-producing cells. This implies the presence of intact HBV particles encapsulated by the host membrane.

The presence of exosome-encapsulated HBV particles was consequently also verified by suppressing the morphogenesis of MVBs or exosomes. Impairment of MVB- or exosome-generation with small molecule inhibitors has significantly inhibited the release of host membrane-encapsulated HBV particles as well. Likewise, silencing of exosome-related proteins caused a diminution of exosome output, which compromised the budding efficiency of wrapped HBV.

Moreover, electron microscopy images of ultra-thin sections combined with immunogold staining visualized the hidden virus in the exosomal structure. Additionally, the presence of LHBs on the surface of exosomes derived from HBV-expressing cells was also observed.

As expected, these exosomal membrane-wrapped HBV particles can spread productive infection in differentiated HepaRG cells. In HBV-susceptible cells, as LHBs on the membrane surface, this type of exosomal HBV appeared to be uptaken in an NTCP receptor-dependent manner.

Taken together these data indicate that a fraction of intact HBV virions can be released as exosomes. This reveals a so far not described release pathway for HBV. Exosomes hijacked by HBV act as a transporter impacting the dissemination of the virus.

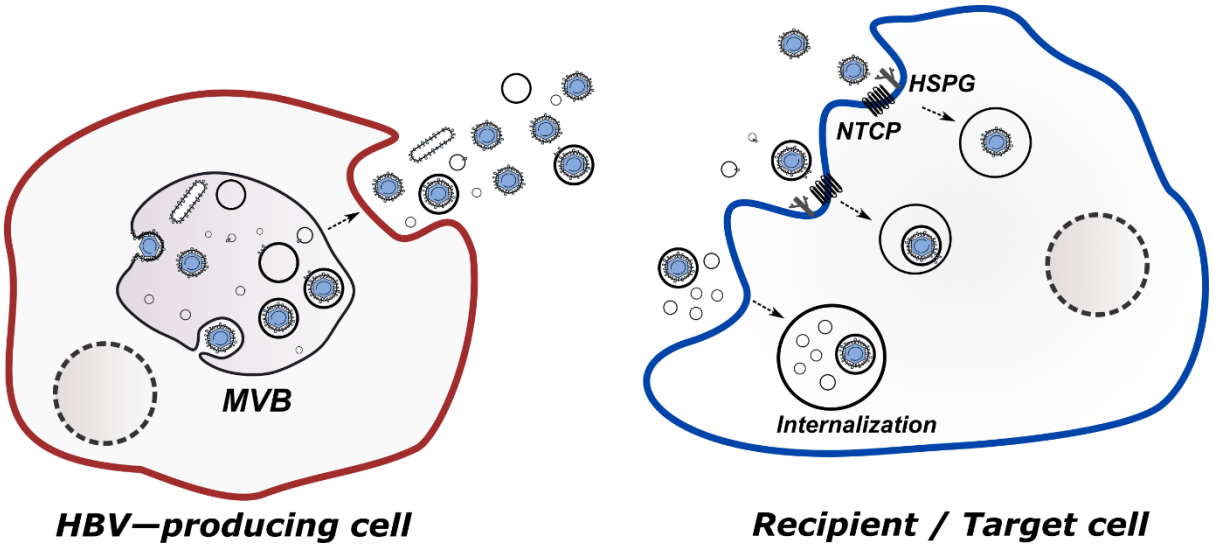

Figure 26. Schematic representation of the release and uptake pathways of exosomal HBV discovered in this study. In HBV-producing cells, host exosomes, free HBV particles, and HBV subviral filaments are released extracellularly by means of the MVB platform. Concurrently, exosomal HBV is also released via this channel, yet the mechanisms regulating this are unclear. In recipient/target cell, free HBV viral particles enter cells via a receptor-mediated approach (HSPGs and NTCP). While exosomal HBV is taken up by target cells by endocytosis (exosomal properties mediated) or receptor-dependent manner.

8 Zusammenfassung

Derzeit sind schätzungsweise 296 Millionen Menschen weltweit chronisch mit dem Hepatitis-B-Virus (HBV) infiziert und die Folgen einer HBV-Infektion führen jedes Jahr zu mehr als 620.000 Todesfällen, was sie zu einer der häufigsten Infektionskrankheiten der Welt macht. Obwohl sichere und wirksame HBV-Impfstoffe das Auftreten neuer HBV-Infektionen in den meisten Ländern verringert haben, gibt es immer noch etwa 1,5 Millionen Neuinfektionen pro Jahr. HBV stellt nach wie vor ein großes Gesundheitsproblem dar, da es in vielen Ländern mit hoher Prävalenz keine groß angelegte Impfstrategie gibt, viele Menschen mit chronischer HBV-Infektion nicht rechtzeitig und wirksam behandelt werden können und eine vollständige Heilung der chronischen Infektion noch lange nicht erreicht ist.

Das Hepatitis-B-Virus (HBV) ist ein kleines, umhülltes DNA-Virus und gehört zur Familie der Hepadnaviridae. Die äußere Hülle, die die drei viralen Oberflächenproteine LHBs, MHBs und SHBs beinhaltet, umgibt das Nukleokapsid. Die Gesamtheit aller HBV-Oberflächenproteine wird als HBsAg bezeichnet. Das ikosaedrische Nukleokapsid wird durch das Kernprotein (HBcAg) gebildet und trägt das partielle doppelsträngige DNA-Genom von etwa 3,2 kb. Das HBV-Genom besteht aus 4 offenen Leserahmen, die für die virale Polymerase (P), das Kernantigen (HBcAg) oder seine sekretorische Variante e-Antigen (HBeAg), die Oberflächenproteine (HBsAg) und das regulatorische X-Protein (HBx) kodieren. Zusätzlich zu den infektiösen Viruspartikeln setzen HBV-produzierende Zellen nicht-infektiöse subvirale Partikel frei, die nur aus HBsAg bestehen und denen ein Genom und alle anderen HBV-Proteine fehlen. Es lassen sich zwei Formen unterscheiden: 22 nm große Sphären und lange Filamente. Während die Sphären hauptsächlich aus SHBs bestehen und nur geringe Mengen an LHBs und MHBs enthalten, zeichnen sich die Filamente durch einen höheren Gehalt an LHBs aus. Darüber hinaus werden nackte Kapside ohne Hülle freigesetzt.

In den letzten 50 Jahren sind die grundlegenden Prinzipien des Lebenszyklus und der Morphogenese des Hepatitis-B-Virus (HBV) aufgeklärt worden. Diese bilden eine wichtige und wirksame Grundlage für aktuelle HBV-Behandlungen und die Entwicklung von Impfstoffen. Seit seiner Entdeckung wurde das HBV als ein umhülltes DNA-Virus mit einem Durchmesser von 42 nm identifiziert. Es wird immer deutlicher, dass die Freisetzung von HBV-Virionen und -Filamenten von der Maschinerie des endosomalen Sortierkomplexes (*endosomal sorting complex required for transport,* ESCRT) und den Wirtsmembran-*Trafficking*-Systemen abhängig ist. Für eine effiziente Freisetzung aus der Wirtszelle werden multivesikuläre Körper (*multi vesicular bodies*, MVBs) als Plattform für das *Budding* und den Austritt von HBV angenommen, wobei das reife Nukleokapsid von der Virushülle eingekapselt wird und dann über den exosomalen Freisetzungsweg aus den Zellen entweicht, wenn die MVBs mit der Plasmamembran verschmelzen. Es ist klar, dass HBV das

vesikuläre System des Wirts nutzt, um seine Selbstorganisation und Verbreitung zu vervollständigen, indem es mit Faktoren interagiert, die die Exosomenbildung vermitteln. Die Überschneidung mit der Exosomenbiogenese, bei der MVBs als Freisetzungsplattformen verwendet werden, eröffnet somit die Möglichkeit der Freisetzung exosomaler HBV-Partikel.

Zusätzlich zu den Viruspartikeln setzen Wirtszellen auch eine große Anzahl extrazellulärer Vesikel frei. Exosomen sind eine Unterart dieser Vesikel, die in Lipiddoppelschichten eingeschlossen sind und eine Größe von etwa 30 bis 150 nm aufweisen; sie teilen denselben Knospungsweg mit vielen Virionen. Insbesondere werden internalisierte Cargos in intraluminale Vesikel (ILVs) sortiert, die durch invertierte Knospung innerhalb eines intrazellulären Endosoms gebildet werden, was zum Auftreten von späten Endosomen führt und als MVBs bezeichnet wird. ILVs können abgebaut werden, während MVBs zu Lysosomen heranreifen. Alternativ könnten MVBs dann mit der Plasmamembran verschmelzen und ihre ILVs als Exosomen in die extrazelluläre Umgebung entlassen. Im Gegensatz zur Bildung von Mikrovesikeln (100-1000 nm) durch Abspaltung von Plasmamembranen werden Exosomen also durch Exozytose von mit ILVs versehenen MVBs gebildet. Es wurde nachgewiesen, dass Zellen vieler Spezies Exosomen in die extrazelluläre Umgebung freisetzen, und sie können auch in einer Vielzahl von Körperflüssigkeiten, einschließlich Plasma, Speichel und Urin, nachgewiesen werden.

Einmal freigesetzt macht die Eigenschaft des mit Exosomen assoziierten bioaktiven Materials, Teil einer Multikomponenten-Transporteinheit zu sein, dass es funktionell von einer Zelle zur anderen übertragbar ist. Die von Exosomen genutzten Eintrittsstrategien hängen von der Verteilung der Proteine und Lipide sowohl auf der Membran des Exosoms als auch auf der Zielzelle ab. Die Aufnahme von Exosomen scheint durch Endozytose oder Membranfusion zu erfolgen, was sich teilweise mit den Eintrittswegen einiger Viren überschneidet. Die von den Exosomen mitgeführten Inhalte können nach der Fusion direkt in das Zytosol der Empfängerzellen freigesetzt werden oder mit den Exosomen in das endosomale Recyclingsystem gelangen. Exosomen werden heute als zusätzlicher Träger für die lokale oder periphere interzelluläre Kommunikation angesehen - diese Art der Exosomen-vermittelten Übertragung spielt bei mehreren physiologischen Prozessen eine wichtige Rolle.

Eine wachsende Zahl von Studien belegt, dass Exosomen eine vielfältige Rolle bei der viralen Pathogenese und Übertragung spielen. Sowohl behüllte als auch unbehüllte Viren können in Exosomen eingeschlossen werden. Biochemische Analysen haben ergeben, dass die prototypischen unbehüllten Hepatitis-A- und Hepatitis-E-Viren aus infizierten Zellen als "quasi-umhüllte Viren" freigesetzt werden, indem sie vollständig in Membranen eingeschlossen werden, die Exosomen ähneln. In ähnlicher Weise kann eine produktive

HCV-Übertragung *in vitro* durch Exosomen verursacht werden, die aus HCV-infizierten Hepatomzellen freigesetzt werden. Mehrere Studien deuten auch darauf hin, dass Exosomen, die aus HIV-infizierten Zellen freigesetzt werden, den Infektionsprozess beeinflussen, da sie von HIV abgeleitete Virulenzfaktoren enthalten.

Die Tarnung viraler Komponenten oder sogar intakter Virionen in Exosomen erleichtert es Viren, sich der immunologischen Detektion zu entziehen, und ermöglicht die interzelluläre Ausbreitung von Viren durch exosomalen „Freiflug“. Die enge Verflechtung von Exosomen-Biogenese und HBV-Egression führt daher zu der Hypothese dieser Studie, ob intakte *de novo* synthetisierte Viren in HBV-produzierende Zellen freigesetzt werden können, indem sie in Exosomen verkapselt werden.

Um die mögliche Rolle von Exosomen bei der Freisetzung und Verbreitung von HBV zu klären, wurden die Eigenschaften von Exosomen, die aus den Kulturmedien menschlicher Hepatomzelllinien gereinigt wurden, systematisch analysiert. Im Allgemeinen handelt es sich bei Exosomen um kleine Vesikel im Größenbereich von 30 bis 150 nm mit einer Auftriebsdichte in bestimmten Medien von 1.08 bis 1.20 g/cm^3, was der Dichte vieler Viruspartikel entspricht. Bei der Anreicherung von Exosomen durch differentielle Ultrazentrifugation werden viele Viruspartikel parallel ausgefällt. Daher ist eine effizientere Trennmethode erforderlich, um ihre jeweiligen Funktionen zu untersuchen. In dieser Studie wurde zum ersten Mal gezeigt, dass Exosomen und HBV-Virionen in einem Jodixanol-Gradienten auf der Grundlage ihrer differentiellen Sedimentation ausreichend getrennt werden können. Dieser Gradient wurde auch verwendet, um Exosomen von HIV-Partikeln und umhüllte Viren ("eHAV") von Picornaviren zu trennen. Dies bot die Möglichkeit, exosomale Cargos im Detail zu untersuchen.

Die Fraktionierung des Gradienten zeigte, dass zwei Populationen infektiöser Viruspartikel aus den Kulturmedien HBV-produzierender Zellen abgetrennt werden konnten. Die Population im Peak mit niedriger Dichte migrierte mit den Exosomenmarkern. Im Gegensatz dazu handelte es sich bei der Population, die in den Fraktionen mit hoher Dichte erschien, um die klassischen HBV-Virionen, d.h. rcDNA-haltige Nukleokapside, die von der HBV-Hülle eingekapselt sind. Die prozentualen Profile der Exosom-assoziierten genomischen HBV-DNA und HBcAg im gesamten Input des Gradienten betrugen etwa 1,76 % bzw. 2,04 %.

Anschließend wurde die Charakterisierung dieser Population mit geringer Dichte, nämlich der hoch gereinigten Exosomenfraktion, systematisch untersucht. Da die Exosomenmembran und die äußere Hülle des HBV-Virus empfindlich auf Detergenzien reagieren, wurde durch die Behandlung mit einem schonenden Detergenz die Exosomenstruktur aufgebrochen und HBsAg in den Exosomen nachgewiesen. Gleichzeitig

führte eine milde und begrenzte NP-40-Behandlung von hoch gereinigten Exosomen und eine andere Kombination von Dichtegradientenzentrifugation zur Freisetzung von intaktem HBV-Virus aus Exosomen, die von HBV-produzierenden Zellen erzeugt wurden. Dies deutet auf das Vorhandensein von intakten HBV-Partikeln hin, die von der Wirtsmembran eingekapselt sind.

Folglich wurde das Vorhandensein von in Exosomen eingekapselten HBV-Partikeln auch durch Unterdrückung der Morphogenese von MVBs oder Exosomen nachgewiesen. Die Beeinträchtigung der MVB- oder Exosomenbildung mit verschiedenen niedermolekularen Inhibitoren hemmte auch deutlich die Freisetzung von in der Wirtsmembran eingekapselten HBV-Partikeln. Allerdings wurden in Zellen mit diesen Inhibitoren eine vergleichbare HBV-Replikation und HBsAg-Produktion beobachtet wie in unbehandelten Zellen. In ähnlicher Weise führte das *Silencing* der Exosom-zugehörigen Proteine Alix und SDCBP zu einer Verringerung der Exosomenproduktion im Vergleich zu Zellen, die nicht mit diesen Inhibitoren behandelt wurden, was gleichzeitig die Effizienz des *Budding* von eingekapseltem HBV beeinträchtigte. Diese Daten deuten darauf hin, dass die Hemmung der Exosomenbildung/-freisetzung die Freisetzung von membranverkapselten HBV-Partikeln verhindert.

Darüber hinaus wurden Ultradünnschnitte von fixierten Exosomen analysiert, um das Vorhandensein von HBV-Virionen in Exosomen zu beobachten. Die Transmissionselektronenmikroskopie von in Epoxidharz eingebetteten Schnitten und mit Methylcellulose/Uranylacetat gefärbten Kryoschnitten zeigte, dass Viruspartikel mit einem Durchmesser von etwa 45 nm häufig in exosomalen Strukturen nachgewiesen wurden. Darüber hinaus wurde die dichte Virushülle, die das Nukleokapsid umgibt, an membranumhüllten viralen Strukturen in Kryoschnitten nachgewiesen. Die Immunogoldmarkierung mit einem Anti-CD63-Antikörper oder einem Antiserum gegen die preS1/preS2-Strukturdomäne wies ebenfalls auf das Vorhandensein von sequestriertem Virus im Lumen des Exosoms hin. Das Vorhandensein von LHBs auf der Oberfläche von Exosomen, die von HBV-exprimierenden Zellen stammen, wurde ebenfalls beobachtet. Die Verfügbarkeit dieses LHBs verleiht dieser Art von Exosomen die Fähigkeit, als Immunogene wie subvirale Partikel zu wirken und die neutralisierende Wirkung von Anti-HBs-Antikörpern gegen HBV-Virionen zu verringern.

Um zu untersuchen, ob die aus HBV-produzierenden Zellen stammenden Exosomen infektiös sind, wurden die aus dem Jodixanol-Gradienten abgetrennten exosomalen Fraktionen hergestellt und zur Infektion von HBV-nicht-empfänglichen HepG2-Zellen oder HBV-empfänglichen differenzierten HepaRG-Zellen verwendet. Die Ergebnisse zeigten, dass diese mit exosomaler Membran überzogenen HBV-Partikel eine produktive Infektion in

differenzierten HepaRG-Zellen verbreiten konnten. Mit LHBs auf der Membranoberfläche schien diese Art von exosomalem HBV in HBV-empfänglichen Zellen auf eine NTCP-Rezeptor-abhängige Weise aufgenommen zu werden. In HepG2-Zellen mit demselben Input funktionierte dies jedoch nicht. Dies könnte daran liegen, dass HBV als Fracht bzw. LHBs eingebettet in exosomale Membranen als Rezeptor wirken, der die Zielspezifität dieser Exosomen in HepG2-Zellen beeinflusst, während die Zahl der anderen Arten von Exosomen nicht ausreicht, um eine Infektion in HepG2-Zellen auszulösen. Dies schließt die Möglichkeit einer Exosomen-abhängigen Aufnahme des eingekapselten Virus durch Wechselwirkungen zwischen Exosomen und Zelloberfläche nicht aus, wenn eine große Anzahl von Exosomen vorhanden ist, die kein LHBs auf der Oberfläche tragen.

Zusammengefasst deuten diese Daten darauf hin, dass ein Teil der intakten HBV-Virionen als Exosomen freigesetzt werden kann, was einen bisher unbeschriebenen Weg der HBV-Freisetzung beschreibt. Wie die zuvor entdeckten quasi-umhüllten HAV- und HEV-Viren nutzt HBV die bereits vorhandene Exosomen-Biogenese für seine eigene Zusammensetzung und Replikation. Dieser bisher unentdeckte Typ von HBV-Partikeln, der den exosomalen Weg nutzt, um eine Wirtsmembranhülle zu besetzen, würde die klassische Definition von HBV als umhülltes Partikel verwischen lassen und möglicherweise das herkömmliche Verständnis des HBV-Lebenszyklus verändern. Außerdem könnten diese HBV-Partikel tragenden Exosomen eine Infektion in differenzierte HepaRG-Zellen übertragen. Es ist wahrscheinlich, dass diese bisher unbekannte Strategie der Verkapselung von HBV-Partikeln in Exosomen eine Strategie ist, um Immunreaktionen zu umgehen und die Partikel speziell in Hepatozyten zu halten, die vom Schutz der exosomalen Membranen umgeben sind. Darüber hinaus tragen exosomale HBV wahrscheinlich zu der HBV-DNA und den Antigenen bei, die in Geweben außerhalb der Leber nachgewiesen werden. Dies deutet darauf hin, dass die von HBV genutzten Exosomen als Transporter fungieren, die die Verbreitung des Virus beeinflussen können.

9 References

[1] BLUMBERG BS, ALTER HJ, VISNICH S. A "NEW" ANTIGEN IN LEUKEMIA SERA. JAMA 1965;191:541–6.

[2] Trepo C. A brief history of hepatitis milestones. Liver international official journal of the International Association for the Study of the Liver 2014;34 Suppl 1:29–37.

[3] Block TM, Alter HJ, London WT, Bray M. A historical perspective on the discovery and elucidation of the hepatitis B virus. Antiviral research 2016;131:109–23.

[4] Trépo C, Chan HLY, Lok A. Hepatitis B virus infection. Lancet (London, England) 2014;384(9959):2053–63.

[5] Organization WH. Progress report on HIV, viral hepatitis and sexually transmitted infections 2019: accountability for the global health sector strategies, 2016–2021; 2019.

[6] Wandera BO, Onyango DM, Musyoki SK. Hepatitis B virus genetic multiplicity and the associated HBV lamivudine resistance mutations in HBV/HIV co-infection in Western Kenya: A review article. Infection, genetics and evolution journal of molecular epidemiology and evolutionary genetics in infectious diseases 2021:105197.

[7] Gerlich WH. Medical virology of hepatitis B: how it began and where we are now. Virology journal 2013;10:239.

[8] Lavanchy D. Viral hepatitis: global goals for vaccination. Journal of clinical virology the official publication of the Pan American Society for Clinical Virology 2012;55(4):296–302.

[9] Glebe D, König A. Molecular virology of hepatitis B virus and targets for antiviral intervention. Intervirology 2014;57(3-4):134–40.

[10] Jiménez-Mendoza JC, Rivera-López FE, González-Lara MF, Valdez-Echeverría RD, Castro-Narro GE, Tore A et al. Seroprevalence of hepatitis B and C viruses in moderate and severe COVID-19 inpatients: A cross-sectional study at a referral center in Mexico. Annals of hepatology 2022;27(3):100684.

[11] Schweitzer A, Horn J, Mikolajczyk RT, Krause G, Ott JJ. Estimations of worldwide prevalence of chronic hepatitis B virus infection: a systematic review of data published between 1965 and 2013. Lancet (London, England) 2015;386(10003):1546–55.

[12] Schädler S, Hildt E. HBV life cycle: entry and morphogenesis. Viruses 2009;1(2):185–209.

[13] Locarnini S. Molecular virology of hepatitis B virus. Seminars in liver disease 2004;24 Suppl 1:3–10.

[14] Landers TA, Greenberg HB, Robinson WS. Structure of hepatitis B Dane particle DNA and nature of the endogenous DNA polymerase reaction. Journal of virology 1977;23(2):368–76.

[15] Glebe D, Bremer CM. The molecular virology of hepatitis B virus. Seminars in liver disease 2013;33(2):103–12.

[16] Seeger C, Ganem D, Varmus HE. Biochemical and genetic evidence for the hepatitis B virus replication strategy. Science (New York, N.Y.) 1986;232(4749):477–84.

[17] Lien JM, Aldrich CE, Mason WS. Evidence that a capped oligoribonucleotide is the primer for duck hepatitis B virus plus-strand DNA synthesis. Journal of virology 1986;57(1):229–36.

[18] Tong S, Revill P. Overview of hepatitis B viral replication and genetic variability. Journal of hepatology 2016;64(1 Suppl):S4-S16.

[19] Slagle BL, Andrisani OM, Bouchard MJ, Lee CGL, Ou J-HJ, Siddiqui A. Technical standards for hepatitis B virus X protein (HBx) research. Hepatology (Baltimore, Md.) 2015;61(4):1416–24.

[20] Yu H, Yuan Q, Ge S-X, Wang H-Y, Zhang Y-L, Chen Q-R et al. Molecular and phylogenetic analyses suggest an additional hepatitis B virus genotype "I". PloS one 2010;5(2):e9297.
[21] Kramvis A, Kew M, François G. Hepatitis B virus genotypes. Vaccine 2005;23(19):2409–23.
[22] Norder H, Couroucé A-M, Coursaget P, Echevarria JM, Lee S-D, Mushahwar IK et al. Genetic diversity of hepatitis B virus strains derived worldwide: genotypes, subgenotypes, and HBsAg subtypes. Intervirology 2004;47(6):289–309.
[23] Tatematsu K, Tanaka Y, Kurbanov F, Sugauchi F, Mano S, Maeshiro T et al. A genetic variant of hepatitis B virus divergent from known human and ape genotypes isolated from a Japanese patient and provisionally assigned to new genotype J. Journal of virology 2009;83(20):10538–47.
[24] Bancroft WH, Mundon FK, Russell PK. Detection of additional antigenic determinants of hepatitis B antigen. Journal of immunology (Baltimore, Md. 1950) 1972;109(4):842–8.
[25] Le Bouvier GL. The heterogeneity of Australia antigen. The Journal of infectious diseases 1971;123(6):671–5.
[26] Okamoto H, Imai M, Tsuda F, Tanaka T, Miyakawa Y, Mayumi M. Point mutation in the S gene of hepatitis B virus for a d/y or w/r subtypic change in two blood donors carrying a surface antigen of compound subtype adyr or adwr. Journal of virology 1987;61(10):3030–4.
[27] Araujo NM, Waizbort R, Kay A. Hepatitis B virus infection from an evolutionary point of view: how viral, host, and environmental factors shape genotypes and subgenotypes. Infection, genetics and evolution journal of molecular epidemiology and evolutionary genetics in infectious diseases 2011;11(6):1199–207.
[28] Sunbul M. Hepatitis B virus genotypes: global distribution and clinical importance. World journal of gastroenterology 2014;20(18):5427–34.
[29] Kramvis A, Kew MC. Relationship of genotypes of hepatitis B virus to mutations, disease progression and response to antiviral therapy. Journal of viral hepatitis 2005;12(5):456–64.
[30] Lin C-L, Kao J-H. Clinical implications of hepatitis B virus variants. Journal of the Formosan Medical Association = Taiwan yi zhi 2010;109(5):321–5.
[31] Hu J, Liu K. Complete and Incomplete Hepatitis B Virus Particles: Formation, Function, and Application. Viruses 2017;9(3).
[32] Mauss S. Hepatology–A clinical textbook| 2020| Mauss, Berg, Rockstroh, Sarrazin, Wedemeyer [WWW Document]. URL https://www.hepatologytextbook.com/download/hepatology2020.pdf 2020.
[33] Howard CR. The biology of hepadnaviruses. The Journal of general virology 1986;67 (Pt 7):1215–35.
[34] Zlotnick A, Cheng N, Conway JF, Booy FP, Steven AC, Stahl SJ et al. Dimorphism of hepatitis B virus capsids is strongly influenced by the C-terminus of the capsid protein. Biochemistry 1996;35(23):7412–21.
[35] Crowther RA, Kiselev NA, Böttcher B, Berriman JA, Borisova GP, Ose V et al. Three-dimensional structure of hepatitis B virus core particles determined by electron cryomicroscopy. Cell 1994;77(6):943–50.
[36] Koschel M, Thomssen R, Bruss V. Extensive mutagenesis of the hepatitis B virus core gene and mapping of mutations that allow capsid formation. Journal of virology 1999;73(3):2153–60.

[37] Ponsel D, Bruss V. Mapping of amino acid side chains on the surface of hepatitis B virus capsids required for envelopment and virion formation. Journal of virology 2003;77(1):416–22.
[38] Selzer L, Katen SP, Zlotnick A. The hepatitis B virus core protein intradimer interface modulates capsid assembly and stability. Biochemistry 2014;53(34):5496–504.
[39] Li H-C, Huang E-Y, Su P-Y, Wu S-Y, Yang C-C, Lin Y-S et al. Nuclear export and import of human hepatitis B virus capsid protein and particles. PLoS pathogens 2010;6(10):e1001162.
[40] Eckhardt SG, Milich DR, McLachlan A. Hepatitis B virus core antigen has two nuclear localization sequences in the arginine-rich carboxyl terminus. Journal of virology 1991;65(2):575–82.
[41] Liu K, Luckenbaugh L, Ning X, Xi J, Hu J. Multiple roles of core protein linker in hepatitis B virus replication. PLoS pathogens 2018;14(5):e1007085.
[42] Thornton SM, Walker S, Zuckerman JN. Management of hepatitis B virus infections in two gibbons and a western lowland gorilla in a zoological collection. The Veterinary record 2001;149(4):113–5.
[43] Albin C, Robinson WS. Protein kinase activity in hepatitis B virus. Journal of virology 1980;34(1):297–302.
[44] Bruss V, Vieluf K. Functions of the internal pre-S domain of the large surface protein in hepatitis B virus particle morphogenesis. Journal of virology 1995;69(11):6652–7.
[45] Schmitt S, Glebe D, Alving K, Tolle TK, Linder M, Geyer H et al. Analysis of the pre-S2 N- and O-linked glycans of the M surface protein from human hepatitis B virus. The Journal of biological chemistry 1999;274(17):11945–57.
[46] Schmitt S, Glebe D, Tolle TK, Lochnit G, Linder D, Geyer R et al. Structure of pre-S2 N- and O-linked glycans in surface proteins from different genotypes of hepatitis B virus. The Journal of general virology 2004;85(Pt 7):2045–53.
[47] Dobrica M-O, Lazar C, Branza-Nichita N. N-Glycosylation and N-Glycan Processing in HBV Biology and Pathogenesis. Cells 2020;9(6).
[48] Julithe R, Abou-Jaoudé G, Sureau C. Modification of the hepatitis B virus envelope protein glycosylation pattern interferes with secretion of viral particles, infectivity, and susceptibility to neutralizing antibodies. Journal of virology 2014;88(16):9049–59.
[49] Lambert C, Prange R. Dual topology of the hepatitis B virus large envelope protein: determinants influencing post-translational pre-S translocation. The Journal of biological chemistry 2001;276(25):22265–72.
[50] Awe K, Lambert C, Prange R. Mammalian BiP controls posttranslational ER translocation of the hepatitis B virus large envelope protein. FEBS letters 2008;582(21-22):3179–84.
[51] Lambert C, Prange R. Chaperone action in the posttranslational topological reorientation of the hepatitis B virus large envelope protein: Implications for translocational regulation. Proceedings of the National Academy of Sciences of the United States of America 2003;100(9):5199–204.
[52] Gripon P, Le Seyec J, Rumin S, Guguen-Guillouzo C. Myristylation of the hepatitis B virus large surface protein is essential for viral infectivity. Virology 1995;213(2):292–9.
[53] Bruss V. A short linear sequence in the pre-S domain of the large hepatitis B virus envelope protein required for virion formation. Journal of virology 1997;71(12):9350–7.
[54] Mauss S, Berg T, Rockstroh J, Sarrazin C, Wedemeyer H, Kamps BS. Hepatology: a clinical textbook: flying publisher Düsseldorf, Germany; 2010.
[55] Prange R, Streeck RE. Novel transmembrane topology of the hepatitis B virus envelope proteins. The EMBO journal 1995;14(2):247–56.

[56] Hildt E, Munz B, Saher G, Reifenberg K, Hofschneider PH. The PreS2 activator MHBs(t) of hepatitis B virus activates c-raf-1/Erk2 signaling in transgenic mice. The EMBO journal 2002;21(4):525–35.
[57] Hildt E, Saher G, Bruss V, Hofschneider PH. The hepatitis B virus large surface protein (LHBs) is a transcriptional activator. Virology 1996;225(1):235–9.
[58] Heermann KH, Kruse F, Seifer M, Gerlich WH. Immunogenicity of the gene S and Pre-S domains in hepatitis B virions and HBsAg filaments. Intervirology 1987;28(1):14–25.
[59] Peiffer K-H, Kuhnhenn L, Jiang B, Mondorf A, Vermehren J, Knop V et al. Divergent preS Sequences in Virion-Associated Hepatitis B Virus Genomes and Subviral HBV Surface Antigen Particles From HBV e Antigen-Negative Patients. The Journal of infectious diseases 2018;218(1):114–23.
[60] Heermann KH, Goldmann U, Schwartz W, Seyffarth T, Baumgarten H, Gerlich WH. Large surface proteins of hepatitis B virus containing the pre-s sequence. Journal of virology 1984;52(2):396–402.
[61] Ning X, Basagoudanavar SH, Liu K, Luckenbaugh L, Wei D, Wang C et al. Capsid Phosphorylation State and Hepadnavirus Virion Secretion. Journal of virology 2017;91(9).
[62] Schormann W, Kraft A, Ponsel D, Bruss V. Hepatitis B virus particle formation in the absence of pregenomic RNA and reverse transcriptase. Journal of virology 2006;80(8):4187–90.
[63] Sakamoto Y, Yamada G, Mizuno M, Nishihara T, Kinoyama S, Kobayashi T et al. Full and empty particles of hepatitis B virus in hepatocytes from patients with HBsAg-positive chronic active hepatitis. Laboratory investigation; a journal of technical methods and pathology 1983;48(6):678–82.
[64] Jansen L, Kootstra NA, van Dort KA, Takkenberg RB, Reesink HW, Zaaijer HL. Hepatitis B Virus Pregenomic RNA Is Present in Virions in Plasma and Is Associated With a Response to Pegylated Interferon Alfa-2a and Nucleos(t)ide Analogues. The Journal of infectious diseases 2016;213(2):224–32.
[65] Huang Y-W, Takahashi S, Tsuge M, Chen C-L, Wang T-C, Abe H et al. On-treatment low serum HBV RNA level predicts initial virological response in chronic hepatitis B patients receiving nucleoside analogue therapy. Antiviral therapy 2015;20(4):369–75.
[66] Shirani K, Nokhodian Z, Kassaian N, Adibi P, Naeini AE, Ataei B. The prevalence of isolated hepatitis B core antibody and its related risk factors among male injected drug users in Isfahan prisons. Advanced biomedical research 2015;4:17.
[67] Gish RG, Basit SA, Ryan J, Dawood A, Protzer U. Hepatitis B core antibody: role in clinical practice in 2020. Current Hepatology Reports 2020;19(3):254–65.
[68] Possehl C, Repp R, Heermann KH, Korec E, Uy A, Gerlich WH. Absence of free core antigen in anti-HBc negative viremic hepatitis B carriers. Archives of virology. Supplementum 1992;4:39–41.
[69] Schulze A, Gripon P, Urban S. Hepatitis B virus infection initiates with a large surface protein-dependent binding to heparan sulfate proteoglycans. Hepatology (Baltimore, Md.) 2007;46(6):1759–68.
[70] Leistner CM, Gruen-Bernhard S, Glebe D. Role of glycosaminoglycans for binding and infection of hepatitis B virus. Cellular microbiology 2008;10(1):122–33.
[71] Patel M, Yanagishita M, Roderiquez G, Bou-Habib DC, Oravecz T, Hascall VC et al. Cell-surface heparan sulfate proteoglycan mediates HIV-1 infection of T-cell lines. AIDS research and human retroviruses 1993;9(2):167–74.
[72] WuDunn D, Spear PG. Initial interaction of herpes simplex virus with cells is binding to heparan sulfate. Journal of virology 1989;63(1):52–8.

[73] Giroglou T, Florin L, Schäfer F, Streeck RE, Sapp M. Human papillomavirus infection requires cell surface heparan sulfate. Journal of virology 2001;75(3):1565–70.
[74] Chen Y, Maguire T, Hileman RE, Fromm JR, Esko JD, Linhardt RJ et al. Dengue virus infectivity depends on envelope protein binding to target cell heparan sulfate. Nature medicine 1997;3(8):866–71.
[75] Barth H, Schafer C, Adah MI, Zhang F, Linhardt RJ, Toyoda H et al. Cellular binding of hepatitis C virus envelope glycoprotein E2 requires cell surface heparan sulfate. The Journal of biological chemistry 2003;278(42):41003–12.
[76] Lindblom A, Fransson LA. Endothelial heparan sulphate: compositional analysis and comparison of chains from different proteoglycan populations. Glycoconjugate journal 1990;7(6):545–62.
[77] Verrier ER, Colpitts CC, Bach C, Heydmann L, Weiss A, Renaud M et al. A targeted functional RNA interference screen uncovers glypican 5 as an entry factor for hepatitis B and D viruses. Hepatology (Baltimore, Md.) 2016;63(1):35–48.
[78] Sureau C, Salisse J. A conformational heparan sulfate binding site essential to infectivity overlaps with the conserved hepatitis B virus a-determinant. Hepatology (Baltimore, Md.) 2013;57(3):985–94.
[79] Zhao K, Liu A, Xia Y. Insights into Hepatitis B Virus DNA Integration-55 Years after Virus Discovery. Innovation (Cambridge (Mass.)) 2020;1(2):100034.
[80] Slijepcevic D, van de Graaf, Stan F J. Bile Acid Uptake Transporters as Targets for Therapy. Digestive diseases (Basel, Switzerland) 2017;35(3):251–8.
[81] Yan H, Zhong G, Xu G, He W, Jing Z, Gao Z et al. Sodium taurocholate cotransporting polypeptide is a functional receptor for human hepatitis B and D virus. eLife 2012;1:e00049.
[82] Barrera A, Guerra B, Notvall L, Lanford RE. Mapping of the hepatitis B virus pre-S1 domain involved in receptor recognition. Journal of virology 2005;79(15):9786–98.
[83] Glebe D, Urban S, Knoop EV, Cag N, Krass P, Grün S et al. Mapping of the hepatitis B virus attachment site by use of infection-inhibiting preS1 lipopeptides and tupaia hepatocytes. Gastroenterology 2005;129(1):234–45.
[84] Gripon P, Cannie I, Urban S. Efficient inhibition of hepatitis B virus infection by acylated peptides derived from the large viral surface protein. Journal of virology 2005;79(3):1613–22.
[85] Engelke M, Mills K, Seitz S, Simon P, Gripon P, Schnölzer M et al. Characterization of a hepatitis B and hepatitis delta virus receptor binding site. Hepatology (Baltimore, Md.) 2006;43(4):750–60.
[86] Huang H-C, Chen C-C, Chang W-C, Tao M-H, Huang C. Entry of hepatitis B virus into immortalized human primary hepatocytes by clathrin-dependent endocytosis. Journal of virology 2012;86(17):9443–53.
[87] Herrscher C, Pastor F, Burlaud-Gaillard J, Dumans A, Seigneuret F, Moreau A et al. Hepatitis B virus entry into HepG2-NTCP cells requires clathrin-mediated endocytosis. Cellular microbiology 2020;22(8):e13205.
[88] Ni Y, Lempp FA, Mehrle S, Nkongolo S, Kaufman C, Fälth M et al. Hepatitis B and D viruses exploit sodium taurocholate co-transporting polypeptide for species-specific entry into hepatocytes. Gastroenterology 2014;146(4):1070–83.
[89] Iwamoto M, Watashi K, Tsukuda S, Aly HH, Fukasawa M, Fujimoto A et al. Evaluation and identification of hepatitis B virus entry inhibitors using HepG2 cells overexpressing a membrane transporter NTCP. Biochemical and biophysical research communications 2014;443(3):808–13.

[90] Macovei A, Petrareanu C, Lazar C, Florian P, Branza-Nichita N. Regulation of hepatitis B virus infection by Rab5, Rab7, and the endolysosomal compartment. Journal of virology 2013;87(11):6415–27.
[91] Iwamoto M, Saso W, Nishioka K, Ohashi H, Sugiyama R, Ryo A et al. The machinery for endocytosis of epidermal growth factor receptor coordinates the transport of incoming hepatitis B virus to the endosomal network. The Journal of biological chemistry 2020;295(3):800–7.
[92] Somiya M, Sasaki Y, Matsuzaki T, Liu Q, Iijima M, Yoshimoto N et al. Intracellular trafficking of bio-nanocapsule-liposome complex: Identification of fusogenic activity in the pre-S1 region of hepatitis B virus surface antigen L protein. Journal of controlled release official journal of the Controlled Release Society 2015;212:10–8.
[93] Oess S, Hildt E. Novel cell permeable motif derived from the PreS2-domain of hepatitis-B virus surface antigens. Gene therapy 2000;7(9):750–8.
[94] Rodríguez-Crespo I, Gómez-Gutiérrez J, Nieto M, Peterson DL, Gavilanes F. Prediction of a putative fusion peptide in the S protein of hepatitis B virus. The Journal of general virology 1994;75 (Pt 3):637–9.
[95] Stoeckl L, Funk A, Kopitzki A, Brandenburg B, Oess S, Will H et al. Identification of a structural motif crucial for infectivity of hepatitis B viruses. Proceedings of the National Academy of Sciences of the United States of America 2006;103(17):6730–4.
[96] Rabe B, Glebe D, Kann M. Lipid-mediated introduction of hepatitis B virus capsids into nonsusceptible cells allows highly efficient replication and facilitates the study of early infection events. Journal of virology 2006;80(11):5465–73.
[97] Osseman Q, Gallucci L, Au S, Cazenave C, Berdance E, Blondot M-L et al. The chaperone dynein LL1 mediates cytoplasmic transport of empty and mature hepatitis B virus capsids. Journal of hepatology 2018;68(3):441–8.
[98] Panté N, Kann M. Nuclear pore complex is able to transport macromolecules with diameters of about 39 nm. Molecular biology of the cell 2002;13(2):425–34.
[99] Fay N, Panté N. Nuclear entry of DNA viruses. Frontiers in microbiology 2015;6:467.
[100] Chen C, Wang JC-Y, Pierson EE, Keifer DZ, Delaleau M, Gallucci L et al. Importin β Can Bind Hepatitis B Virus Core Protein and Empty Core-Like Particles and Induce Structural Changes. PLoS pathogens 2016;12(8):e1005802.
[101] Schmitz A, Schwarz A, Foss M, Zhou L, Rabe B, Hoellenriegel J et al. Nucleoporin 153 arrests the nuclear import of hepatitis B virus capsids in the nuclear basket. PLoS pathogens 2010;6(1):e1000741.
[102] Gallucci L, Kann M. Nuclear Import of Hepatitis B Virus Capsids and Genome. Viruses 2017;9(1).
[103] Kann M, Sodeik B, Vlachou A, Gerlich WH, Helenius A. Phosphorylation-dependent binding of hepatitis B virus core particles to the nuclear pore complex. The Journal of cell biology 1999;145(1):45–55.
[104] Barrasa MI, Guo JT, Saputelli J, Mason WS, Seeger C. Does a cdc2 kinase-like recognition motif on the core protein of hepadnaviruses regulate assembly and disintegration of capsids? Journal of virology 2001;75(4):2024–8.
[105] Lan YT, Li J, Liao W, Ou J. Roles of the three major phosphorylation sites of hepatitis B virus core protein in viral replication. Virology 1999;259(2):342–8.
[106] Lupberger J, Schaedler S, Peiran A, Hildt E. Identification and characterization of a novel bipartite nuclear localization signal in the hepatitis B virus polymerase. World journal of gastroenterology 2013;19(44):8000–10.
[107] Königer C, Wingert I, Marsmann M, Rösler C, Beck J, Nassal M. Involvement of the host DNA-repair enzyme TDP2 in formation of the covalently closed circular DNA

persistence reservoir of hepatitis B viruses. Proceedings of the National Academy of Sciences of the United States of America 2014;111(40):E4244-53.
[108] Kitamura K, Que L, Shimadu M, Koura M, Ishihara Y, Wakae K et al. Flap endonuclease 1 is involved in cccDNA formation in the hepatitis B virus. PLoS pathogens 2018;14(6):e1007124.
[109] Wei L, Ploss A. Core components of DNA lagging strand synthesis machinery are essential for hepatitis B virus cccDNA formation. Nature microbiology 2020;5(5):715–26.
[110] Wei L, Ploss A. Hepatitis B virus cccDNA is formed through distinct repair processes of each strand. Nature communications 2021;12(1):1591.
[111] Majka J, Burgers PMJ. The PCNA-RFC families of DNA clamps and clamp loaders. Progress in nucleic acid research and molecular biology 2004;78:227–60.
[112] Bruning JB, Shamoo Y. Structural and thermodynamic analysis of human PCNA with peptides derived from DNA polymerase-delta p66 subunit and flap endonuclease-1. Structure (London, England 1993) 2004;12(12):2209–19.
[113] Wei L, Ploss A. Mechanism of Hepatitis B Virus cccDNA Formation. Viruses 2021;13(8).
[114] Werle-Lapostolle B, Bowden S, Locarnini S, Wursthorn K, Petersen J, Lau G et al. Persistence of cccDNA during the natural history of chronic hepatitis B and decline during adefovir dipivoxil therapy. Gastroenterology 2004;126(7):1750–8.
[115] Boyd A, Lacombe K, Lavocat F, Maylin S, Miailhes P, Lascoux-Combe C et al. Decay of ccc-DNA marks persistence of intrahepatic viral DNA synthesis under tenofovir in HIV-HBV co-infected patients. Journal of hepatology 2016;65(4):683–91.
[116] Bourne EJ, Dienstag JL, Lopez VA, Sander TJ, Longlet JM, Hall JG et al. Quantitative analysis of HBV cccDNA from clinical specimens: correlation with clinical and virological response during antiviral therapy. Journal of viral hepatitis 2007;14(1):55–63.
[117] Huang Q, Zhou B, Cai D, Zong Y, Wu Y, Liu S et al. Rapid Turnover of Hepatitis B Virus Covalently Closed Circular DNA Indicated by Monitoring Emergence and Reversion of Signature-Mutation in Treated Chronic Hepatitis B Patients. Hepatology (Baltimore, Md.) 2021;73(1):41–52.
[118] Hu J, Protzer U, Siddiqui A. Revisiting Hepatitis B Virus: Challenges of Curative Therapies. Journal of virology 2019;93(20).
[119] Rall LB, Standring DN, Laub O, Rutter WJ. Transcription of hepatitis B virus by RNA polymerase II. Molecular and cellular biology 1983;3(10):1766–73.
[120] Belloni L, Poliicino T, Cimino L, Raffa G, Raimondo G, Levrero M. 56 HBX BINDS IN VIVO ON THE HBV MINICHROMOSOME, MODIFIES THE EPIGENETIC REGULATION OF CCC-DNA FUNCTION AND POTENTIATES HBV REPLICATION. Journal of hepatology 2008(48):S25.
[121] Tsukuda S, Watashi K. Hepatitis B virus biology and life cycle. Antiviral research 2020;182:104925.
[122] Luo L, Chen S, Gong Q, Luo N, Lei Y, Guo J et al. Hepatitis B virus X protein modulates remodelling of minichromosomes related to hepatitis B virus replication in HepG2 cells. International journal of molecular medicine 2013;31(1):197–204.
[123] Pollicino T, Belloni L, Raffa G, Pediconi N, Squadrito G, Raimondo G et al. Hepatitis B virus replication is regulated by the acetylation status of hepatitis B virus cccDNA-bound H3 and H4 histones. Gastroenterology 2006;130(3):823–37.
[124] Koumbi L, Karayiannis P. The Epigenetic Control of Hepatitis B Virus Modulates the Outcome of Infection. Frontiers in microbiology 2015;6:1491.

[125] Bartenschlager R, Schaller H. The amino-terminal domain of the hepadnaviral P-gene encodes the terminal protein (genome-linked protein) believed to prime reverse transcription. The EMBO journal 1988;7(13):4185–92.
[126] Junker-Niepmann M, Bartenschlager R, Schaller H. A short cis-acting sequence is required for hepatitis B virus pregenome encapsidation and sufficient for packaging of foreign RNA. The EMBO journal 1990;9(10):3389–96.
[127] Bartenschlager R, Schaller H. Hepadnaviral assembly is initiated by polymerase binding to the encapsidation signal in the viral RNA genome. The EMBO journal 1992;11(9):3413–20.
[128] Ganem D, Pollack JR, Tavis J. Hepatitis B virus reverse transcriptase and its many roles in hepadnaviral genomic replication. Infectious agents and disease 1994;3(2-3):85–93.
[129] Jeong JK, Yoon GS, Ryu WS. Evidence that the 5'-end cap structure is essential for encapsidation of hepatitis B virus pregenomic RNA. Journal of virology 2000;74(12):5502–8.
[130] Knaus T, Nassal M. The encapsidation signal on the hepatitis B virus RNA pregenome forms a stem-loop structure that is critical for its function. Nucleic acids research 1993;21(17):3967–75.
[131] Hu J, Boyer M. Hepatitis B virus reverse transcriptase and epsilon RNA sequences required for specific interaction in vitro. Journal of virology 2006;80(5):2141–50.
[132] Jones SA, Boregowda R, Spratt TE, Hu J. In vitro epsilon RNA-dependent protein priming activity of human hepatitis B virus polymerase. Journal of virology 2012;86(9):5134–50.
[133] Pollack JR, Ganem D. An RNA stem-loop structure directs hepatitis B virus genomic RNA encapsidation. Journal of virology 1993;67(6):3254–63.
[134] Pollack JR, Ganem D. Site-specific RNA binding by a hepatitis B virus reverse transcriptase initiates two distinct reactions: RNA packaging and DNA synthesis. Journal of virology 1994;68(9):5579–87.
[135] Hu J, Seeger C. Hepadnavirus Genome Replication and Persistence. Cold Spring Harbor perspectives in medicine 2015;5(7):a021386.
[136] Stahl M, Retzlaff M, Nassal M, Beck J. Chaperone activation of the hepadnaviral reverse transcriptase for template RNA binding is established by the Hsp70 and stimulated by the Hsp90 system. Nucleic acids research 2007;35(18):6124–36.
[137] Hu J, Toft DO, Seeger C. Hepadnavirus assembly and reverse transcription require a multi-component chaperone complex which is incorporated into nucleocapsids. The EMBO journal 1997;16(1):59–68.
[138] Chain BM, Myers R. Variability and conservation in hepatitis B virus core protein. BMC microbiology 2005;5:33.
[139] Birnbaum F, Nassal M. Hepatitis B virus nucleocapsid assembly: primary structure requirements in the core protein. Journal of virology 1990;64(7):3319–30.
[140] Gallina A, Bonelli F, Zentilin L, Rindi G, Muttini M, Milanesi G. A recombinant hepatitis B core antigen polypeptide with the protamine-like domain deleted self-assembles into capsid particles but fails to bind nucleic acids. Journal of virology 1989;63(11):4645–52.
[141] Zheng J, Schödel F, Peterson DL. The structure of hepadnaviral core antigens. Identification of free thiols and determination of the disulfide bonding pattern. The Journal of biological chemistry 1992;267(13):9422–9.
[142] Zhou S, Standring DN. Hepatitis B virus capsid particles are assembled from core-protein dimer precursors. Proceedings of the National Academy of Sciences of the United States of America 1992;89(21):10046–50.

[143] Nassal M, Rieger A, Steinau O. Topological analysis of the hepatitis B virus core particle by cysteine-cysteine cross-linking. Journal of molecular biology 1992;225(4):1013–25.
[144] Ceres P, Zlotnick A. Weak protein-protein interactions are sufficient to drive assembly of hepatitis B virus capsids. Biochemistry 2002;41(39):11525–31.
[145] Bourne CR, Katen SP, Fulz MR, Packianathan C, Zlotnick A. A mutant hepatitis B virus core protein mimics inhibitors of icosahedral capsid self-assembly. Biochemistry 2009;48(8):1736–42.
[146] Tan Z, Pionek K, Unchwaniwala N, Maguire ML, Loeb DD, Zlotnick A. The interface between hepatitis B virus capsid proteins affects self-assembly, pregenomic RNA packaging, and reverse transcription. Journal of virology 2015;89(6):3275–84.
[147] Liao W, Ou JH. Phosphorylation and nuclear localization of the hepatitis B virus core protein: significance of serine in the three repeated SPRRR motifs. Journal of virology 1995;69(2):1025–9.
[148] Gazina EV, Fielding JE, Lin B, Anderson DA. Core protein phosphorylation modulates pregenomic RNA encapsidation to different extents in human and duck hepatitis B viruses. Journal of virology 2000;74(10):4721–8.
[149] Heger-Stevic J, Zimmermann P, Lecoq L, Böttcher B, Nassal M. Hepatitis B virus core protein phosphorylation: Identification of the SRPK1 target sites and impact of their occupancy on RNA binding and capsid structure. PLoS pathogens 2018;14(12):e1007488.
[150] Jiang B, Hildt E. Intracellular Trafficking of HBV Particles. Cells 2020;9(9).
[151] Patel N, White SJ, Thompson RF, Bingham R, Weiß EU, Maskell DP et al. HBV RNA pre-genome encodes specific motifs that mediate interactions with the viral core protein that promote nucleocapsid assembly. Nature microbiology 2017;2:17098.
[152] Liaw Y-F, Zoulim F. Hepatitis B virus in human diseases: Springer; 2016.
[153] Pley C, Lourenço J, McNaughton AL, Matthews PC. Spacer Domain in Hepatitis B Virus Polymerase: Plugging a Hole or Performing a Role? Journal of virology 2022;96(9):e0005122.
[154] Wang GH, Seeger C. Novel mechanism for reverse transcription in hepatitis B viruses. Journal of virology 1993;67(11):6507–12.
[155] Nassal M, Rieger A. A bulged region of the hepatitis B virus RNA encapsidation signal contains the replication origin for discontinuous first-strand DNA synthesis. Journal of virology 1996;70(5):2764–73.
[156] Wang GH, Seeger C. The reverse transcriptase of hepatitis B virus acts as a protein primer for viral DNA synthesis. Cell 1992;71(4):663–70.
[157] Wang X, Hu J. Distinct requirement for two stages of protein-primed initiation of reverse transcription in hepadnaviruses. Journal of virology 2002;76(12):5857–65.
[158] Lin L, Wan F, Hu J. Functional and structural dynamics of hepadnavirus reverse transcriptase during protein-primed initiation of reverse transcription: effects of metal ions. Journal of virology 2008;82(12):5703–14.
[159] Abraham TM, Loeb DD. Base pairing between the 5' half of epsilon and a cis-acting sequence, phi, makes a contribution to the synthesis of minus-strand DNA for human hepatitis B virus. Journal of virology 2006;80(9):4380–7.
[160] Abraham TM, Loeb DD. The topology of hepatitis B virus pregenomic RNA promotes its replication. Journal of virology 2007;81(21):11577–84.
[161] Lien JM, Petcu DJ, Aldrich CE, Mason WS. Initiation and termination of duck hepatitis B virus DNA synthesis during virus maturation. Journal of virology 1987;61(12):3832–40.

[162] Loeb DD, Hirsch RC, Ganem D. Sequence-independent RNA cleavages generate the primers for plus strand DNA synthesis in hepatitis B viruses: implications for other reverse transcribing elements. The EMBO journal 1991;10(11):3533–40.
[163] Haines KM, Loeb DD. The sequence of the RNA primer and the DNA template influence the initiation of plus-strand DNA synthesis in hepatitis B virus. Journal of molecular biology 2007;370(3):471–80.
[164] Mueller-Hill K, Loeb DD. cis-Acting sequences 5E, M, and 3E interact to contribute to primer translocation and circularization during reverse transcription of avian hepadnavirus DNA. Journal of virology 2002;76(9):4260–6.
[165] Lewellyn EB, Loeb DD. Base pairing between cis-acting sequences contributes to template switching during plus-strand DNA synthesis in human hepatitis B virus. Journal of virology 2007;81(12):6207–15.
[166] Karayiannis P. Hepatitis B virus: virology, molecular biology, life cycle and intrahepatic spread. Hepatology international 2017;11(6):500–8.
[167] Nassal M. Hepatitis B viruses: reverse transcription a different way. Virus research 2008;134(1-2):235–49.
[168] Yang W, Summers J. Integration of hepadnavirus DNA in infected liver: evidence for a linear precursor. Journal of virology 1999;73(12):9710–7.
[169] Staprans S, Loeb DD, Ganem D. Mutations affecting hepadnavirus plus-strand DNA synthesis dissociate primer cleavage from translocation and reveal the origin of linear viral DNA. Journal of virology 1991;65(3):1255–62.
[170] Mason WS, Jilbert AR, Summers J. Clonal expansion of hepatocytes during chronic woodchuck hepatitis virus infection. Proceedings of the National Academy of Sciences of the United States of America 2005;102(4):1139–44.
[171] Summers J, Mason WS. Residual integrated viral DNA after hepadnavirus clearance by nucleoside analog therapy. Proceedings of the National Academy of Sciences of the United States of America 2004;101(2):638–40.
[172] Mason WS, Seeger C. Hepadnaviruses: molecular biology and pathogenesis: Springer Science & Business Media; 2012.
[173] Summers J, Smith PM, Horwich AL. Hepadnavirus envelope proteins regulate covalently closed circular DNA amplification. Journal of virology 1990;64(6):2819–24.
[174] Summers J, Smith PM, Huang MJ, Yu MS. Morphogenetic and regulatory effects of mutations in the envelope proteins of an avian hepadnavirus. Journal of virology 1991;65(3):1310–7.
[175] Gao W, Hu J. Formation of hepatitis B virus covalently closed circular DNA: removal of genome-linked protein. Journal of virology 2007;81(12):6164–74.
[176] Köck J, Rösler C, Zhang J-J, Blum HE, Nassal M, Thoma C. Generation of covalently closed circular DNA of hepatitis B viruses via intracellular recycling is regulated in a virus specific manner. PLoS pathogens 2010;6(9):e1001082.
[177] Rost M, Mann S, Lambert C, Döring T, Thomé N, Prange R. Gamma-adaptin, a novel ubiquitin-interacting adaptor, and Nedd4 ubiquitin ligase control hepatitis B virus maturation. The Journal of biological chemistry 2006;281(39):29297–308.
[178] Bartusch C, Döring T, Prange R. Rab33B Controls Hepatitis B Virus Assembly by Regulating Core Membrane Association and Nucleocapsid Processing. Viruses 2017;9(6).
[179] Li J, Liu Y, Wang Z, Liu K, Wang Y, Liu J et al. Subversion of cellular autophagy machinery by hepatitis B virus for viral envelopment. Journal of virology 2011;85(13):6319–33.

[180] Sir D, Tian Y, Chen W, Ann DK, Yen T-SB, Ou J-HJ. The early autophagic pathway is activated by hepatitis B virus and required for viral DNA replication. Proceedings of the National Academy of Sciences of the United States of America 2010;107(9):4383–8.
[181] Löffler-Mary H, Dumortier J, Klentsch-Zimmer C, Prange R. Hepatitis B virus assembly is sensitive to changes in the cytosolic S loop of the envelope proteins. Virology 2000;270(2):358–67.
[182] Poisson F, Severac A, Hourioux C, Goudeau A, Roingeard P. Both pre-S1 and S domains of hepatitis B virus envelope proteins interact with the core particle. Virology 1997;228(1):115–20.
[183] Bruss V, Lu X, Thomssen R, Gerlich WH. Post-translational alterations in transmembrane topology of the hepatitis B virus large envelope protein. The EMBO journal 1994;13(10):2273–9.
[184] Li H, Yan L, Shi Y, Lv D, Shang J, Bai L et al. Hepatitis B virus infection: overview. Hepatitis B virus infection 2020:1–16.
[185] Hoffmann J, Boehm C, Himmelsbach K, Donnerhak C, Roettger H, Weiss TS et al. Identification of α-taxilin as an essential factor for the life cycle of hepatitis B virus. Journal of hepatology 2013;59(5):934–41.
[186] Lambert C, Döring T, Prange R. Hepatitis B virus maturation is sensitive to functional inhibition of ESCRT-III, Vps4, and gamma 2-adaptin. Journal of virology 2007;81(17):9050–60.
[187] Stieler JT, Prange R. Involvement of ESCRT-II in hepatitis B virus morphogenesis. PloS one 2014;9(3):e91279.
[188] Watanabe T, Sorensen EM, Naito A, Schott M, Kim S, Ahlquist P. Involvement of host cellular multivesicular body functions in hepatitis B virus budding. Proceedings of the National Academy of Sciences of the United States of America 2007;104(24):10205–10.
[189] Jiang B, Himmelsbach K, Ren H, Boller K, Hildt E. Subviral Hepatitis B Virus Filaments, like Infectious Viral Particles, Are Released via Multivesicular Bodies. Journal of virology 2015;90(7):3330–41.
[190] Patient R, Hourioux C, Roingeard P. Morphogenesis of hepatitis B virus and its subviral envelope particles. Cellular microbiology 2009;11(11):1561–70.
[191] Patient R, Hourioux C, Sizaret P-Y, Trassard S, Sureau C, Roingeard P. Hepatitis B virus subviral envelope particle morphogenesis and intracellular trafficking. Journal of virology 2007;81(8):3842–51.
[192] Huovila AP, Eder AM, Fuller SD. Hepatitis B surface antigen assembles in a post-ER, pre-Golgi compartment. The Journal of cell biology 1992;118(6):1305–20.
[193] Patzer EJ, Nakamura GR, Simonsen CC, Levinson AD, Brands R. Intracellular assembly and packaging of hepatitis B surface antigen particles occur in the endoplasmic reticulum. Journal of virology 1986;58(3):884–92.
[194] Bardens A, Döring T, Stieler J, Prange R. Alix regulates egress of hepatitis B virus naked capsid particles in an ESCRT-independent manner. Cellular microbiology 2011;13(4):602–19.
[195] Chou S-F, Tsai M-L, Huang J-Y, Chang Y-S, Shih C. The Dual Role of an ESCRT-0 Component HGS in HBV Transcription and Naked Capsid Secretion. PLoS pathogens 2015;11(10):e1005123.
[196] Schorey JS, Cheng Y, Singh PP, Smith VL. Exosomes and other extracellular vesicles in host-pathogen interactions. EMBO reports 2015;16(1):24–43.
[197] Piper RC, Katzmann DJ. Biogenesis and function of multivesicular bodies. Annual review of cell and developmental biology 2007;23:519–47.

[198] Muralidharan-Chari V, Clancy JW, Sedgwick A, D'Souza-Schorey C. Microvesicles: mediators of extracellular communication during cancer progression. Journal of cell science 2010;123(Pt 10):1603–11.
[199] Doyle LM, Wang MZ. Overview of Extracellular Vesicles, Their Origin, Composition, Purpose, and Methods for Exosome Isolation and Analysis. Cells 2019;8(7).
[200] Edelstein L, Smythies JR, Quesenberry PJ, Noble D. Exosomes: A Clinical Compendium: Academic Press; 2019.
[201] Gurung S, Perocheau D, Touramanidou L, Baruteau J. The exosome journey: from biogenesis to uptake and intracellular signalling. Cell communication and signaling CCS 2021;19(1):47.
[202] van Dongen HM, Masoumi N, Witwer KW, Pegtel DM. Extracellular Vesicles Exploit Viral Entry Routes for Cargo Delivery. Microbiology and molecular biology reviews MMBR 2016;80(2):369–86.
[203] Meldolesi J. Exosomes and Ectosomes in Intercellular Communication. Current biology CB 2018;28(8):R435-R444.
[204] Yuyama K, Igarashi Y. Physiological and pathological roles of exosomes in the nervous system. Biomolecular concepts 2016;7(1):53–68.
[205] Banjade S, Zhu L, Jorgensen JR, Suzuki SW, Emr SD. Recruitment and organization of ESCRT-0 and ubiquitinated cargo via condensation. Science advances 2022;8(13):eabm5149.
[206] Ren X, Kloer DP, Kim YC, Ghirlando R, Saidi LF, Hummer G et al. Hybrid structural model of the complete human ESCRT-0 complex. Structure (London, England 1993) 2009;17(3):406–16.
[207] Schmidt O, Teis D. The ESCRT machinery. Current biology CB 2012;22(4):R116-20.
[208] Prag G, Watson H, Kim YC, Beach BM, Ghirlando R, Hummer G et al. The Vps27/Hse1 complex is a GAT domain-based scaffold for ubiquitin-dependent sorting. Developmental cell 2007;12(6):973–86.
[209] Lu Q, Hope LW, Brasch M, Reinhard C, Cohen SN. TSG101 interaction with HRS mediates endosomal trafficking and receptor down-regulation. Proceedings of the National Academy of Sciences of the United States of America 2003;100(13):7626–31.
[210] Bache KG, Slagsvold T, Cabezas A, Rosendal KR, Raiborg C, Stenmark H. The growth-regulatory protein HCRP1/hVps37A is a subunit of mammalian ESCRT-I and mediates receptor down-regulation. Molecular biology of the cell 2004;15(9):4337–46.
[211] Bishop N, Woodman P. TSG101/mammalian VPS23 and mammalian VPS28 interact directly and are recruited to VPS4-induced endosomes. The Journal of biological chemistry 2001;276(15):11735–42.
[212] Kostelansky MS, Schluter C, Tam YYC, Lee S, Ghirlando R, Beach B et al. Molecular architecture and functional model of the complete yeast ESCRT-I heterotetramer. Cell 2007;129(3):485–98.
[213] Gill DJ, Teo H, Sun J, Perisic O, Veprintsev DB, Emr SD et al. Structural insight into the ESCRT-I/-II link and its role in MVB trafficking. The EMBO journal 2007;26(2):600–12.
[214] Wollert T, Hurley JH. Molecular mechanism of multivesicular body biogenesis by ESCRT complexes. Nature 2010;464(7290):864–9.
[215] Hierro A, Sun J, Rusnak AS, Kim J, Prag G, Emr SD et al. Structure of the ESCRT-II endosomal trafficking complex. Nature 2004;431(7005):221–5.
[216] Im YJ, Hurley JH. Integrated structural model and membrane targeting mechanism of the human ESCRT-II complex. Developmental cell 2008;14(6):902–13.

[217] Teo H, Perisic O, González B, Williams RL. ESCRT-II, an endosome-associated complex required for protein sorting: crystal structure and interactions with ESCRT-III and membranes. Developmental cell 2004;7(4):559–69.
[218] Henne WM, Buchkovich NJ, Emr SD. The ESCRT pathway. Developmental cell 2011;21(1):77–91.
[219] Hurley JH, Emr SD. The ESCRT complexes: structure and mechanism of a membrane-trafficking network. Annual review of biophysics and biomolecular structure 2006;35:277–98.
[220] Nickerson DP, Russell MRG, Odorizzi G. A concentric circle model of multivesicular body cargo sorting. EMBO reports 2007;8(7):644–50.
[221] Babst M, Wendland B, Estepa EJ, Emr SD. The Vps4p AAA ATPase regulates membrane association of a Vps protein complex required for normal endosome function. The EMBO journal 1998;17(11):2982–93.
[222] Teng F, Fussenegger M. Shedding Light on Extracellular Vesicle Biogenesis and Bioengineering. Advanced science (Weinheim, Baden-Wurttemberg, Germany) 2020;8(1):2003505.
[223] Katoh K, Shibata H, Suzuki H, Nara A, Ishidoh K, Kominami E et al. The ALG-2-interacting protein Alix associates with CHMP4b, a human homologue of yeast Snf7 that is involved in multivesicular body sorting. The Journal of biological chemistry 2003;278(40):39104–13.
[224] Villarroya-Beltri C, Baixauli F, Gutiérrez-Vázquez C, Sánchez-Madrid F, Mittelbrunn M. Sorting it out: regulation of exosome loading. Seminars in cancer biology 2014;28:3–13.
[225] Elias RD, Ma W, Ghirlando R, Schwieters CD, Reddy VS, Deshmukh L. Proline-rich domain of human ALIX contains multiple TSG101-UEV interaction sites and forms phosphorylation-mediated reversible amyloids. Proceedings of the National Academy of Sciences of the United States of America 2020;117(39):24274–84.
[226] Pashkova N, Gakhar L, Winistorfer SC, Sunshine AB, Rich M, Dunham MJ et al. The yeast Alix homolog Bro1 functions as a ubiquitin receptor for protein sorting into multivesicular endosomes. Developmental cell 2013;25(5):520–33.
[227] Keren-Kaplan T, Attali I, Estrin M, Kuo LS, Farkash E, Jerabek-Willemsen M et al. Structure-based in silico identification of ubiquitin-binding domains provides insights into the ALIX-V:ubiquitin complex and retrovirus budding. The EMBO journal 2013;32(4):538–51.
[228] Ghossoub R, Lembo F, Rubio A, Gaillard CB, Bouchet J, Vitale N et al. Syntenin-ALIX exosome biogenesis and budding into multivesicular bodies are controlled by ARF6 and PLD2. Nature communications 2014;5:3477.
[229] Baietti MF, Zhang Z, Mortier E, Melchior A, Degeest G, Geeraerts A et al. Syndecan-syntenin-ALIX regulates the biogenesis of exosomes. Nature cell biology 2012;14(7):677–85.
[230] Putz U, Howitt J, Lackovic J, Foot N, Kumar S, Silke J et al. Nedd4 family-interacting protein 1 (Ndfip1) is required for the exosomal secretion of Nedd4 family proteins. The Journal of biological chemistry 2008;283(47):32621–7.
[231] Trajkovic K, Hsu C, Chiantia S, Rajendran L, Wenzel D, Wieland F et al. Ceramide triggers budding of exosome vesicles into multivesicular endosomes. Science (New York, N.Y.) 2008;319(5867):1244–7.
[232] Laulagnier K, Grand D, Dujardin A, Hamdi S, Vincent-Schneider H, Lankar D et al. PLD2 is enriched on exosomes and its activity is correlated to the release of exosomes. FEBS letters 2004;572(1-3):11–4.

[233] Matsuo H, Chevallier J, Mayran N, Le Blanc I, Ferguson C, Fauré J et al. Role of LBPA and Alix in multivesicular liposome formation and endosome organization. Science (New York, N.Y.) 2004;303(5657):531–4.
[234] Strauss K, Goebel C, Runz H, Möbius W, Weiss S, Feussner I et al. Exosome secretion ameliorates lysosomal storage of cholesterol in Niemann-Pick type C disease. The Journal of biological chemistry 2010;285(34):26279–88.
[235] Perez-Hernandez D, Gutiérrez-Vázquez C, Jorge I, López-Martín S, Ursa A, Sánchez-Madrid F et al. The intracellular interactome of tetraspanin-enriched microdomains reveals their function as sorting machineries toward exosomes. The Journal of biological chemistry 2013;288(17):11649–61.
[236] Zimmerman B, Kelly B, McMillan BJ, Seegar TCM, Dror RO, Kruse AC et al. Crystal Structure of a Full-Length Human Tetraspanin Reveals a Cholesterol-Binding Pocket. Cell 2016;167(4):1041-1051.e11.
[237] Verweij FJ, van Eijndhoven, Monique A J, Hopmans ES, Vendrig T, Wurdinger T, Cahir-McFarland E et al. LMP1 association with CD63 in endosomes and secretion via exosomes limits constitutive NF-κB activation. The EMBO journal 2011;30(11):2115–29.
[238] Votteler J, Sundquist WI. Virus budding and the ESCRT pathway. Cell host & microbe 2013;14(3):232–41.
[239] Rheinemann L, Sundquist WI. Virus Budding. Encyclopedia of Virology 2021:519–28.
[240] Blondot M-L, Bruss V, Kann M. Intracellular transport and egress of hepatitis B virus. Journal of hepatology 2016;64(1 Suppl):S49-S59.
[241] Prange R. Host factors involved in hepatitis B virus maturation, assembly, and egress. Medical microbiology and immunology 2012;201(4):449–61.
[242] Feng Z, Hensley L, McKnight KL, Hu F, Madden V, Ping L et al. A pathogenic picornavirus acquires an envelope by hijacking cellular membranes. Nature 2013;496(7445):367–71.
[243] Nagashima S, Takahashi M, Kobayashi T, Nishizawa T, Nishiyama T, Primadharsini PP et al. Characterization of the Quasi-Enveloped Hepatitis E Virus Particles Released by the Cellular Exosomal Pathway. Journal of virology 2017;91(22).
[244] Nagashima S, Takahashi M, Jirintai S, Tanaka T, Nishizawa T, Yasuda J et al. Tumour susceptibility gene 101 and the vacuolar protein sorting pathway are required for the release of hepatitis E virions. The Journal of general virology 2011;92(Pt 12):2838–48.
[245] Nagashima S, Takahashi M, Jirintai, Tanaka T, Yamada K, Nishizawa T et al. A PSAP motif in the ORF3 protein of hepatitis E virus is necessary for virion release from infected cells. The Journal of general virology 2011;92(Pt 2):269–78.
[246] Kenney SP, Pudupakam RS, Huang Y-W, Pierson FW, LeRoith T, Meng X-J. The PSAP motif within the ORF3 protein of an avian strain of the hepatitis E virus is not critical for viral infectivity in vivo but plays a role in virus release. Journal of virology 2012;86(10):5637–46.
[247] Chen Y-H, Du W, Hagemeijer MC, Takvorian PM, Pau C, Cali A et al. Phosphatidylserine vesicles enable efficient en bloc transmission of enteroviruses. Cell 2015;160(4):619–30.
[248] Yang JE, Rossignol ED, Chang D, Zaia J, Forrester I, Raja K et al. Complexity and ultrastructure of infectious extracellular vesicles from cells infected by non-enveloped virus. Scientific reports 2020;10(1):7939.
[249] Feng Z, Hirai-Yuki A, McKnight KL, Lemon SM. Naked Viruses That Aren't Always Naked: Quasi-Enveloped Agents of Acute Hepatitis. Annual review of virology 2014;1(1):539–60.

[250] Dreux M, Garaigorta U, Boyd B, Décembre E, Chung J, Whitten-Bauer C et al. Short-range exosomal transfer of viral RNA from infected cells to plasmacytoid dendritic cells triggers innate immunity. Cell host & microbe 2012;12(4):558–70.
[251] Santiana M, Ghosh S, Ho BA, Rajasekaran V, Du W-L, Mutsafi Y et al. Vesicle-Cloaked Virus Clusters Are Optimal Units for Inter-organismal Viral Transmission. Cell host & microbe 2018;24(2):208-220.e8.
[252] Parent LJ, Bennett RP, Craven RC, Nelle TD, Krishna NK, Bowzard JB et al. Positionally independent and exchangeable late budding functions of the Rous sarcoma virus and human immunodeficiency virus Gag proteins. Journal of virology 1995;69(9):5455–60.
[253] Puffer BA, Parent LJ, Wills JW, Montelaro RC. Equine infectious anemia virus utilizes a YXXL motif within the late assembly domain of the Gag p9 protein. Journal of virology 1997;71(9):6541–6.
[254] Pornillos O, Higginson DS, Stray KM, Fisher RD, Garrus JE, Payne M et al. HIV Gag mimics the Tsg101-recruiting activity of the human Hrs protein. The Journal of cell biology 2003;162(3):425–34.
[255] Lee S, Joshi A, Nagashima K, Freed EO, Hurley JH. Structural basis for viral late-domain binding to Alix. Nature structural & molecular biology 2007;14(3):194–9.
[256] Garnier L, Wills JW, Verderame MF, Sudol M. WW domains and retrovirus budding. Nature 1996;381(6585):744–5.
[257] Macias MJ, Wiesner S, Sudol M. WW and SH3 domains, two different scaffolds to recognize proline-rich ligands. FEBS letters 2002;513(1):30–7.
[258] Rotin D, Kumar S. Physiological functions of the HECT family of ubiquitin ligases. Nature reviews. Molecular cell biology 2009;10(6):398–409.
[259] El Najjar F, Schmitt AP, Dutch RE. Paramyxovirus glycoprotein incorporation, assembly and budding: a three way dance for infectious particle production. Viruses 2014;6(8):3019–54.
[260] Duan Z, Hu Z, Zhu J, Xu H, Chen J, Liu H et al. Mutations in the FPIV motif of Newcastle disease virus matrix protein attenuate virus replication and reduce virus budding. Archives of virology 2014;159(7):1813–9.
[261] Schmitt AP, Leser GP, Morita E, Sundquist WI, Lamb RA. Evidence for a new viral late-domain core sequence, FPIV, necessary for budding of a paramyxovirus. Journal of virology 2005;79(5):2988–97.
[262] Popov S, Popova E, Inoue M, Göttlinger HG. Human immunodeficiency virus type 1 Gag engages the Bro1 domain of ALIX/AIP1 through the nucleocapsid. Journal of virology 2008;82(3):1389–98.
[263] Popov S, Popova E, Inoue M, Göttlinger HG. Divergent Bro1 domains share the capacity to bind human immunodeficiency virus type 1 nucleocapsid and to enhance virus-like particle production. Journal of virology 2009;83(14):7185–93.
[264] Bello NF, Dussupt V, Sette P, Rudd V, Nagashima K, Bibollet-Ruche F et al. Budding of retroviruses utilizing divergent L domains requires nucleocapsid. Journal of virology 2012;86(8):4182–93.
[265] Dussupt V, Javid MP, Abou-Jaoudé G, Jadwin JA, La Cruz J de, Nagashima K et al. The nucleocapsid region of HIV-1 Gag cooperates with the PTAP and LYPXnL late domains to recruit the cellular machinery necessary for viral budding. PLoS pathogens 2009;5(3):e1000339.
[266] Calistri A, Del Vecchio C, Salata C, Celestino M, Celegato M, Göttlinger H et al. Role of the feline immunodeficiency virus L-domain in the presence or absence of Gag

processing: involvement of ubiquitin and Nedd4-2s ligase in viral egress. Journal of cellular physiology 2009;218(1):175–82.

[267] Chung H-Y, Morita E, Schwedler U von, Müller B, Kräusslich H-G, Sundquist WI. NEDD4L overexpression rescues the release and infectivity of human immunodeficiency virus type 1 constructs lacking PTAP and YPXL late domains. Journal of virology 2008;82(10):4884–97.

[268] Jadwin JA, Rudd V, Sette P, Challa S, Bouamr F. Late domain-independent rescue of a release-deficient Moloney murine leukemia virus by the ubiquitin ligase itch. Journal of virology 2010;84(2):704–15.

[269] Usami Y, Popov S, Popova E, Göttlinger HG. Efficient and specific rescue of human immunodeficiency virus type 1 budding defects by a Nedd4-like ubiquitin ligase. Journal of virology 2008;82(10):4898–907.

[270] Weiss ER, Popova E, Yamanaka H, Kim HC, Huibregtse JM, Göttlinger H. Rescue of HIV-1 release by targeting widely divergent NEDD4-type ubiquitin ligases and isolated catalytic HECT domains to Gag. PLoS pathogens 2010;6(9):e1001107.

[271] Kian Chua P, Lin M-H, Shih C. Potent inhibition of human Hepatitis B virus replication by a host factor Vps4. Virology 2006;354(1):1–6.

[272] Urata S, Yasuda J, de la Torre, Juan Carlos. The z protein of the new world arenavirus tacaribe virus has bona fide budding activity that does not depend on known late domain motifs. Journal of virology 2009;83(23):12651–5.

[273] Gardiner C, Di Vizio D, Sahoo S, Théry C, Witwer KW, Wauben M et al. Techniques used for the isolation and characterization of extracellular vesicles: results of a worldwide survey. Journal of extracellular vesicles 2016;5:32945.

[274] Théry C, Amigorena S, Raposo G, Clayton A. Isolation and characterization of exosomes from cell culture supernatants and biological fluids. Current protocols in cell biology 2006;Chapter 3:Unit 3.22.

[275] Kowal J, Arras G, Colombo M, Jouve M, Morath JP, Primdal-Bengtson B et al. Proteomic comparison defines novel markers to characterize heterogeneous populations of extracellular vesicle subtypes. Proceedings of the National Academy of Sciences of the United States of America 2016;113(8):E968-77.

[276] Sidhom K, Obi PO, Saleem A. A Review of Exosomal Isolation Methods: Is Size Exclusion Chromatography the Best Option? International journal of molecular sciences 2020;21(18).

[277] Konadu KA, Huang MB, Roth W, Armstrong W, Powell M, Villinger F et al. Isolation of Exosomes from the Plasma of HIV-1 Positive Individuals. Journal of visualized experiments JoVE 2016(107).

[278] Cantin R, Diou J, Bélanger D, Tremblay AM, Gilbert C. Discrimination between exosomes and HIV-1: purification of both vesicles from cell-free supernatants. Journal of immunological methods 2008;338(1-2):21–30.

[279] Wang Y-T, Shi T, Srivastava S, Kagan J, Liu T, Rodland KD. Proteomic Analysis of Exosomes for Discovery of Protein Biomarkers for Prostate and Bladder Cancer. Cancers 2020;12(9).

[280] Nordin JZ, Lee Y, Vader P, Mäger I, Johansson HJ, Heusermann W et al. Ultrafiltration with size-exclusion liquid chromatography for high yield isolation of extracellular vesicles preserving intact biophysical and functional properties. Nanomedicine nanotechnology, biology, and medicine 2015;11(4):879–83.

[281] Hong C-S, Funk S, Muller L, Boyiadzis M, Whiteside TL. Isolation of biologically active and morphologically intact exosomes from plasma of patients with cancer. Journal of extracellular vesicles 2016;5:29289.

[282] Welton JL, Webber JP, Botos L-A, Jones M, Clayton A. Ready-made chromatography columns for extracellular vesicle isolation from plasma. Journal of extracellular vesicles 2015;4:27269.
[283] Yang D, Zhang W, Zhang H, Zhang F, Chen L, Ma L et al. Progress, opportunity, and perspective on exosome isolation - efforts for efficient exosome-based theranostics. Theranostics 2020;10(8):3684–707.
[284] Lobb RJ, Becker M, Wen SW, Wong CSF, Wiegmans AP, Leimgruber A et al. Optimized exosome isolation protocol for cell culture supernatant and human plasma. Journal of extracellular vesicles 2015;4:27031.
[285] Heinemann ML, Vykoukal J. Sequential Filtration: A Gentle Method for the Isolation of Functional Extracellular Vesicles. Methods in molecular biology (Clifton, N.J.) 2017;1660:33–41.
[286] Musumeci T, Leonardi A, Bonaccorso A, Pignatello R, Puglisi G. Tangential Flow Filtration Technique: An Overview on Nanomedicine Applications. Pharmaceutical nanotechnology 2018;6(1):48–60.
[287] Peterson MF, Otoc N, Sethi JK, Gupta A, Antes TJ. Integrated systems for exosome investigation. Methods (San Diego, Calif.) 2015;87:31–45.
[288] Soda N, Rehm BHA, Sonar P, Nguyen N-T, Shiddiky MJA. Advanced liquid biopsy technologies for circulating biomarker detection. Journal of materials chemistry. B 2019;7(43):6670–704.
[289] Kang Y-T, Kim YJ, Bu J, Cho Y-H, Han S-W, Moon B-I. High-purity capture and release of circulating exosomes using an exosome-specific dual-patterned immunofiltration (ExoDIF) device. Nanoscale 2017;9(36):13495–505.
[290] Aden DP, Fogel A, Plotkin S, Damjanov I, Knowles BB. Controlled synthesis of HBsAg in a differentiated human liver carcinoma-derived cell line. Nature 1979;282(5739):615–6.
[291] Knowles BB, Howe CC, Aden DP. Human hepatocellular carcinoma cell lines secrete the major plasma proteins and hepatitis B surface antigen. Science (New York, N.Y.) 1980;209(4455):497–9.
[292] Ladner SK, Otto MJ, Barker CS, Zaifert K, Wang GH, Guo JT et al. Inducible expression of human hepatitis B virus (HBV) in stably transfected hepatoblastoma cells: a novel system for screening potential inhibitors of HBV replication. Antimicrobial agents and chemotherapy 1997;41(8):1715–20.
[293] Gripon P, Rumin S, Urban S, Le Seyec J, Glaise D, Cannie I et al. Infection of a human hepatoma cell line by hepatitis B virus. Proceedings of the National Academy of Sciences of the United States of America 2002;99(24):15655–60.
[294] Heermann KH, Goldmann U, Schwartz W, Seyffarth T, Baumgarten H, Gerlich WH. Large surface proteins of hepatitis B virus containing the pre-s sequence. Journal of virology 1984;52(2):396–402.
[295] Dragovic RA, Gardiner C, Brooks AS, Tannetta DS, Ferguson DJP, Hole P et al. Sizing and phenotyping of cellular vesicles using Nanoparticle Tracking Analysis. Nanomedicine nanotechnology, biology, and medicine 2011;7(6):780–8.
[296] Towbin H, Gordon J. Immunoblotting and dot immunobinding--current status and outlook. Journal of immunological methods 1984;72(2):313–40.
[297] Tokuyasu KT. A technique for ultracryotomy of cell suspensions and tissues. The Journal of cell biology 1973;57(2):551–65.
[298] Liou W, Geuze HJ, Slot JW. Improving structural integrity of cryosections for immunogold labeling. Histochemistry and cell biology 1996;106(1):41–58.

[299] Griffiths G. Fine structure immunocytochemistry: Springer Science & Business Media; 2012.
[300] Hajibagheri MN. Electron Microscopy: Methods and Protocols: Springer Science & Business Media; 1999.
[301] Oorschot V, Wit H de, Annaert WG, Klumperman J. A novel flat-embedding method to prepare ultrathin cryosections from cultured cells in their in situ orientation. The journal of histochemistry and cytochemistry official journal of the Histochemistry Society 2002;50(8):1067–80.
[302] Almeida JD, Rubenstein D, Stott EJ. New antigen-antibody system in Australia-antigen-positive hepatitis. Lancet (London, England) 1971;2(7736):1225–7.
[303] Kumeda N, Ogawa Y, Akimoto Y, Kawakami H, Tsujimoto M, Yanoshita R. Characterization of Membrane Integrity and Morphological Stability of Human Salivary Exosomes. Biological & pharmaceutical bulletin 2017;40(8):1183–91.
[304] Elgner F, Ren H, Medvedev R, Ploen D, Himmelsbach K, Boller K et al. The Intracellular Cholesterol Transport Inhibitor U18666A Inhibits the Exosome-Dependent Release of Mature Hepatitis C Virus. Journal of virology 2016;90(24):11181–96.
[305] Choi H, Mun JY. Structural analysis of exosomes using different types of Electron microscopy. Applied Microscopy 2017;47(3):171–5.
[306] Wang J, Cao D, Yang J. Exosomes in Hepatitis B Virus Transmission and Related Immune Response. The Tohoku journal of experimental medicine 2020;252(4):309–20.
[307] Fu Y, Zhang L, Zhang F, Tang T, Zhou Q, Feng C et al. Exosome-mediated miR-146a transfer suppresses type I interferon response and facilitates EV71 infection. PLoS pathogens 2017;13(9):e1006611.
[308] Hurwitz SN, Nkosi D, Conlon MM, York SB, Liu X, Tremblay DC et al. CD63 Regulates Epstein-Barr Virus LMP1 Exosomal Packaging, Enhancement of Vesicle Production, and Noncanonical NF-κB Signaling. Journal of virology 2017;91(5).
[309] Lenassi M, Cagney G, Liao M, Vaupotic T, Bartholomeeusen K, Cheng Y et al. HIV Nef is secreted in exosomes and triggers apoptosis in bystander CD4+ T cells. Traffic (Copenhagen, Denmark) 2010;11(1):110–22.
[310] Deschamps T, Kalamvoki M. Extracellular Vesicles Released by Herpes Simplex Virus 1-Infected Cells Block Virus Replication in Recipient Cells in a STING-Dependent Manner. Journal of virology 2018;92(18).
[311] Gould SJ, Booth AM, Hildreth JEK. The Trojan exosome hypothesis. Proceedings of the National Academy of Sciences of the United States of America 2003;100(19):10592–7.
[312] Nolte-'t Hoen E, Cremer T, Gallo RC, Margolis LB. Extracellular vesicles and viruses: Are they close relatives? Proceedings of the National Academy of Sciences of the United States of America 2016;113(33):9155–61.
[313] Deng L, Jiang W, Wang X, Merz A, Hiet M-S, Chen Y et al. Syntenin regulates hepatitis C virus sensitivity to neutralizing antibody by promoting E2 secretion through exosomes. Journal of hepatology 2019;71(1):52–61.
[314] Narayanan A, Iordanskiy S, Das R, van Duyne R, Santos S, Jaworski E et al. Exosomes derived from HIV-1-infected cells contain trans-activation response element RNA. The Journal of biological chemistry 2013;288(27):20014–33.
[315] He N, Liu M, Hsu J, Xue Y, Chou S, Burlingame A et al. HIV-1 Tat and host AFF4 recruit two transcription elongation factors into a bifunctional complex for coordinated activation of HIV-1 transcription. Molecular cell 2010;38(3):428–38.
[316] Feng Z. Quasi-enveloped hepatitis virus assembly and release. Advances in virus research 2020;108:315–36.

[317] Dane DS, Cameron CH, Briggs M. Virus-like particles in serum of patients with Australia-antigen-associated hepatitis. Lancet (London, England) 1970;1(7649):695–8.
[318] Schädler S, Hildt E. HBV life cycle: entry and morphogenesis. Viruses 2009;1(2):185–209.
[319] Gangalum RK, Atanasov IC, Zhou ZH, Bhat SP. AlphaB-crystallin is found in detergent-resistant membrane microdomains and is secreted via exosomes from human retinal pigment epithelial cells. The Journal of biological chemistry 2011;286(5):3261–9.
[320] Higgins ME, Davies JP, Chen FW, Ioannou YA. Niemann-Pick C1 is a late endosome-resident protein that transiently associates with lysosomes and the trans-Golgi network. Molecular genetics and metabolism 1999;68(1):1–13.
[321] Datta A, Kim H, Lal M, McGee L, Johnson A, Moustafa AA et al. Manumycin A suppresses exosome biogenesis and secretion via targeted inhibition of Ras/Raf/ERK1/2 signaling and hnRNP H1 in castration-resistant prostate cancer cells. Cancer letters 2017;408:73–81.
[322] Catalano M, O'Driscoll L. Inhibiting extracellular vesicles formation and release: a review of EV inhibitors. Journal of extracellular vesicles 2020;9(1):1703244.
[323] Lyu L, Wang H, Li B, Qin Q, Qi L, Nagarkatti M et al. A critical role of cardiac fibroblast-derived exosomes in activating renin angiotensin system in cardiomyocytes. Journal of molecular and cellular cardiology 2015;89(Pt B):268–79.
[324] Hu Y, Yan C, Mu L, Huang K, Li X, Tao D et al. Fibroblast-Derived Exosomes Contribute to Chemoresistance through Priming Cancer Stem Cells in Colorectal Cancer. PloS one 2015;10(5):e0125625.
[325] Richards KE, Zeleniak AE, Fishel ML, Wu J, Littlepage LE, Hill R. Cancer-associated fibroblast exosomes regulate survival and proliferation of pancreatic cancer cells. Oncogene 2017;36(13):1770–8.
[326] Charrier A, Chen R, Chen L, Kemper S, Hattori T, Takigawa M et al. Exosomes mediate intercellular transfer of pro-fibrogenic connective tissue growth factor (CCN2) between hepatic stellate cells, the principal fibrotic cells in the liver. Surgery 2014;156(3):548–55.
[327] Che Y, Shi X, Shi Y, Jiang X, Ai Q, Shi Y et al. Exosomes Derived from miR-143-Overexpressing MSCs Inhibit Cell Migration and Invasion in Human Prostate Cancer by Downregulating TFF3. Molecular therapy. Nucleic acids 2019;18:232–44.
[328] Nagashima S, Jirintai S, Takahashi M, Kobayashi T, Tanggis, Nishizawa T et al. Hepatitis E virus egress depends on the exosomal pathway, with secretory exosomes derived from multivesicular bodies. The Journal of general virology 2014;95(Pt 10):2166–75.
[329] Wang T, Fang L, Zhao F, Wang D, Xiao S. Exosomes Mediate Intercellular Transmission of Porcine Reproductive and Respiratory Syndrome Virus. Journal of virology 2018;92(4).
[330] Friand V, David G, Zimmermann P. Syntenin and syndecan in the biogenesis of exosomes. Biology of the cell 2015;107(10):331–41.
[331] Mir B, Goettsch C. Extracellular Vesicles as Delivery Vehicles of Specific Cellular Cargo. Cells 2020;9(7).
[332] Kashyap R, Balzano M, Lechat B, Lambaerts K, Egea-Jimenez AL, Lembo F et al. Syntenin-knock out reduces exosome turnover and viral transduction. Scientific reports 2021;11(1):4083.
[333] Jiang W, Ma P, Deng L, Liu Z, Wang X, Liu X et al. Hepatitis A virus structural protein pX interacts with ALIX and promotes the secretion of virions and foreign proteins through exosome-like vesicles. Journal of extracellular vesicles 2020;9(1):1716513.

[334] Strack B, Calistri A, Craig S, Popova E, Göttlinger HG. AIP1/ALIX is a binding partner for HIV-1 p6 and EIAV p9 functioning in virus budding. Cell 2003;114(6):689–99.
[335] Schwedler UK von, Stuchell M, Müller B, Ward DM, Chung H-Y, Morita E et al. The protein network of HIV budding. Cell 2003;114(6):701–13.
[336] Martin-Serrano J, Yarovoy A, Perez-Caballero D, Bieniasz PD. Divergent retroviral late-budding domains recruit vacuolar protein sorting factors by using alternative adaptor proteins. Proceedings of the National Academy of Sciences of the United States of America 2003;100(21):12414–9.
[337] Carlton JG, Martin-Serrano J. Parallels between cytokinesis and retroviral budding: a role for the ESCRT machinery. Science (New York, N.Y.) 2007;316(5833):1908–12.
[338] Carlton JG, Agromayor M, Martin-Serrano J. Differential requirements for Alix and ESCRT-III in cytokinesis and HIV-1 release. Proceedings of the National Academy of Sciences of the United States of America 2008;105(30):10541–6.
[339] Hurley JH. The ESCRT complexes. Critical reviews in biochemistry and molecular biology 2010;45(6):463–87.
[340] Platta HW, Abrahamsen H, Thoresen SB, Stenmark H. Nedd4-dependent lysine-11-linked polyubiquitination of the tumour suppressor Beclin 1. The Biochemical journal 2012;441(1):399–406.
[341] Panwalkar V, Neudecker P, Schmitz M, Lecher J, Schulte M, Medini K et al. The Nedd4-1 WW Domain Recognizes the PY Motif Peptide through Coupled Folding and Binding Equilibria. Biochemistry 2016;55(4):659–74.
[342] Kikonyogo A, Bouamr F, Vana ML, Xiang Y, Aiyar A, Carter C et al. Proteins related to the Nedd4 family of ubiquitin protein ligases interact with the L domain of Rous sarcoma virus and are required for gag budding from cells. Proceedings of the National Academy of Sciences of the United States of America 2001;98(20):11199–204.
[343] Sette P, Jadwin JA, Dussupt V, Bello NF, Bouamr F. The ESCRT-associated protein Alix recruits the ubiquitin ligase Nedd4-1 to facilitate HIV-1 release through the LYPXnL L domain motif. Journal of virology 2010;84(16):8181–92.
[344] Ninomiya M, Inoue J, Krueger EW, Chen J, Cao H, Masamune A et al. The Exosome-Associated Tetraspanin CD63 Contributes to the Efficient Assembly and Infectivity of the Hepatitis B Virus. Hepatology communications 2021;5(7):1238–51.
[345] Baghaei K, Tokhanbigli S, Asadzadeh H, Nmaki S, Reza Zali M, Hashemi SM. Exosomes as a novel cell-free therapeutic approach in gastrointestinal diseases. Journal of cellular physiology 2019;234(7):9910–26.
[346] Emerson SU, Nguyen HT, Torian U, Burke D, Engle R, Purcell RH. Release of genotype 1 hepatitis E virus from cultured hepatoma and polarized intestinal cells depends on open reading frame 3 protein and requires an intact PXXP motif. Journal of virology 2010;84(18):9059–69.
[347] Yamada K, Takahashi M, Hoshino Y, Takahashi H, Ichiyama K, Nagashima S et al. ORF3 protein of hepatitis E virus is essential for virion release from infected cells. The Journal of general virology 2009;90(Pt 8):1880–91.
[348] Graff J, Nguyen H, Yu C, Elkins WR, St Claire M, Purcell RH et al. The open reading frame 3 gene of hepatitis E virus contains a cis-reactive element and encodes a protein required for infection of macaques. Journal of virology 2005;79(11):6680–9.
[349] Jung MK, Mun JY. Sample Preparation and Imaging of Exosomes by Transmission Electron Microscopy. Journal of visualized experiments JoVE 2018(131).
[350] Kim SB, Kim HR, Park MC, Cho S, Goughnour PC, Han D et al. Caspase-8 controls the secretion of inflammatory lysyl-tRNA synthetase in exosomes from cancer cells. The Journal of cell biology 2017;216(7):2201–16.

[351] Heijnen HF, Schiel AE, Fijnheer R, Geuze HJ, Sixma JJ. Activated platelets release two types of membrane vesicles: microvesicles by surface shedding and exosomes derived from exocytosis of multivesicular bodies and alpha-granules. Blood 1999;94(11):3791–9.
[352] Choi H, Mun JY. Structural analysis of exosomes using different types of electron microscopy. Applied Microscopy 2017;47(3):171–5.
[353] Rydell GE, Prakash K, Norder H, Lindh M. Hepatitis B surface antigen on subviral particles reduces the neutralizing effect of anti-HBs antibodies on hepatitis B viral particles in vitro. Virology 2017;509:67–70.
[354] Sanada T, Hirata Y, Naito Y, Yamamoto N, Kikkawa Y, Ishida Y et al. Transmission of HBV DNA Mediated by Ceramide-Triggered Extracellular Vesicles. Cellular and molecular gastroenterology and hepatology 2017;3(2):272–83.
[355] Yang Y, Han Q, Hou Z, Zhang C, Tian Z, Zhang J. Exosomes mediate hepatitis B virus (HBV) transmission and NK-cell dysfunction. Cellular & molecular immunology 2017;14(5):465–75.
[356] Keir ME, Butte MJ, Freeman GJ, Sharpe AH. PD-1 and its ligands in tolerance and immunity. Annual review of immunology 2008;26:677–704.
[357] Notario L, Redondo-Antón J, Alari-Pahissa E, Albentosa A, Leiva M, Lopez D et al. CD69 Targeting Enhances Anti-vaccinia Virus Immunity. Journal of virology 2019;93(19).
[358] Chen R, Zhao X, Wang Y, Xie Y, Liu J. Hepatitis B virus X protein is capable of down-regulating protein level of host antiviral protein APOBEC3G. Scientific reports 2017;7:40783.
[359] Temme S, Eis-Hübinger AM, McLellan AD, Koch N. The herpes simplex virus-1 encoded glycoprotein B diverts HLA-DR into the exosome pathway. Journal of immunology (Baltimore, Md. 1950) 2010;184(1):236–43.
[360] Plazolles N, Humbert J-M, Vachot L, Verrier B, Hocke C, Halary F. Pivotal advance: The promotion of soluble DC-SIGN release by inflammatory signals and its enhancement of cytomegalovirus-mediated cis-infection of myeloid dendritic cells. Journal of leukocyte biology 2011;89(3):329–42.
[361] Mack M, Kleinschmidt A, Brühl H, Klier C, Nelson PJ, Cihak J et al. Transfer of the chemokine receptor CCR5 between cells by membrane-derived microparticles: a mechanism for cellular human immunodeficiency virus 1 infection. Nature medicine 2000;6(7):769–75.
[362] Rozmyslowicz T, Majka M, Kijowski J, Murphy SL, Conover DO, Poncz M et al. Platelet- and megakaryocyte-derived microparticles transfer CXCR4 receptor to CXCR4-null cells and make them susceptible to infection by X4-HIV. AIDS (London, England) 2003;17(1):33–42.
[363] Datta S, Chatterjee S, Veer V, Chakravarty R. Molecular biology of the hepatitis B virus for clinicians. Journal of clinical and experimental hepatology 2012;2(4):353–65.
[364] Watashi K, Wakita T. Hepatitis B Virus and Hepatitis D Virus Entry, Species Specificity, and Tissue Tropism. Cold Spring Harbor perspectives in medicine 2015;5(8):a021378.
[365] Chen N-L, Bai L, Deng T, Zhang C, Kong Q-Y, Chen H. Expression of hepatitis B virus antigen and Helicobacter pylori infection in gastric mucosa of patients with chronic liver disease. Hepatobiliary & pancreatic diseases international HBPD INT 2004;3(2):223–5.
[366] Park SC, Jeong S-H, Kim J, Han CJ, Kim YC, Choi KS et al. High prevalence of hepatitis B virus infection in patients with B-cell non-Hodgkin's lymphoma in Korea. Journal of medical virology 2008;80(6):960–6.

[367] Dejean A, Lugassy C, Zafrani S, Tiollais P, Brechot C. Detection of hepatitis B virus DNA in pancreas, kidney and skin of two human carriers of the virus. The Journal of general virology 1984;65 (Pt 3):651–5.
[368] Kong D, Di Wu, Wang T, Li T, Xu S, Chen F et al. Detection of viral antigens in renal tissue of glomerulonephritis patients without serological evidence of hepatitis B virus and hepatitis C virus infection. International journal of infectious diseases IJID official publication of the International Society for Infectious Diseases 2013;17(7):e535-8.
[369] Ramakrishnaiah V, Thumann C, Fofana I, Habersetzer F, Pan Q, Ruiter PE de et al. Exosome-mediated transmission of hepatitis C virus between human hepatoma Huh7.5 cells. Proceedings of the National Academy of Sciences of the United States of America 2013;110(32):13109–13.
[370] Longatti A, Boyd B, Chisari FV. Virion-independent transfer of replication-competent hepatitis C virus RNA between permissive cells. Journal of virology 2015;89(5):2956–61.
[371] Ko HL, Lam TH, Ng H, Toh J, Wang LW, Ren EC. Identification of Slug and SOX7 as transcriptional repressors binding to the hepatitis B virus core promoter. Journal of hepatology 2017.
[372] Seeger C, Mason WS. Hepatitis B virus biology. Microbiology and molecular biology reviews MMBR 2000;64(1):51–68.
[373] Schaller H, Fischer M. Transcriptional control of hepadnavirus gene expression. Current topics in microbiology and immunology 1991;168:21–39.
[374] Ganem D, Varmus HE. The molecular biology of the hepatitis B viruses. Annual review of biochemistry 1987;56:651–93.

10 Declaration of collaboration

Except where stated otherwise by reference or acknowledgment, the work presented was generated by myself under the supervision of my advisors during my doctoral studies. All contributions from colleagues are explicitly referenced in the thesis. The material listed below was obtained in the context of collaborative research:

Fig. 23 Ultrathin section of exosomes released from HepAD38 cells visualized by transmission electron microscopy.

Collaboration partners: Prof. Dr. Jacomine Krijnse-Locker, Dr. Susanne Tonnemacher and Regina Eberle

Institution: Loewe Center DRUID, Paul-Ehrlich-Institute, Langen, Germany

Contributions: Epon-embedded exosome sectioning and Exosome cryo-sectioning

My contributions: sample preparation, electron microscope analysis, immuno-gold labeling, data collection, image plotting

Whenever a figure, table or text is identical to a previous publication, it is stated explicitly in the thesis that copyright permission and/or co-author agreement has been obtained.

The following parts of the thesis have been previously published:

All figures shown in the results section, except for Figure 12B, Figure 14B, Figure 14C and Figure 18 are modified from a manuscript that is in press (Wu et al., 2022) and therefore do not violate copyright guidelines.

11 Declaration of an oath

D E C L A R A T I O N

I herewith declare that I have not previously participated in any doctoral examination procedure in a mathematics or natural science discipline.

Frankfurt am Main, ...(Date) ..... (Signature)

Author's Declaration

I herewith declare that I have produced my doctoral dissertation on the topic of

Analysis of the relevance of exosomes for the spread of hepatitis B virus

independently and using only the tools indicated therein. In particular, all references borrowed from external sources are clearly acknowledged and identified.

I confirm that I have respected the principles of good scientific practice and have not made use of the services of any commercial agency in respect of my doctorate.

Frankfurt am Main, ...(Date) ..... (Signature)

12 Publications

Peer-reviewed first author publications

Wu, Q., Glitscher, M., Tonnemacher, S., Schollmeier, A., Raupach J., Zahn T., Eberle R., Krijnse-Locker J., Basic M. and Hildt, E., 2022. Detection of intact hepatitis B virions in exosomes. *Cellular and Molecular Gastroenterology and Hepatology*, **in press**.

Wu, Q., Yu, H., Wei, W., Cheng, Y., Huang, S., Shi, H., Liu, S., Xia, J., Jia, H. and Hao, L., 2018. Linkage disequilibrium and functional analysis of PRE1 insertion together with SNPs in the promoter region of IGFBP7 gene in different pig breeds. *Journal of applied genetics*, *59*(2), pp.231-241.

Peer-reviewed co-author publications

Jiang, B., Wen, X., **Wu, Q.**, Bender, D., Carra, G., Basic, M., Kubesch, A., Peiffer, K.H., Boller, K. and Hildt, E., 2020. The N-terminus makes the difference: impact of genotype-specific disparities in the N-terminal part of the hepatitis B virus large surface protein on morphogenesis of viral and subviral particles. *Cells*, *9*(8), p.1898.

Wang, C., Liu, S., **Wu, Q.**, Cheng, Y., Feng, T., Song, J., Yang, R., Geng, H., Lu, G., Wang, S. and Hao, L., 2020. Porcine IGF-1R synonymous mutations in the intracellular domain affect cell proliferation and alter kinase activity. *International journal of biological macromolecules*, *152*, pp.147-153.

Jiang, B., **Wu, Q.**, Kuhnhenn, L., Akhras, S., Spengler, C., Boller, K., Peiffer, K.H. and Hildt, E., 2019. Formation of semi-enveloped particles as a unique feature of a hepatitis B virus PreS1 deletion mutant. *Alimentary Pharmacology & Therapeutics*, *50*(8), pp.940-954.

Poster presentations

13th Annual Meeting, Retreat on Biomedical Research of the Paul-Ehrlich-Institute, 2019, Ronneburg, Germany
Topic: Analysis of the relevance of exosomes for the spread of hepatitis B virus

14th Annual Meeting, Retreat on Biomedical Research of the Paul-Ehrlich-Institute, 2020, Ronneburg, Germany
Topic: Analysis of the relevance of exosomes for the spread of hepatitis B virus

29th Annual Meeting of the Society of Virology, 2019, Düsseldorf, Germany.
Topic 1: Analysis of the relevance of exosomes for the spread of hepatitis B virus
Topic 2: Impact of genotype on hepatitis B virus life cycle

30th Annual Meeting of the Society of Virology, 2021, digital, Germany.
Topic: Analysis of the relevance of exosomes for the spread of hepatitis B virus

HBV International Meeting 2021, Toronto, Canada
Topic: Exosomes participate in the life cycle of hepatitis B virus